FEBRUARY 2024

M.Sc. in Material Science and Engineering

HÜSEYİN FAAL

REPUBLIC OF TÜRKİYE

GAZİANTEP UNIVERSITY

GRADUATE SCHOOL OF NATURAL & APPLIED SCIENCES

Mn-Cu ALLOY BASED FLEXIBLE ELECTRODE FOR SUPERCAPACITOR APPLICATIONS

M.Sc. THESIS

IN

MATERIAL SCIENCE AND ENGINEERING

BY

HÜSEYİN FAAL

FEBRUARY 2024

Mn-Cu ALLOY BASED FLEXIBLE ELECTRODE FOR SUPERCAPACITOR APPLICATIONS

M.Sc. Thesis

in

Material Science and Engineering

Gaziantep University

Supervisor

Assoc. Prof. Dr. Abdulcabbar YAVUZ

by

Hüseyin FAAL

February 2024

©2024[Gaziantep University]

I hereby declare that all information in this document has been obtained and presented in accordance with academic rules and ethical conduct. I also declare that, as required by these rules and conduct, I have fully cited and referenced all material and results that are not original to this work.

Hüseyin FAAL

ABSTRACT

Mn-Cu ALLOY BASED FLEXIBLE ELECTRODE FOR SUPERCAPACITOR APPLICATIONS

FAAL, Hüseyin
M.Sc.Thesis in Metallurgy And Materials Engineering
Supervisor: Assoc. Prof. Dr. Abdulcabbar YAVUZ

February 2024

98 pages

Significant advancements have been made in the application of technologies utilizing flexible screens and sensors. However, progress in the field of flexible energy storage devices has been quite limited. Research on flexible energy storage electrodes is essential due to the critical role of flexibility and stretchability in wearable, biomedical, and portable electronic devices. This study investigates the electrochemical properties of flexible Mn-Cu alloy-coated films, filaments, and fabric graphite samples for supercapacitors. The electrochemical synthesis of Mn-Cu-based hybrid graphite is conducted using a deep eutectic solvent ionic liquid at various static voltages. Following the electrochemical deposition performance in Ethaline deep eutectic solvent, electrodes obtained are evaluated for electrochemical properties at various scan rates in different electrolytes. These electrolytes include sodium sulfate (Na_2SO_4), potassium hydroxide (KOH), a mixture of sodium sulfate and potassium hydroxide (Na_2SO_4 + KOH), and hydrochloric acid (HCl). The performance of the electrodes is examined through chronocoulometry, chronoamperometry, and cyclic voltammetry (CV) studies. Subsequently, non-electrochemical methods such as X-ray diffraction (XRD) and Fourier-transform infrared spectroscopy (FTIR) are employed for the characterization of these hybrid electrodes. The research aims to enhance the capacitance, energy, and power performance of supercapacitors. To achieve this goal, electrochemical processes were thoroughly examined to enhance the electrochemical properties of the electrodes. The obtained data indicate that Mn-Cu alloy-based stretchable graphite electrodes offer high specific capacitance values. These examination results are promising for use in supercapacitor technology applications.

Keywords: Energy Storage; Supercapacitor; Mn-Cu Alloy; Flexible Electrode; Deep Eutectic Solvent.

ÖZET

SÜPERKAPASİTÖR UYGULAMALARI İÇİN Mn-Cu ALAŞIM BAZLI ESNEK ELEKTROT

FAAL, Hüseyin
Yüksek Lisans Tezi, Metalurji ve Malzeme Mühendisliği
Danışman: Doç. Dr. Abdulcabbar YAVUZ

Şubat 2024

98 sayfa

Esnek ekranlar ve sensörlerin kullanan teknolojilerin uygulamalarında dikkate değer ilerlemeler kaydedilmiştir. Ancak, esnek enerji depolama cihazları alanında ilerleme oldukça sınırlı kalmıştır. Giyilebilir, biyomedikal ve taşınabilir elektronik cihazlarda esneklik ve gerilebilirliğin kritik rolü nedeniyle esnek enerji depolama elektrotları üzerine araştırma yapılması önemlidir. Bu çalışma, süperkapasitörler için esneklik özelliğine sahip Mn-Cu alaşım ile kaplanmış film, filament, kumaş grafit numunelerin elektrokimyasal özelliklerini incelemektedir. Mn-Cu bazlı hibrit grafitin elektrokimyasal sentezi, çeşitli statik voltajlarda derin ötektik çözücü iyonik sıvı kullanılarak gerçekleştirdi. Etaline derin ötektik çözücü içinde elektrokimyasal birikme ile elde edilen elektrotların ardından, farklı elektrolitlerde çeşitli tarama hızlarında elektrokimyasal özellikleri açısından değerlendirildi. Bu elektrolitler arasında sodyum sülfat (Na_2SO_4), potasyum hidroksit (KOH), sodyum sülfat ve potasyum hidroksitin karışımı (Na_2SO_4 + KOH) ve hidroklorik asit (HCl) vardır. Elektrotların performansı kronokulometri, kronoamperometri ve döngüsel voltametri (CV) çalışmaları aracılığıyla incelendi. Daha sonra bu hibrit elektrotların karakterizasyonunu incelemek için X-ışını kırınımı (XRD) ve Fourier dönüşümlü kızılötesi spektroskopisi (FTIR) gibi elektrokimyasal olmayan yöntemler kullanıldı. Araştırma, süperkapasitörlerin kapasitansını, enerjisini ve güç performansını artırmayı amaçlamaktadır. Bu amaca ulaşmak için, elektrotların elektrokimyasal özelliklerini geliştirmek amacıyla elektrokimyasal işlemler kapsamlı bir şekilde incelenmiştir. Elde edilen veriler, Mn-Cu alaşımı bazlı gerilebilir grafit elektrotların yüksek spesifik kapasitans değerleri sunduğunu göstermektedir. Bu inceleme sonuçları süperkapasitör teknoloji uygulamalarında kullanım için umut vericidir.

Anahtar Kelimeler: Enerji Depolama; Süperkapasitör; Mn-Cu Alaşımı; Esnek Elektrot; Derin Ötektik Çözücü.

''Dedicated to my family''

ACKNOWLEDGEMENTS

First and foremost, I would like to express my deep gratitude to my advisor, Assoc. Prof. Dr. Abdulcabbar YAVUZ, for the support provided throughout every stage of this project.

Subsequently, I wish to express my appreciation to the Department of Metallurgical and Materials Engineering for their assistance in meeting the requirements of this project.

Moreover, I am grateful to my family, and friends for their unwavering support, and love during this challenging journey. Their steadfast backing has propelled me forward at every step of this project.

TABLE OF CONTENTS

LIST OF TABLES

Page

LIST OF FIGURES

Page

LIST OF SYMBOLS

Mn	Manganese
Cu	Copper
$MnCl_2$	Manganese Chloride
$CuCl_2$	Copper Chloride
Na_2SO_4	Sodium Sulfate
KOH	Potassium Hydroxide
DES	Deep Eutectic Solvent
Pt	Platinum
W	Watt
V	Voltage
Π	Pi number
I	Current
M	Molarity
Å	Angstrom
°	Degree
°C	Centigrade Celsius
%	Percentage
ε_0	The permittivity of free space
C	Capacitance
q, Q	Charge
CV	Cyclic Voltammogram
EDLC	Electric Double Layer Capacitor
XRD	X-Ray Diffraction
FTIR	Fourier Transform Infrared Spectroscopy

CHAPTER I
INTRODUCTION

1.1 Overview of the Thesis Study

As we approach the end of the first quarter of the twenty-first century, it is obvious that the increase in energy and electricity consumption has produced a serious issues. Rapid population increase and changing consumer habits are the two main causes of this global problem because rapid population could spend more energy. Additionally, daily life in many countries has been changed due to technological improvement. Almost all technological devices (mobile phones, computers, electrical vehicals, household goods etc.) are based on energy consumption. A sizeable amount of the total energy consumption is jointly accounted for by the industrial, transportation, and construction sectors. Global energy demand could be anticipated to double by 2050 and triple by the end of the century. Increasing the efficiency of the current traditional energy systems alone might not be sufficient to meet this demand sustainably [1],[2].

It seems that conventional energy sources have harmful environmental effects that lead to ecological problems such as acid rain, ground-level ozone production, air and water pollution, global warming, and ozone layer depletion. The quick depletion of available fossil fuel resources has also compelled energy supply firms around the world to think about ways to increase the efficiency and economy of the use of current energy sources as well as to take action to develop new energy resources. Renewable energy sources were created as a result of overcoming these difficulties and improving the sustainability of energy storage techniques, and they offer significant advantages both economically and environmentally [1],[3],[4].

In terms of energy usage and power management, energy storage technologies are crucial. It contributes to a sustainable, safe, and clean way of future energy needs. There are numerous techniques for energy storage including capacitors and supercapacitors [5],[6]; sodium-sulfur (NaS), lithium-ion, nickel-cadmium (Ni-Cd) and lead-acid batteries [7],[8]; fuel cells, mechanically pumped hydropower [7], compressed air energy storage systems (CAES), and flywheels. Supercapacitors

technologies with fast charge-discharge capabilities have become increasingly prominent as a case of the need for high-power applications, maintaining energy quality, and satisfying continuous energy demand [1], [9]–[13].

Even though the use of supercapacitors is a new electrochemical energy storage technology that does not have a long history; numerous scienties, researchers and componies have focused on this system recently. In energy storage systems, supercapacitors are critical components as they can swiftly meet energy demands because of their quick energy storage and release capabilities. This aids energy systems in absorbing abrupt power spikes or emergencies. Supercapacitors are particularly cost-effective because of their long lifespan and ability to resist thousands of charge-discharge cycles. They generally require low maintenance fee. They could be an eco-friendly form of energy storage because they do not have chemicals that could be toxic for the environment and could be recycled. Supercapacitors might therefore be crucial components of energy storage systems in the future [4],[11],[14].

Basically two conducting electrodes (positive and negative electrodes), an electrolyte, and a separator form supercapacitors. Some supercapacitors are based on the principle of electrostatic storage, which is achieved by supplying a constant direct current voltage between two double layers (electrodes) that are spaced apart by a thin layer of dielectric or insulating material. These kind of supercapacitors are referred to as electric double-layer capacitors (EDLC). Energy could be stored through an electrolyte solution between two solid electrolytes. Pseudocapacitors and hybrid supercapacitors (their details are given in Section 2) are other main categories of supercapacitors within the context of energy storage techniques [13],[15],[16]. The representation of EDLC, psudocapacitor and hybrit supercapacitors are presented in **Figure 1.1.**

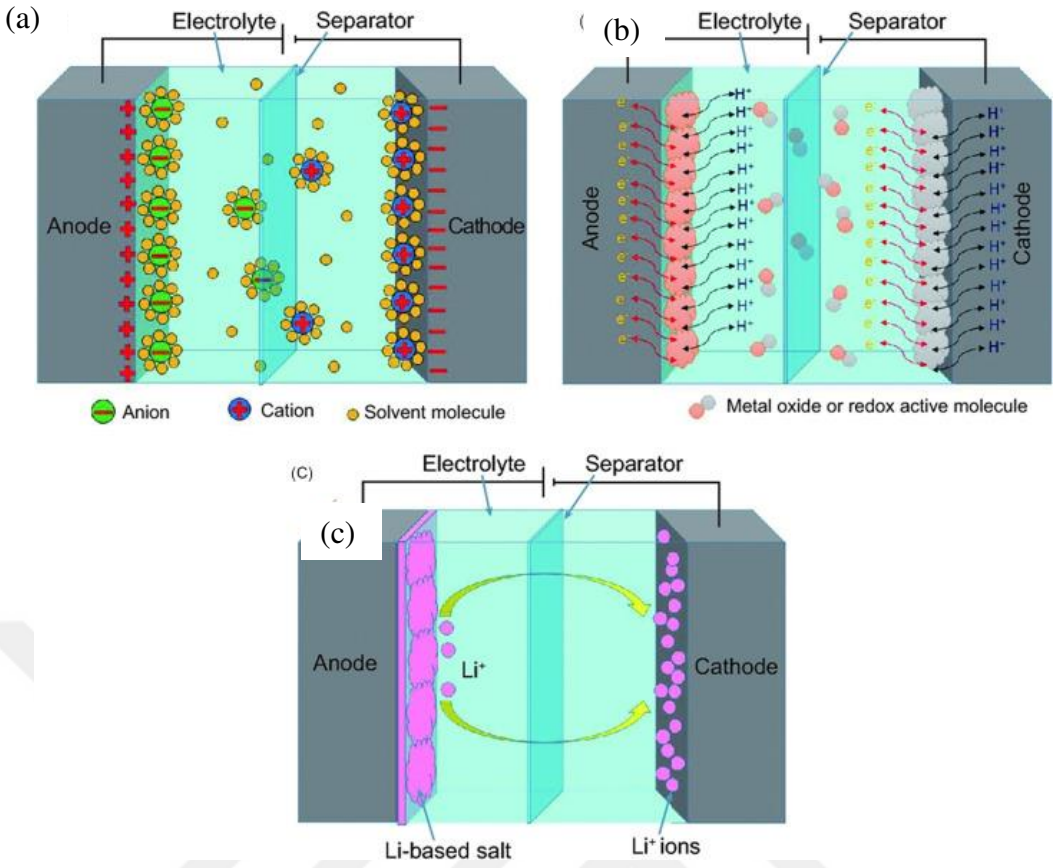

Figure 1.1 The visual representation of **(a)** an electrical double-layer capacitor (EDLC), **(b)** a pseudo-capacitor, and **(c)** a hybrid supercapacitor [15]

Electric double-layer capacitors (EDLCs) improve storage capacities by increasing electrical conductivity, increasing the surface area of the electrodes, and reducing pore size. Through the accumulation of charges at the electrode-electrolyte interfaces, this approach offers storage capability. [2], [16], [17]. Pseudocapacitors, on the other hand, store energy by reversible multi-electron redox faradaic reactions. Pseudocapacitors could have higher energy density and specific capacitance than EDLCs. This may suggest that energy storage devices can be improved using various techniques and tailored for various uses [14]–[16].

Pseudocapacitors could have higher specific capacitance values while EDLCs generally have higher cyclic stability and power performance. As the name implies, hybrid systems also give the option of combining the power source of a capacitor-like electrode (EDLC structure) with the energy source of a battery-like electrode (pseudocapacitor) in the same cell [7],[15],[17]. The EDLC generally consist of carbon based materials. The materials of pseudocapacitors are oxide, hydroxide and

sulphide based metals/alloys. Additionally conducting polymers are also the materials of pseudocapacitors. When different materials belonging to EDLC and pseudocapacitors are combined, hybrid supercapacitors could be obtained.

The main components with a significant impact on the performance of supercapacitors are electrodes and electrolytes [17]**.** The elements that store and release this energy are identified as electrodes [18]. Electrolytes are defined as those that provide energy storage and release processes at the interface and facilitate the movement of ions. Therefore, the selection of the correct electrolyte and electrode is important for supercapacitors' performance and efficiency [17]. Therefore we have focused on the combination both electrode and electrolyte in this thesis.

The material, structure, conductivity, surface area and electrochemical properties of the electrode are critical factors that influence the electrode's selection. For instance, combination of EDLC and pseudocapacitive materials could be fabricated for high-performance supercapacitor. In this work, active alloy-coated flexible graphite electrodes have been studied to analyse supercapacitor performance. These coatings could cause more surface area of the electrode and increase the interaction with the electrolyte. Thus, electrode selection could increase the energy storage capacity by enabling more interaction on the electrolyte interface of the electrodes [16],[18].

This thesis aims to examine how graphite electrodes [19] coated with effective metals such as manganese (Mn) [17] and copper (Cu) [19] affect the performance of supercapacitors. This process is obtained in the context of a comparison of various electrolytes such as sodium sulfate (Na_2SO_4) [20], potassium hydroxide (KOH) [21], a mixture of sodium sulfate + potassium hydroxide (Na_2SO_4 + KOH) [20] and hydrochloric acid (HCl) [22]. Structural and compositional characterisation of the coating are presented. The energy storage capacity and performance of supercapacitors consisting of modified electrode and appropriate electrolyte combinations are tested.

1.2 Aim of the Thesis

The main aim of the study is to analyze how the interactions between selected electrodes, electrolytes, and how their variations could influence supercapacitor performance. This could be used for development and optimization of

supercapacitor technology. In this thesis; electrodes, electrolytes, and the interactions between these two components have been reserached. The resulting data could be used to evaluate the parameters effecting supercapacitor properties. This research could contribute to our understanding of how these electrolyte and electrodes could affect supercapacitor performance. Mn-Cu based electrodes have been electrodeposited on graphite layer, graphite wire and graphite fabric. Electrodeposition conditions of the alloys on graphite based substrate have been studied. After coating process, modified electrodes have been transferred to various electrolytes such as sodium sulfate (Na_2SO_4), potassium hydroxide (KOH), sodium sulfate and potassium hydroxide mixture (Na_2SO_4 + KOH) and hydrochloric acid (HCl) in order to compare their electrochemical performance.

As a result of the electrochemical experiment studies, manganese-copper-coated graphite film, wire, and fabric could provide more interaction at the electrode-electrolyte interface in addition to improving the surface properties of sample electrodes. In this context, these alloy coatings and surface enhancement processes are assumed to lead to positive changes in energy storage capacity. This work could release the interactions between selected electrodes and electrolytes affecting supercapacitor performance.

1.3 Structure of the Thesis Study

This thesis consists of four main chapters, and each chapter explains the general structure and content of the study in detail;

I. The first chapter, the introduction, introduces the subject of the study, determines the general purpose of the thesis, presents its aim, and summarizes the chapter structure of the thesis.

II. The second chapter, theory and literature study, discusses the basic concepts and energy storage systems in detail. The history of supercapacitors, their working principle, and their comparison with other energy storage systems are the basic elements of this section. Additionally, the non-electrochemical characterization techniques (XRD, FTIR) and electrochemical characterization techniques (chronoculometry, chronoamperometry, cyclic voltammetry) used in this study are briefly described.

III. The third chapter, experimental procedures, describes in detail the experimental equipment, chemicals used, and how the experiments were performed. Experimental procedures such as the preparation processes of electrodes, coating solutions, electrolyte solutions, and cyclic voltammetry studies of manganese-copper-coated graphite films, wire, and fabrics are explained in detail in this section. Information on how non-electrochemical and electrochemical characterization techniques were applied in each study is included in this section.

IV. The fourth chapter, results and discussion, presents the findings obtained from the three-chapter experimental studies, the predictions of the study, the effective inferences derived from them, and the synthesis results. This chapter is also a section where the thesis discusses the hypothesis regarding the aims of the thesis using relevant graphs, figures, and tables, compares the study results, and evaluates the contributions of the thesis to the literature based on these results.

V. The fifth chapter, conclusion, gives summary of the work.

The reader is guided through the introduction, theoretical literature, experimental procedures, and the results and discussion by this structure, which serves as a detailed plan of action for this thesis study.

CHAPTER II
LITERATURE REVIEW AND THEORY

2.1 Energy Storage Systems

Energy storage systems have been improved as a form of technology to provide energy for the technological devices. Energy storage systems could also reduce power outages in cities, balance global energy supply and demand, and give the future generation of customers more effective access to renewable energy sources. The historical development of energy storage devices spans a significant amount of time. The process, which began with mechanical energy storage techniques like hydroelectric power plants, to the present day, to great innovative developments such as the invention of batteries and capacitors and the long-term storage of chemical energy within these electronic materials.

The Russia-Ukraine war in 2022 caused a great crisis in our country and Europe. This crisis raised serious concerns about the security and stability of the energy supply. The reliance on fossil fuels was observed as unsustainable. This war and similar crisis have showed once again that there could be a serious need for alternative energy sources in the world. For this reason, large investments and studies have been carried out to diversify the energy supply in the world and to develop renewable energy sources [23].

Energy storage systems play a pivotal role in addressing the inherent intermittency and variability of many renewable energy sources. These sources are highly dependent on environmental factors, which cause yearly variations in energy production. For this reason, energy demand and supply are not always precisely balanced, which could result in imbalances (IRENA (2023), World Energy Transitions Outlook 2023, Volume 1, International Renewable Energy Agency, n.d.).

The importance of energy storage systems becomes apparent in this situation. When the primary sources are unavailable or insufficient, these systems serve as a bridge, ensuring that the excess energy produced from alternative sources is effectively stored and made available. Energy storage systems offer a dependable and

consistent power supply, fulfilling the ever-changing demands of the need, by efficiently controlling and utilizing this stored energy [24].

Depending on how the energy is stored, it can be categorized into four main groups mechanical, thermal, chemical, and electromagnetic energy storage illustrated in **Figure 2.1** Each storage method has its costs and technological specifications [7].

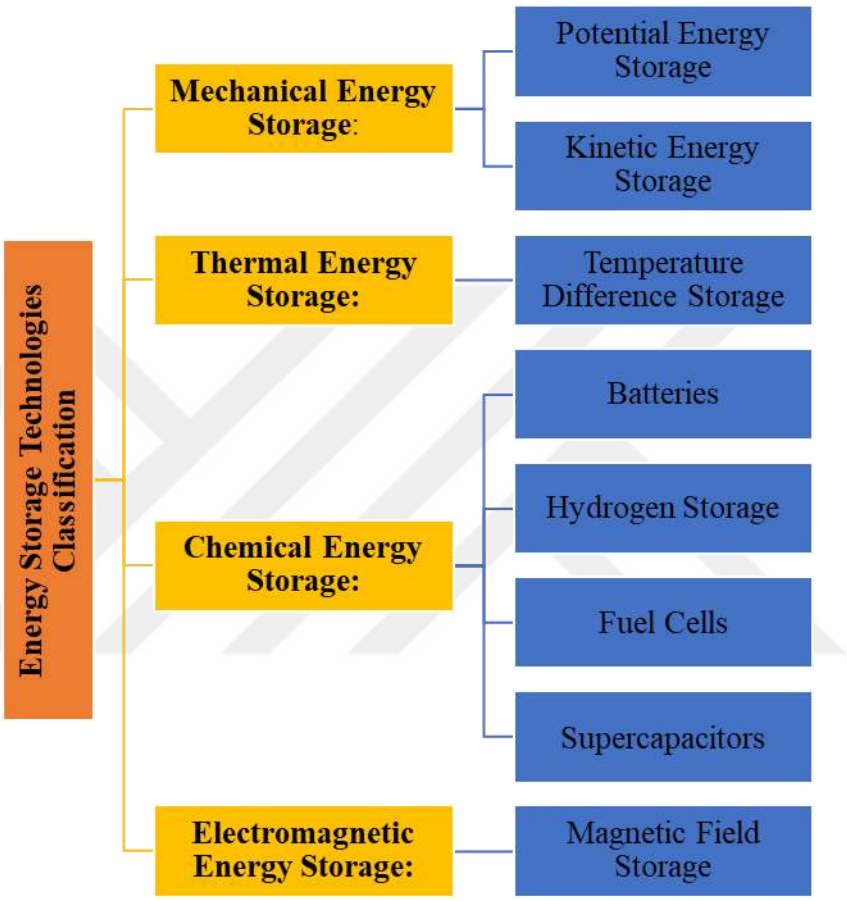

Figure 2.1 Schematic view of the classifications of energy storage technologies

2.2 Batteries

It is defined electrochemical apparatus that converts chemical energy into electric energy as a battery. There are two essential components of batteries. These are electrolyte and electrodes as anode and cathode. Their chemistries, properties could effect their performance [2].

Batteries lead to the initiation of important technological processes by converting chemical energy into electrical power. The principle is formed from the movement of electrical charge per unit of time through redox reactions. Redox reactions involve the movement of electrons along an electrical circuit from one electron cell

source to another. To produce the required output voltage and capacity with the reason of one

or more cells need to be linked in series, parallel, or both in series and parallel. Each cell has a anode and cathode which could be negative and positive electrodes depending on charging/discharging type. The electrolyte facilitate the chemical reaction between these two electrodes [25],[26].

A primary battery is a set of non-rechargeable, disposable cells that is used up completely. In contrast, secondary batteries are a cell group that can be charged again and again after use. They could also have a high power density and high discharge rate. The differences between primary and secondary batteries are illustrated in [27].

Table 2.1 Comparision of primary and secondary batteries

Primary Batteries	**Secondary Batteries**
Designed to be non-rechargeable	Designed to be Rechargeable
Meant to be used once	Meant to be used multiple times
Generally lower cost	Generally higher cost
Generally simpler manufacturing process	Generally complex manufacturing process
Lower lifecycle	Longer lifecycle
A limited number of charge-discharge cycles	Multiple numbers of charge-discharge cycles

In addition to the development of storage devices that convert the energy obtained from several different chemical reactions into electrical energy, innovative research for new battery types continues unabated. Although there are many studies and inventions on this subject, a brief review of the most common of these are presented here.

Nickel-cadmium (Ni-Cd) batteries made of nickel and cadmium (Ni-Cd) running on electrochemical reactions between nickel hydroxide (NiOOH) and cadmium (Cd). They have a wide range of purposes and have been used for a very long period in various applications. The main application areas of Ni-Cd batteries are portable devices, electric vehicles, emergency lighting vehicles, etc [28].

Ni-Cd batteries provide several beneficial features, including a high energy density and quick charging and discharging speeds. In comparison to other battery kinds that is a recommended option because of their longevity and durability. On the other hand, if the disadvantages are mentioned, they contain cadmium, which can be detrimental to the environment and need suitable recycling procedures [27],[28]. Additionally, compared to other contemporary battery types, their energy density and performance traits could be poorer. Considering their lengthy history of usage and wide range of applications, Ni-Cd batteries still occupy an important position. However other battery types might become more popular in the future due to increased competition and the creation of new battery technology [28].

Lithium-ion battery is generally as in all battery types, it usually contains a positively charged cathode, negatively charged anode, separator, electrolyte, and positive and negative current collectors making up a Li-ion battery presented in **Figure 2.2**. As a result of losing their electrons during the charging process, the lithium atoms in the anode, the negative electrode of the lithium-ion battery, become ionized. Next, lithium ions start to migrate towards the cathode, the battery's other electrode. A cathode receives the electrolyte through lithium ions (Li^+). Energy is stored as a result of the cathode's electrode material's ability to attract and hold lithium ions. As a result of the discharge cycle's operating principle lithium ions (Li^+) travel reversibly between the cathode and anode electrodes [30],[31].

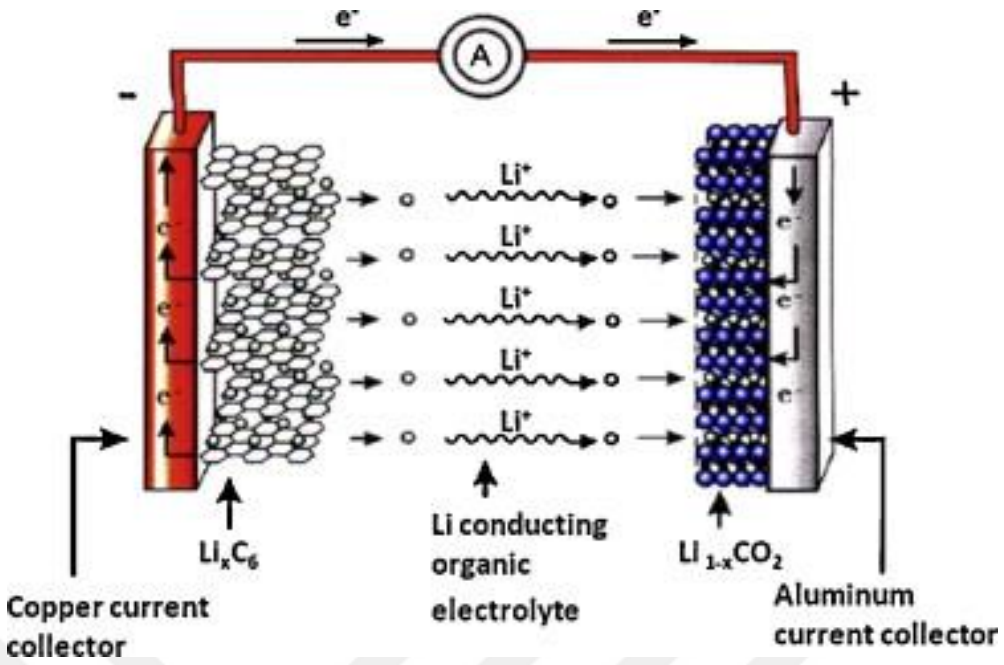

Figure 2.2 Representation of a frequent lithium-ion battery [29]

The low atomic weight of lithium makes lithium-ion batteries lightweight. Some batteries could be more suitable than lithium-ion batteries due to their high energy density, reduced self-discharge, and longer lifecycle. However, they could have some disadvantages such as cost, toxicity and long production process. Rechargeable lithium-ion (Li-ion) batteries are widely used in portable electronic devices and electric vehicles because of their high energy density and relatively long cycle life [32].

In lead-acid batteries, lead (Pb) is used as the negative electrode, lead dioxide (PbO_2) is used as the positive electrode, and sulfuric acid (H_2SO_4) solution is used as an electrolyte to ensure that ion exchange is effective between these electrodes. The representation of such battery is presented in

Figure *2.3*.

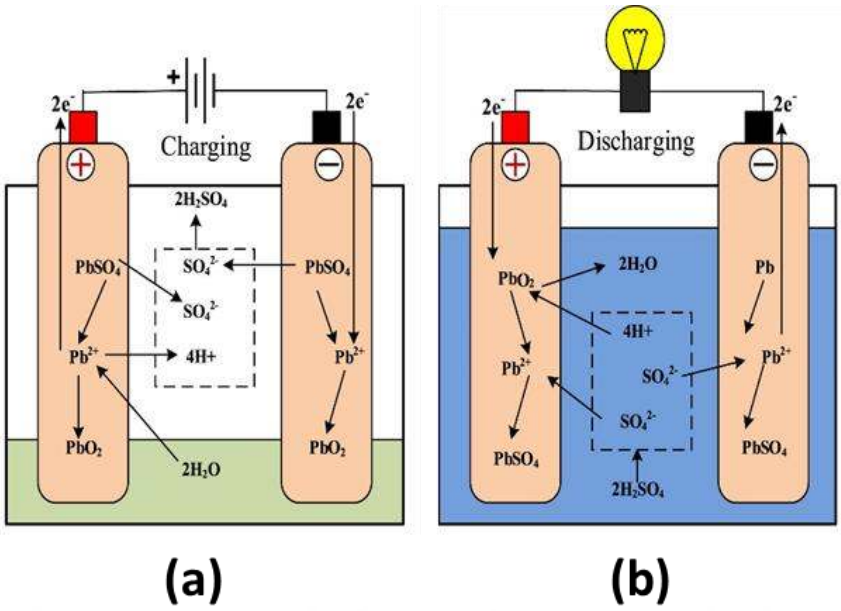

Figure 2.3 Schematic of **(a)** charge phase lead-acid batteries **and (b)** discharge phase lead-acid batteries [26]

During the discharge phase illustrated in

Figure *2.3*b), both electrodes will convert to lead sulfate ($PbSO_4$) and consume the sulfate ions from the electrolyte solution. $PbSO_4$ on the negative plates is reduced to metal during the initial charging process. But, on the positive plates, PbO_2 is formed. A battery undergoes a chemical transformation when it discharges electrical energy into an external circuit. Regularly, this process consumes the device's stored power until its voltage drops completely, and often requires immediate recharging for further use. In contrast, the overall sulfuric acid concentration in the electrolyte-to-charge reaction increases during charging (in **Figure *2.3*a)** [33],[34].

Rechargeable lead-acid batteries are frequently used in automobile batteries because of their various benefits **(as shown in Table 2.2)**, including their high power-to-weight ratio, low price, and flat discharge voltage characteristics. Additionally they could have a simple self-charging feature. Sulfuric acid is also used by lead-acid batteries, which are safer than certain other batteries in terms of safety [35],[36].

Table 2.2 Advantages and limitations of lead acid batteries

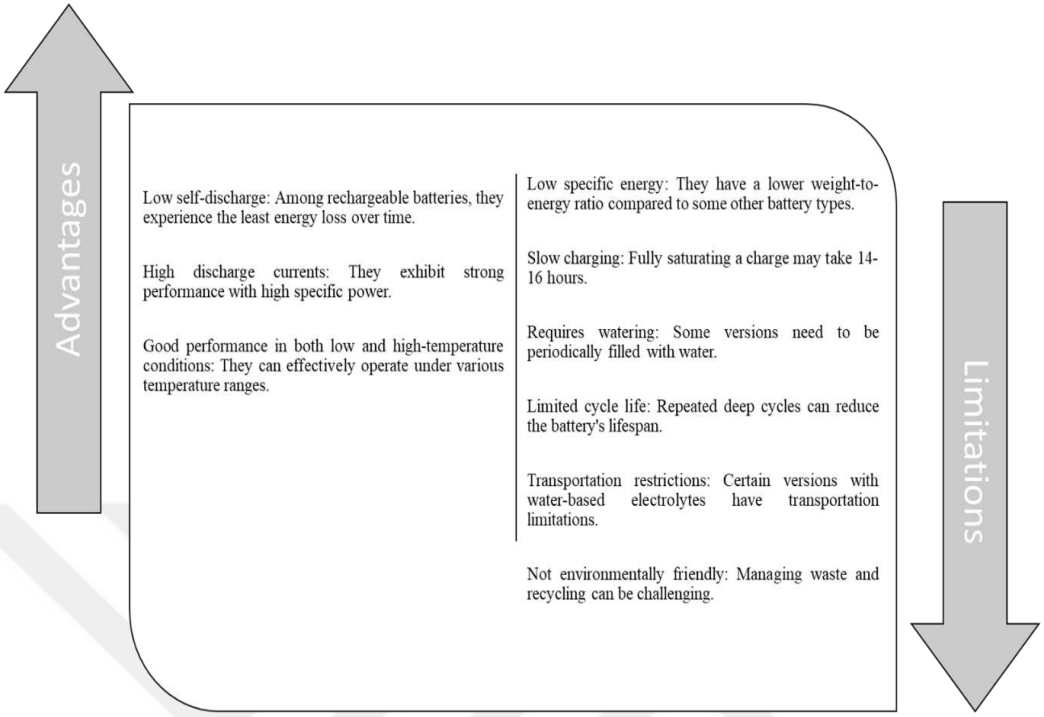

2.3 Fuel Cells

A fuel cell is an electrochemical device that converts chemical energy from a fuel such as hydrogen into electrical energy, similar to batteries. Hydrogen is supplied to the anode, the negatively charged electrode, and oxygen is sent to the cathode, the positively charged electrode. An electric current is generated by the movement of protons through the electrolyte and electrons through an external circuit. Water is produced at the cathode through the reaction between protons and electrons from the external circuit and oxygen in the air. This process produces electrical energy from a fuel cell in the results.

Based on our prior knowledge, energy for consumers can be defined as the readily available form that can be utilised at any time and place as needed. Meeting these requirements can be accomplished using energy storage systems and technologies such batteries, fuel cells, capacitors, and supercapacitors. Discrepancies in features arise due to the different designs of emerging storage technologies such as batteries, fuel cells, capacitors, and supercapacitors, as well as variations in storage concepts. The qualities that differentiate storage technologies are high storage capacity, high

efficiency, low self-discharge and capacity losses, long life, low cost, and energy intensity measured in kWh/kg or kWh/liter [37].

Table 2.3 Comparison of parameters of energy storage devices

Parameter	Fuel Cells	Batteries	Capacitors	Supercapacitors
Charge Time (s)	10 to 300 hrs. Instant charge (refuel).	1–10 hr	10^{-6} – 10^{-3}	1-30
Discharge Time (s)	10 to 300 hrs. Instant charge (refuel).	1-10 hr	10^{-6} – 10^{-3}	1-30
Life	1,500 ~ 10,000 hrs	500 ~ 1,500 cycles	>500,000 cycles	50,000+ hrs Unlimited cycles
Weight (kg)	0.02-5	0.001-10	0.001-10	0.001-230
Power Density (KW/kg)	0.001 to 0.1	0.005 to 0.4	0.25 to 10,000	10 to 120
Energy Density (Wh/kg)	300 to 3,000	8 to 600	0.01 to 0.05	1 to 10

Unlike capacitors, which use a dielectric material like a polymer film or an oxide layer to physically separate the electrical charge. The separation of chemically charged species at the electrical interface between a solid electrode and an electrolyte is the basis for supercapacitors. Due to their quick charging, quick

discharging, longevity, and environmental friendliness, these technologies have high potential [38].

2.4 Supercapacitors

2.4.1 History of Supercapacitors

As a result of an experiment with the Leyden jar, the first foundation of the capacitor was laid by around 1745. The study of the Leyden Jar (shown in **Figure 2.4**), a glass container with metal foil, is credited as the birth of capacitor technology. The jar serves as a dielectric during charging while the metal foils serve as the electrode. Negative (-) and positive (+) charges build up on each electrode, respectively. It starts to charge when a wire is attached to these two metal plate structures. In 1876 Fitzgerald continued the historical development of capacitors in the form of paper ceramics rolled into a roll and coated with wax by incorporating a wax-impregnated dielectric structure with foil electrodes into this development [5],[6],[39].

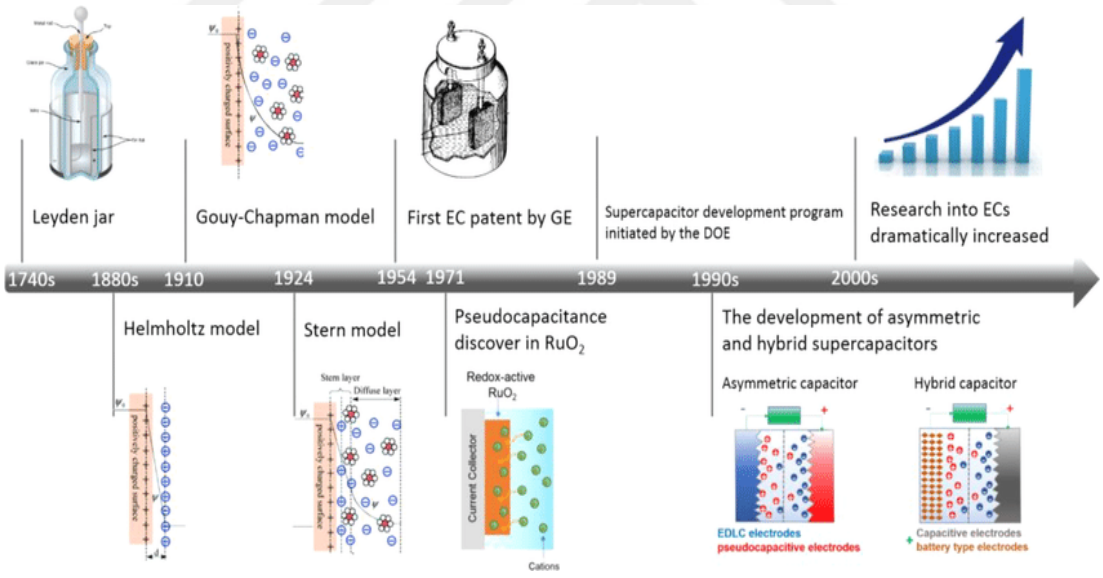

Figure 2.4 Schematic of chronological developments from capacitors to supercapacitors [41]

In 1957, General Electric patented the first supercapacitor with the name electric double-layer capacitors (EDLCs). In 1966, Standard Oil researchers uncovered the double-layer capacitor discovery while studying under their experimental work and opted not to commercialize it. Supercapacitors were created as a result of this

surprising discovery, which created new opportunities for energy storage technology. When NEC Technology Company acquired the license from Standard Oil in 1978, they publicized technology as a potent memory backup option for computers [6],[39],[40].

From 2012 to 2022 (given in **Figure 2.4)**, progress in supercapacitor research, developments in materials and production methods, and optimization R&D studies aimed at increasing performance and reducing costs have continued to increase in the last 10 years [42]. An almost 10-fold increase in research papers published during this period can be observed, making supercapacitor research one of the 'hot' research areas. Research has been extended to electrode materials, but also to studies of electrolytes and separators [42]. Supercapacitors fill the void of batteries and other energy storage technologies due to their high specific capacitance values, low operating voltage ranges, and long charge/discharge cycles. This thesis aims to contribute to the development of supercapacitors with the electrode and electrolyte combination to be used.

2.4.2 Principles of Working Supercapacitor

In the working principle of supercapacitors, positive and negative ions are absorbed on the surfaces of solid electrodes. This is an electrostatic energy storage method that relies on electrostatic capacitors, as shown in **Equation 2.1**.

The fundamental formula that applies to all capacitors can be explained as follows:

$$C = \frac{\varepsilon_0 * \varepsilon r * A}{d} \qquad (2.1)$$

In this equation, the permeability of the air (ε_0), the relative permittivity of the dielectric material (εr), the surface area (A), and the distance (d) between the two electrodes are shown in **Figure 2.5**. The capacitance value of the capacitor is adjusted by changing the surface area and thickness of the dielectric material [6],[15]. Upon increasing surface area or decreasing distance, the capacitance could be increased.

The basic equation (**Equation 2.2**) showing the specific capacitance (C) value in supercapacitors is as follows :

$$C = \frac{2}{A \cdot \Delta V} \int \frac{I \, dV}{v} \qquad (2.2)$$

In which:

- C is the specific capacitance (F cm^{-2}),

- I represents the current density (A cm^{-2}),
- ΔV stands for the potential difference (V),
- v signifies the scan rate (mV s^{-1}),
- A is the area of active materials loaded in the working electrode (cm^2)

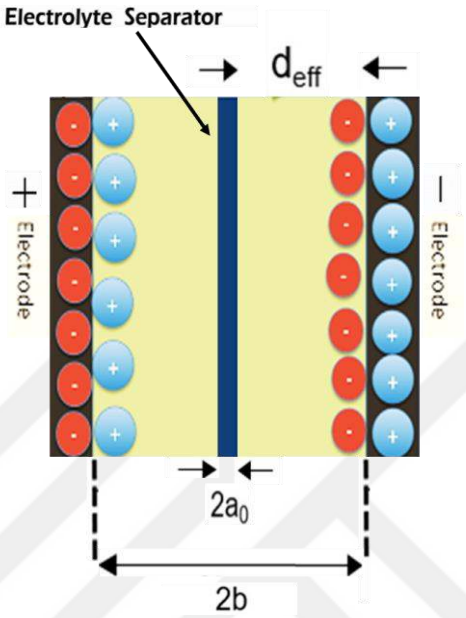

Figure 2.5 View diagram of supercapacitor electrode formed located in the middle of two electrodes separated by a single layer [43]

In this context, energy is stored due to the potential difference between the two solid electrodes. The positive and negative ions in the electrolyte are absorbed on the surfaces of the solid electrodes during charging, under the influence of charging. The cation and anion return to the step-and-step region of the solid electrodes during discharge [44].

➢ **Charging (Loading) Process,**

During charging, ions flowing onto the surfaces of the positive and negative electrodes are adsorbed by the electrodes. These ions accomodate on the electrode surface, forming two layers as far as potential is applied. The electrical double layer creates a space charge region between the charged ions. In this way, a potential difference is obtained on the surfaces of the electrodes. This potential difference enables energy to be stored and used (presented in **Figure 2.6**) [6],[44].

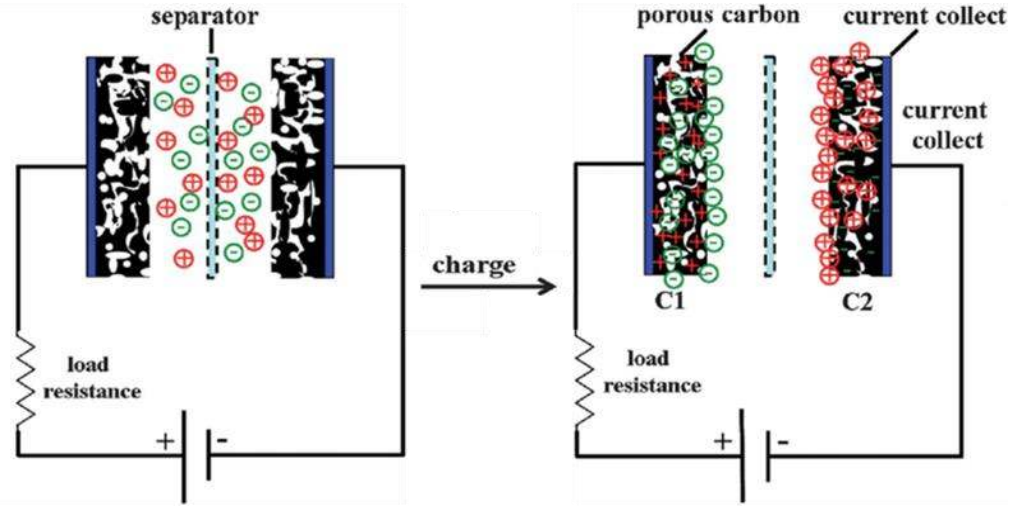

Figure 2.6 Schematic diagram of charging in supercapacitor [45]

➢ **Discharge (Transferring) Process,**

During the discharge process, on contrary to the charging process, the positively charged ions are separated from the negative electrode particles, while the negatively charged ions are separated from the positive electrodes (presented in **Figure 2.7**) especially when potential is removed [6],[15],[44].

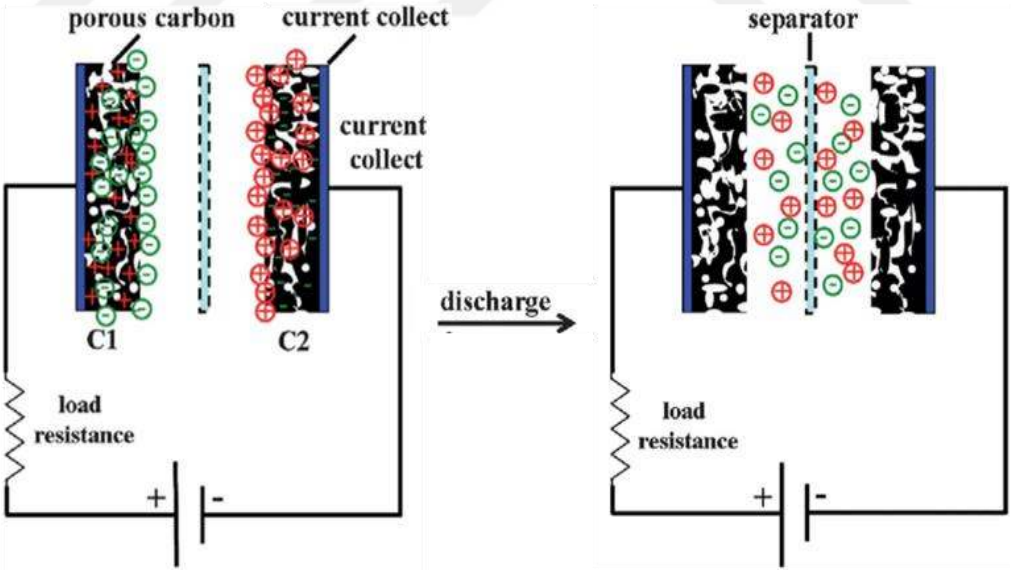

Figure 2.7 Schematic diagram of discharging in supercapacitor [45]

2.4.3 General Properties of Supercapacitors

This stage examines the general properties of supercapacitors in terms of structural, chemical, and operational capacity. A supercapacitor's physical composition and

components are examples of structural features. The main feature of supercapcitor devices are electrodes (positive and negative) and electrolytes.

An electrolyte solution and a solid electrolyte are critical parameters for the properties of supercapacitors. Supercapacitors' performance and physical characteristics are a result of the interaction between their electrode and electrolyte components, whose primary constituents are materials. Electrode materials also would need a high surface area for energy storage [39],[44],[46]. Carbon based materials with a high surface area often serves as the electrode material for EDL capacitors. Carbon materials which are mainly composed of EDLC could be made of carbon-derived compounds, carbon [87] fiber [88] fabric, airgel [89] with various carbon appearances, graphite [90], graphene [91], and carbon nanotubes [46].

Because of its adaptable morphologies and properties, carbon is a versatile element. Additionally, carbon is a crucial material for energy storage applications due to its high abundance and low specific gravity [45],[46]. Metals including nickel [92] [93], ruthenium [94], copper [95], iron [96], manganese [97], cobalt oxide [98] based electrodes and the alloys consisting of at least one of these metals are the main materials in pseudocapacitors. Additionally conducting polymers such as polyaniline [99] and polypyrrole [100] could be used as pseudocapacitors. The final performance of supercapacitors (either EDLC or pseudocapacitores) will be intimately related to the physical and chemical properties of these electrodes given. In this approach, the variety of electrode materials aids in the applications of supercapacitors [46],[47].

Another element that substantially influences the functionality and energy storage capacity of supercapacitors is the electrolyte composition. These electrolytes can be ionic, organic, or aqueous liquids, among other varieties [48]. Ionic-bonded chemicals called electrolytes are made up of ions with positively charged cations and negatively charged anions. These ions make it possible for electrolytes to conduct electricity and dissolve effortlessly in polar solvents like water. Their high ionic conductivity and low viscosity make them distinctive [18],[48].

Finally, the separators that affect the supercapacitor properties. Separators are the supercapacitor components located between the electrodes and regulate ion movement in the electrolyte solution. The separator, a mechanically sturdy part,

helps to efficiently transport ions to the electrodes' surface area while limiting unfavorable material diffusion in the electrolyte [49].

On the other hand, it is also compared to other energy storage systems, supercapacitors have a higher specific power. However, they have less specific energy, nevertheless (see **Figure 2.8**). Supercapacitors are exceptionally adaptable as a stand-alone energy source or in conjunction with batteries as a hybrid system because of the ability to cover several orders of magnitude in both the specific energy and specific power ranges thanks to optimal cell design [46].

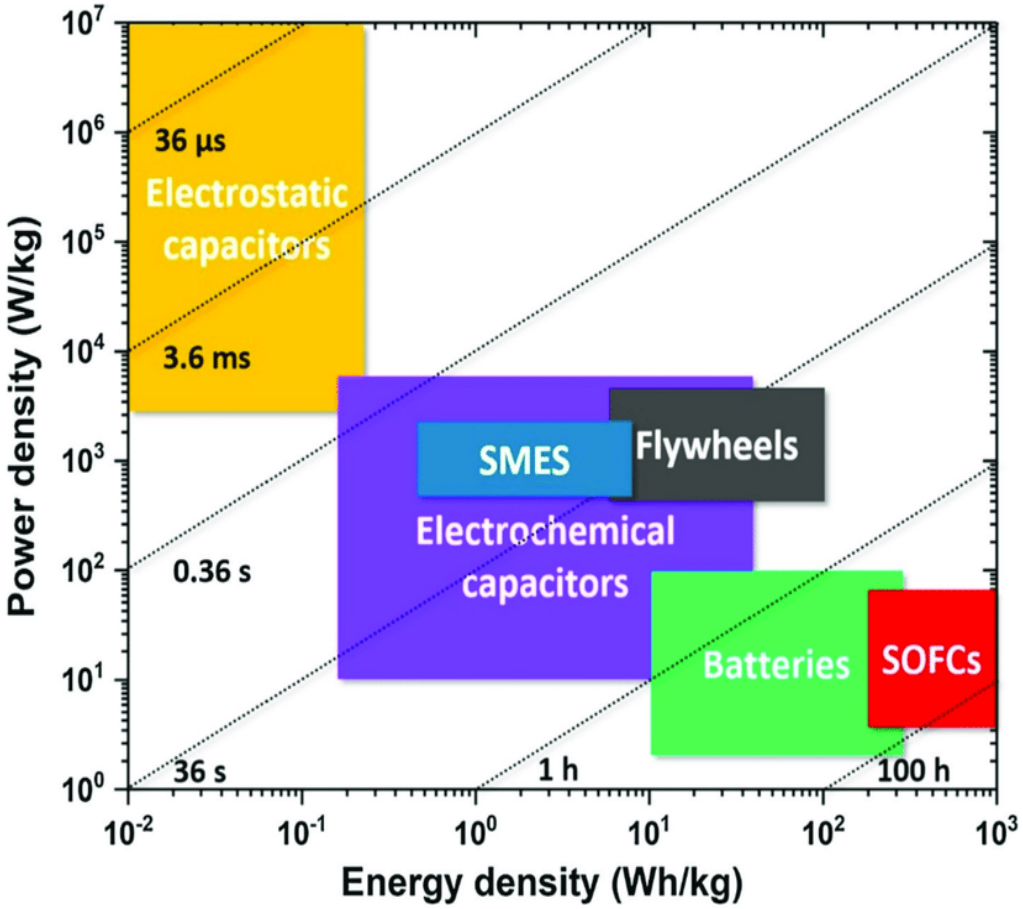

Figure 2.8 The Ragone plot showing the energy and power performance metrics of a variety of energy storage devices [50]

2.5 Types of Supercapacitors

As mentioned in previous section, the working principle of the supercapacitor is based on the storage and distribution of ions from the electrolyte to the surface area of the electrodes. As shown in **Figure 2.9**, energy storage mechanisms; are divided into three different classes: electrochemical double-layer capacitors,

pseudocapacitors, and hybrid supercapacitors [18]. These electrodes are explained below in detail, specifically the fundamental differences in how supercapacitors store energy and how they work.

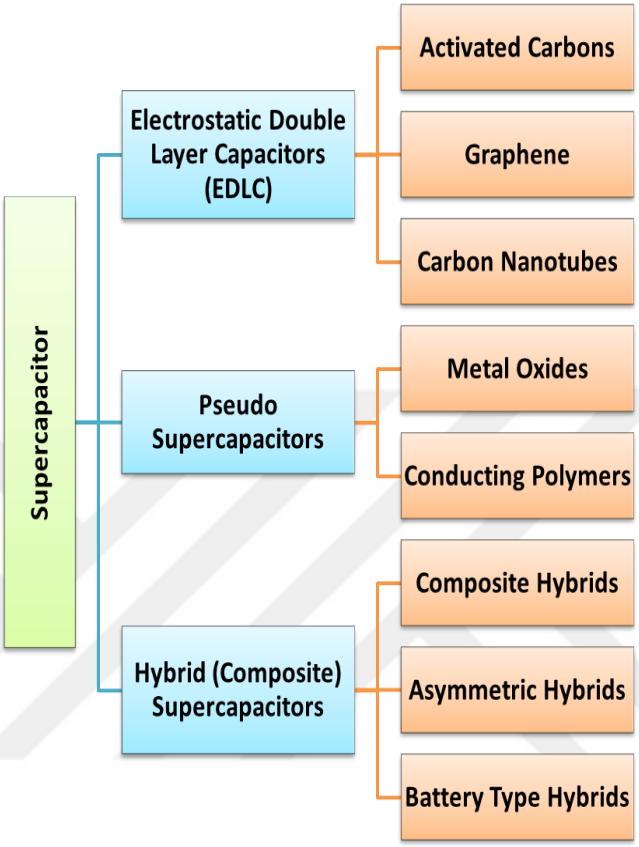

Figure 2.9 Schematic view of the classifications of supercapacitor

2.5.1 Electrostatic Double-Layer Capacitors

Electrostatic double-layer capacitors (EDLCs) are one of the most intriguing energy storage technologies currently available [51]. In the working principle of electrostatic double-layer capacitors, as the name suggests, the ions in the electrolyte spread over the separator and onto the pores on the other side as a result of the potential difference and being stored electrostatically on the electrode surfaces [13].

Today, EDLCs are thought to be the best option for high-power applications. The adsorption of ions to the surface of the electrodes serves as the working foundation for the energy storage mechanism of electrostatic double-layer capacitors [52].

In terms of performance, EDLCs could provide higher power density as energy storage systems with benefits like a long cycle life, the ability to charge and

discharge in a short time (typically in minutes), and a broad range of applications [53]. The main component of EDLC is carbon based materials explained in Section 2.6.1.

2.5.2 Pseudo Supercapacitors

Pseudocapacitance are energy storage systems in which faradic reactions occur on electrode surfaces mediating electron transfers [54]. Fast and reversible faradic reactions that take place on or near the electrode material's surface give rise to pseudocapacitance reaction. As a case, charge builds up on the electrode surface, allowing energy to be stored [55]. This development of energy storage systems known as pseudocapacitance is also connected to the structure of materials, particularly metal oxides and conducting polymers [55].

The development of pseudocapacitance, a type of energy storage device, is also related to the composition of materials, particularly metal oxides, hydroxides and sulphites. In the search for economically favorable, plentiful, and inexpensive metal oxides to display similar characteristics, it has received high attention. The pseudocapacitance qualities of materials like manganese and ruthenium based oxides, for instance, have made them desirable for use in energy storage applications [56].

Charge buildup on electrode surfaces and quick, reversible faradic reactions define this energy storage process. When charging and discharging, these reactions take place. (produced by compounds' bonds). The disadvantage of this system also compared to other energy storage systems is this principle of working, since during charging and discharging the electrodes are stretched and degraded faster compared to the electrostatic storage principle. The system's lifespan (cycles) could be shortened as a result [46],[57],[58]. The materials of pseudocapacitance are explained in detail in Section 2.6.2.

2.5.3 Hybrid (Composite) Supercapacitors

Pseudocapacitors could have low power density and cyclic stability despite having high specific capacitance, while electrostatic double-layer capacitance (EDLC) supercapacitors could have high energy density and high cyclic stability. Hybrid supercapacitors represent a synthesis of these two types of capacitors, which

provide significant advantages in terms of energy storage [59]. Hybrid supercapacitors are also a unique component that combines various charging methods. While EDLC employs an electrostatic mechanism based on charge separation by electrolyte between electrodes to offer energy storage capacity. However, pseudocapacitance employs oxidation and reduction reaction-based charge/discharge mechanisms to offer energy storage capacity. The combination of these two mechanisms enables the unique properties of the two capacitor types, such as fast charge/discharge ability and high energy density of hybrid supercapacitors [59].

Table 2.4 Characteristics of different supercapacitor types.

SC Types	Electrode Materials	Charge Storage Mechanism	Advantage/ Disadvantage
Electric Double-Layer Capacitors (EDLC)	Carbon materials for both electrodes	Charge absorption/desorption at the electrode-electrolyte interface	• High power density, • Good cycling performance , • Low energy density, • Low specific capacitance,
Pseudocapacitors	Metal oxides and conductive polymers	Reversible surface Faradic redox processes	• High capacitance, • High energy density, • Poor cycling performance ,
Hybrid Supercapasitor	Carbon materials and pseudocapacitive materials for anode and cathode. Composites of pseudocapacitive materials with carbon based materials	One electrode with redox reactions and EDLC absorption/desorption for another electrode without Faradic process	• High power density, • High energy density, • Good cycling ability,

Hybrid supercapacitors can be tuned based on the performance of various electrode materials. The total performance of hybrid supercapacitors is determined by factors

such as the chemical characteristics, microstructure, and electroconductivity of these metal oxides, composites, and carbon-based electrodes. By increasing the development of these variables, hybrid supercapacitors containing metal ions like lithium ions can reach better energy storage capacities and power combinations [56],[60].

In this context, hybrid supercapacitors attract attention as a special innovation system that combines various advantages and will have great potential in the field of energy storage in the future compared to other types. The differences between supercapacitor types [61] are summarised in **Table 2.4**.

2.6 Electrolytes for Supercapacitors

A conductive source that ensures the flow of energy is necessary for all devices that store or generate electrical energy based on electrochemical process. Batteries, fuel cells, general capacitors, and supercapacitors are a few examples of these systems. These energy storage systems have an electrolyte that allows ions to flow or conduct. These electrolytes enable quick energy storage or release. Likewise, they are components that permit ion mobility to facilitate high-speed charging and discharging [73].

Electrolytes play a critical role in the operating principles of various energy storage devices and affect the performance of these devices by facilitating or hindering the movement of ions. Because of this, there are different types and characteristics of electrolytes depending on their use. **Figure 2.10** illustrated electrolytes which can be divided into three main categories such as aqueous conventional, solid, and redox electrolytes [74].

In energy storage systems, liquid electrolytes make ions travel between the electrodes, facilitating electrochemical reactions. This enables energy storage devices to be charged and discharged. Ions travel through the liquid electrolyte when an electric current is given to one of the electrodes, reversibly turning chemical energy into electrical energy [75].

In comparison to organic electrolytes, aqueous electrolytes could have higher ion concentrations, capacities, and power densities. This might be due to the lower ionic radius and increased ion concentration. Among the most popular liquid electrolytes are KOH, NaOH, Na_2SO_4, H_2SO_4, NH_4Cl, etc. The energy density is

lowered by the low energy density of liquid electrolytes. Aqueous electrolytes can also be made and used without strict pretreatment requirements [76].

Ionic liquids are liquids consisting of only ions (cations and anions). Salt are generally are solid at room temperature and they could be liquid at high temperatures (typically around 1500 C). However, there are some special salts and they could be liquid at room temperature. These salts are called as room temperature ionic liquids. When salts, acids or bases are dissolved solvent (such as water or organic solvents) for preparation of solutions (electrolytes), the system consists of solvent and ions. However, room temperature ionic liquids have only ions. The main problem of ionic liquids are their high cost. Therefore, Deep Eutectic Solvents, which are mainly cheaper, safer and more environmentally friendly than ionic liquid, could be used instead of room temperature ionic liquids. The Deep Eutectic Solvent used in this work is choline chloride and ethylene glycol based Ethaline.

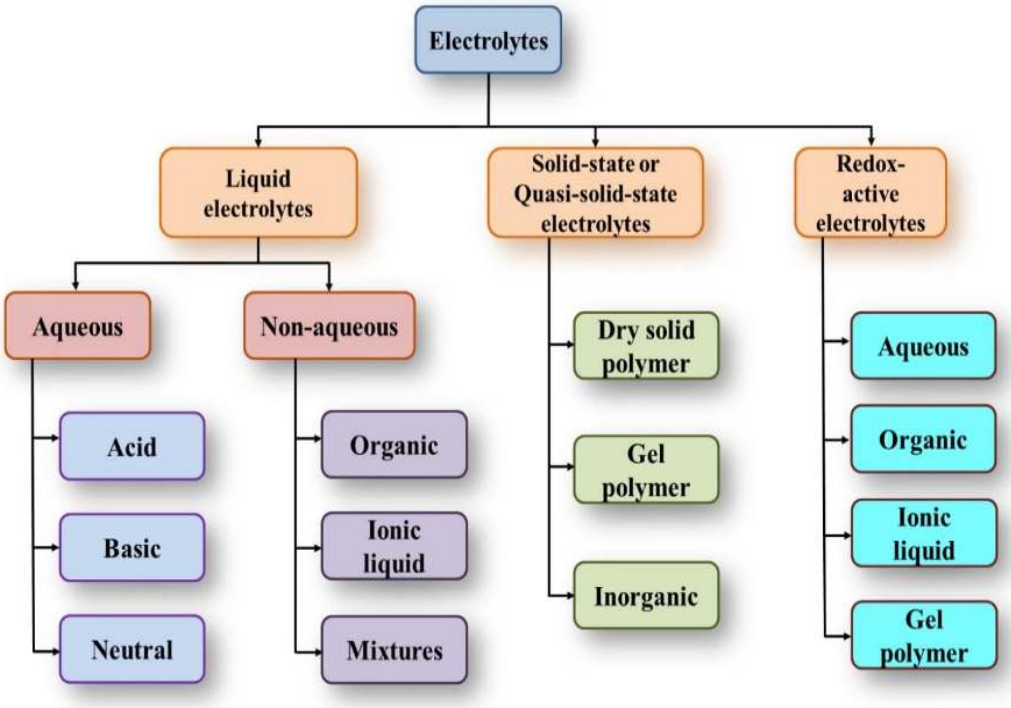

Figure 2.10 Classification flowchart of electrolytes for supercapacitor [77]

Solid electrolytes are also mentioned as an alternative to the usage of conventional (liquid) electrolytes. Solid electrolytes are less dangerous than electrolytes in organic solvents which makes operation safer for energy storage systems such as batteries and supercapasitors. Potential window for aqueos electrolyte is around 1.3

V and it could be enlarged to around 2 V when organic or ionic liquid electrolytes are used. However, solid electrolytes enable higher operating voltages (often >4.5 V), which can enhance battery performance. Alternative battery chemistries, such as Li/O_2 and Li/S batteries, are compatible with solid electrolytes [74],[78]. Different potential windows have been applied in this work to reveal the performance of the electrolyte.

2.7 Electrodes for Supercapacitors

Electrodes are parts that are used to store charge on a capacitor's surface while it is being charged and to release this ion charge when the capacitor is being discharged [62] To develop power-dense supercapacitors, it has been an important area to conduct research and discover applications for these functional materials in the literature.

The common characteristics of these requiring development electrode materials are as follows:

- High surface area,
- Good conductivity,
- High storage capacity,
- Ability to provide energy density,
- Cyclic stability,
- Chemical and physical resistance.

These characteristic features are important factors that determine the performance of supercapacitors and constitute the reason why they are preferred in applications. Therefore, developing and optimizing electrode materials play a critical role in the advancement of supercapacitor technology [63]. Although these types of electrode materials generally vary according to the type of supercapacitor, they can be grouped as composite materials based on carbon, metal oxide, conducting polymer, and derivatives of these materials [64].

2.7.1 Carbon and Its Derivatives Electrodes

The storage mechanism used by carbon materials is an ideal option for Electrochemical double-layer capacitors (EDLC), also known as special capacitors or high capacitance capacitors. These capacitors are used for various applications that require energy storage and rapid energy discharge [64]. Electrodes must

fundamentally have unique benefits for effective application. Electrodes made of carbon have large specific surface areas. As a result, the electrodes' surface has more electroactive sites and may store more charge. Rapid energy discharge is made possible by this feature [65]. Carbon electrodes' capacity to deliver fast power is a result of their ability to store and release energy quickly. This functionality is important for powering devices [62].

Compared to other energy storage electrodes, carbon based electrodes generally have a longer cycle stability. They do not lose significant capacity when charged and discharged cyclically, resulting in cost savings. Carbon electrodes are capable of stable performance over a broad temperature range. This broadens their application and enables them used in a variety of temperature environments [64]. Some examples regarding the types of carbon are presented in **Figure 2.11**. These electrode materials are activated carbon, carbon aerogels, carbon nanotubes, graphene, etc. This provides the flexibility to design electrodes suitable for different applications [67].

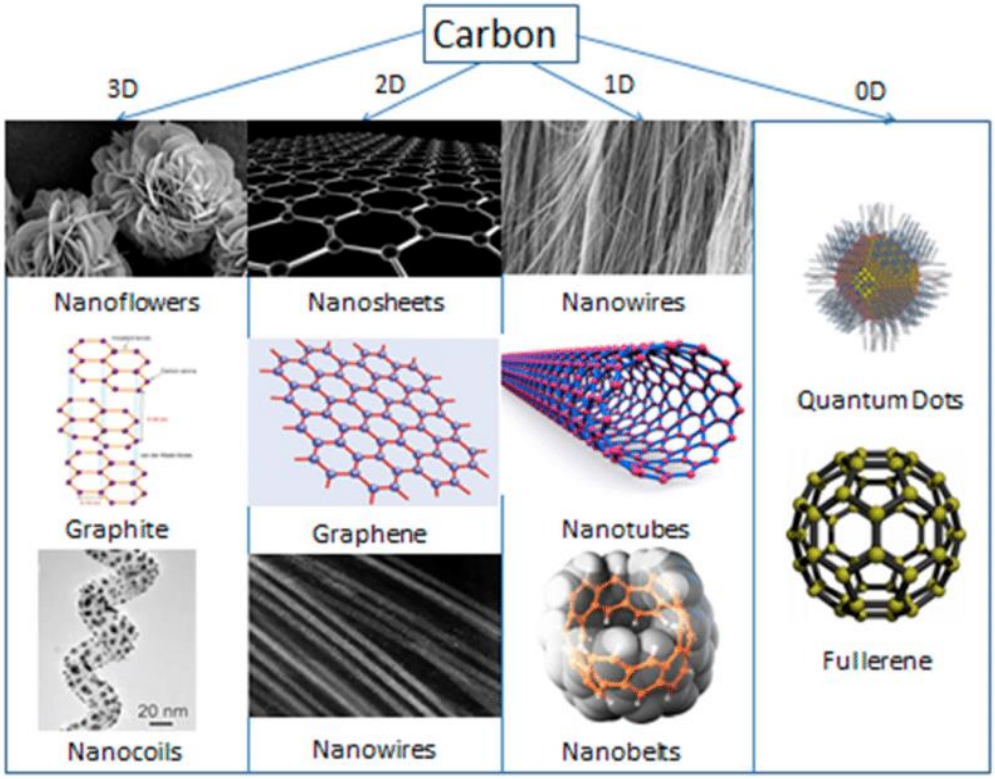

Figure 2.11 Types of carbon structures in all three dimensions [66]

2.7.2 Metal oxides and Conducting Polymers

Pseudocapacitors, which have a faradic manner of storing charges through reversible redox processes in electroactive materials, are storage devices that use electrodes made of metal oxide or conducting polymers. In addition to transition metal oxides (TMOs), which are frequently utilized for pseudocapacitors, there are also conductive polymers and transition metal nitrides (TMNs) and sulphides. For redox processes, these materials have a high working potential. Compared to an EDLC (Electrochemical double-layer capacitor), these pseudocapacitors might have a larger specific capacitance. This is because the electrode's inside as well as its surface have a role in charge storage [64]. The self-discharge of the electrodes having pseudocapacitance behaviour is less probable than that having EDLC behaviour. Metal oxide/hydroxide and conducting polymer based electrodes could be tailored using a variety of procedures. These include hydrothermal synthesis, electrochemical deposition, sol-gel technique, anodic deposition, and spray deposition [65]. These metal oxide-based electrode materials generally have the following characteristics:

- Due to their excellent electrical conductivity, allowing for fast charge/discharge times [68].
- RuO_2 has a high specific capacity, which boosts the energy storage capacity, especially in the metal oxide form [69].
- Metal oxide electrodes have also low ESR (equivalent series resistance), resulting in better power density [69].
- Metal oxides make durable electrodes because they are chemically stable and do not degrade in various chemical conditions [67].

Some metal oxides, particularly ruthenium dioxide, are expensive, which hurts production costs. Therefore some inexpensive metal based electrodes such as copper, cobalt and nickel have been searched recently. Additionally, because metal oxide pores cannot be designed or modified in any manner, they can result in undesirable flaws in the electrodes' microstructure, which might impact their short-term stability [65].

2.7.3 Composite Type Electrodes

A composite material might be used in this kind of supercapacitor to store charges between polarizable electrodes (carbon) and non-polarizable electrodes (metal

oxide or polymer) both faradic and non-faradic processes are used [68]. Carbonaceous materials could be used as electrode in high-performance hybrid supercapacitors (HSCs), and transition metals (sulphides/oxides/hydrosides) are used as electrode materials in aqueous electrolytes [64]. As a result, high energy storage can be achieved using both EDLC and pseudocapacitor-type electrodes. In comparison to other capacitor types, it could be less expensive and has superior cycle stability. These hybrid electrodes are made of composites of carbon and carbon, carbon and metal (alloy) oxide (hydroxide or sulphide), and carbon and conducting polymer [67].

Higher energy and power densities in the supercapacitor might be possible by increasing the effective specific surface area (SSA) in carbon materials. Depending on the effective specific surface area (SSA), carbon materials can attain a high capacitance in carbon-carbon composites [67]. The following properties of these carbon-carbon based composite electrode generally materials are present :

- High capacitance is obtained as the result, as more electrolyte ions may be absorbed and stored, because of the properties wide surface of carbon.
- To enable quick charge and discharge, these composite materials can effectively carry electric current [70].
- Carbon is mechanically resilient, therefore composites made of it are strong and able to resist repeated charge-discharge cycles [70].

For carbon-metal (alloy) oxide (hydroxide/sulphide) composites, the EDLC electrode, which is mostly based on carbonaceous compounds, drives the high power, while the faradic electrode is often responsible for the high capacitance and cyclic stability. Hybrid supercapacitor devices can obtain a greater working potential and a high energy density in a variety of electrolytes thanks to the combined use of both electrodes [67],[71].

These carbon-metal (alloy) oxide (hydroxide) composites based electrode materials generally have the following properties:

- These composites offer methods for both chemical and physical energy storage by combining the pseudocapacitance of metal oxides with the double-layer capacitance of carbon [68].
- These composites can have high specific capacities, due to the interaction between the high surface area of carbon and the high capacitance of metal oxides. Because the carbon components in the

composites are effective electrical conductors, electron transmission is facilitated [71].

- These composites can provide high power and energy densities because of integrated capacitance processes. Additionally, the high capacitance of metal oxides and the mechanical resilience of carbon both contribute to the long-term stability of these composites [72].

For carbon-conducting polymer composites, considering the different types of hybrid, it is considered the most promising supercapacitor electrode material. Due to its high conductivity, easy composite synthesis, and excellent energy storage capacity. However, due to swelling and shrinkage due to repeated cycles (charge/discharge process), the polymer could be susceptible to a rapid deterioration in performance. To avoid this limitation, combining the polymer with carbon materials has been proven to maximize the capacitance value as well as strengthen the stability of the polymer [66],[71].

These carbon-metal oxide composites based electrode materials generally have the following properties:

- In considering the various forms of hybrid, it is regarded as the most promising supercapacitor electrode material for carbon-conducting polymer composites, due to its high energy storage capacity, high conductivity, and ease of composite synthesis [72].

- However, the polymer is also vulnerable to a quick decline in performance due to swelling and shrinkage caused by repeated cycles (charge/discharge process) [67].

- It has been demonstrated that increasing the capacitance value and boosting the polymer's stability can both help to get over this restriction [67].

The specific properties may vary depending on the exact composition and manufacturing process of these composites. Alloy based oxide has been electrodeposited on graphite based substrate. The alloy coating is Mn-Cu based electrode and the substrate is grahite wire (1D), graphite flag (2D) and graphite fabric (3D).

CHAPTER III
EXPERIMENTAL PROCEDURES

This study's main goals are to evaluate the coating conditions applied in various parameters and examine the energy storage effects of manganese-copper alloy-based graphite film coatings. It then aims to examine the condition of coatings on graphite tape, graphite wire, and graphite fabric and compare their energy storage efficiency with appropriately optimized process data. These benchmarking studies are carried out by characterizing these electrodes, which are produced as alloy-based flexible electrodes, with electrochemical and non-electrochemical techniques.

3.1 Equipments Used in the Research

Table 3.1 presents information on the materials and devices used in the thesis and the purpose of the use of the materials. Additionally, materials used during current collector preparation and electrochemical measurements enabled the experiments to be carried out successfully.

The materials used for the graphite substrate current collector (substrate) preparation process;

- **Graphite**, Substrate to be cleaned (%99 pure),
- **Cleaning Cloth**, used to clean the graphite surface,
- **Sandpaper**, 600 microns of sandpaper is used to smooth the surface,
- **Transparent Tape**, used to cover and prepare the substrate surface,
- **Glass Rod**, Tool that helps adhere the tape to the graphite surface,
- **Multimeter**, tool that used to check the conductivity of the graphite-coated tape surface.

Table 3.1 List of Materials and Devices used in this experimental study

Material	Usage Purposes
Laboratory Scale (with ±0.0001 g precision)	Used for precise measurements to determine the accurate amount of materials.
Heating and Stirring Device (with ±3 ^{o}C precision)	Used for maintaining the desired temperature in solutions and ensuring homogeneous mixing. Essential for controlling and accelerating chemical reactions.
Thermometers	Used for measuring temperatures of solutions subjected to different processes. Essential for examining the temperature dependency of chemical reactions and optimizing reaction conditions.
Sample Weighing Containers	Disposable plastic containers are used to place the substances to be weighed.
Weighing Spatula	Used to transfer small amounts of samples to the scale, preventing direct contact with the samples and aiding in precise measurements.
Beakers	Glass containers are used for preparing chemical mixtures in desired quantities. Important for visualizing and mixing reactions.
Stirring Rods	Glass apparatuses are used to facilitate homogeneous mixing of mixtures. Improves the efficiency of chemical reactions.
Stirring Tablet Materials	Thermoset stirring apparatus that aids in the homogeneous mixing of mixtures in beakers. Enhances the effectiveness of mixing.
Drying Device	Used to accelerate the removal of water and moisture remaining on washed materials' surfaces. Ensures dry materials for precise measurements and reactions.

The materials used during electrochemical measurements are;

- **Reference Electrode**, In aqueous solutions, an electrode with a structure containing an AgCl layer covered with Ag wire and a saturated potassium chloride electrolyte in a glass body is used. In deep eutectic solvents (DESs), a silver wire is used as a direct reference electrode.
- **Counter Electrode**, Titanium coated ruthenitum mesh
- **Working Electrode,** In this study thesis, three types of working electrodes (graphite coated tape, graphite wire, and graphite knitted fabric) were used in electrochemical experiments.

3.2 Chemicals in the Experiment

The list of chemicals utilized to produce the findings in this thesis is shown in Error! Reference source not found. It is suitable for laboratory studies of chemical materials used in this thesis. The names of the chemical materials used in the studies, the purity of the chemicals, and the supplier company information are tabulated in the table.

Table 3.2 List of chemicals used during the research in this experimental study

No	Chemical Name	Purity Grade	Supplier Company
1	**Manganese (II) Chloride Dihydrate ($MnCl_2.2H_2O$)**	>%99	Merck
2	**Copper (II) Chloride Dihydrate ($CuCl_2.2H_2O$)**	>%99	Merck
3	**Choline Chloride ($HOC_2H_2N(CH_3)_3Cl$)**	>%99	Alfa Aesar
4	**Mono Ethylene Glycol**	%99	Nebioğlu
5	**Potassium Hydroxide (KOH)**	>%90	Tekkim
6	**Sodium Sulfate (Na_2SO_4)**	>%90	Merck

3.3 Preparation of Electrodes, Deep Eutectic Solvent and Electrolytes

The preparation of the graphite-coated flexible tape electrode is as follows;

- **Surface Cleaning,**

  The first step to clean the surface of bulk graphite substrate to be used is to carefully wipe the main graphite surface from which the samples will be taken with a clean napkin. This process ensures that any visible dirt, dust, or debris on the surface is removed. (Error! Reference source not found.**a**).

- **Sandpaperiing Process,**

  After the cleaning process is completed, 600 micron (mc) sandpaper is used to make the surface smoother. At this stage, the graphite surface is carefully sandpapered until it has a flat structure like a transom. In this way, the substrate surface gains a smooth and homogeneous structure. (Error! Reference source not found.**b**).

- **Taping Process,**

  After the sanding process, the graphite surface reaches a clean and flat structure. Now for basic processing, transparent tape is used to cover the substrate surface and prepare it for further processing. This tape is carefully placed on the graphite surface and the taping process is performed. (Error! Reference source not found.**c**).

- **Pre-film Formation,**

  The tape is adhered to the graphite surface by pressing lightly. This pre-bonding step ensures that the tape adheres properly to the surface.

- **Film Formation,**

  The tape is well adhered to the graphite surface. This step ensures that the tape adheres more firmly to the surface and eliminates possible air bubbles.

- **Full Film Formation,**

  Finally, the tape is completely adhered to the graphite surface, leaving no loose edges or gaps. This step allows the tape to form a tight bond with the graphite surface. (Error! Reference source not found.**d**).

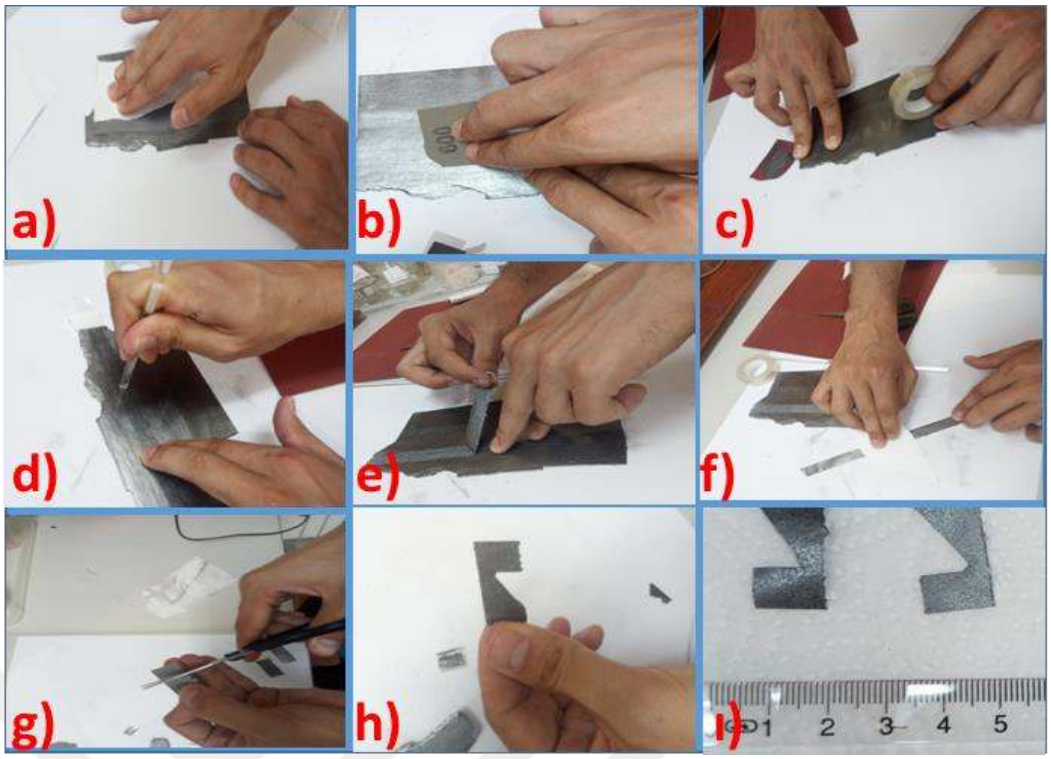

Figure 3.1 Photographs showing the preparation of flexible tape graphite substrate; a) Cleaning the surface of the graphite; b) Sandpapiring the surface of the graphite; c) Covering the substrate surface with a tape; d) adhered to the graphite surface by pressing lightly with glass rod; e) Removing thin flexible graphite film from the graphite surface; f) Homogenising the surface of the graphite tape; g) Cutting the flexible graphite tape; h) Obtaining a graphite film sample of 1 cm^2 size; ı) The obtained samples are preserved for the electrode coating test steps after quality standard control.

- **Flexible Graphit Film Production,**

  As a result of the banding process, the graphite surface is covered with tape, and a flexible graphit film is formed. This flexible graphit film is removed from the graphite surface to obtain a thin flexible substrate. (Error! Reference source not found.**e & 3.1f**).

- **Sample Collection,**

  The samples are prepared by measuring and cutting the flexible graphit coated tape (Error! Reference source not found.**g**) to the desired size (1

cm²). These samples have been used as current collector. (Error! Reference source not found.**h & 3.1ı**).

After the preparation of the graphite-coated flexible tape electrode, the next step in the experimental process is the selection and preparation of the Deep Eutectic Solvent, which is listed as follows:

- **Preparation of Deep Eutectic Solvent**

  In the initial stage, a Deep Eutectic Solvent, the Ethaline solution was prepared. The essential components for producing Ethaline are the mixture of choline chloride (ChCl) and ethylene glycol (EG).

- **Weighing of Chemical Components and Solution Preparation,**

  Initially, the ChCl (**Figure 3.2a**) and EG (**Figure 3.2b**) components were individually weighed on precision balances. In total, 100 grams of ChCl and 88 grams of EG were measured (**Figure 3.2c**). Subsequently, 88 grams of EG were transferred into a beaker, and 100 grams of ChCl were added, completing the weighing process (**Figure 3.2d**).

- **Preheat Stage**,

  First, the mixture of choline chloride (ChCl) and ehylene glycol (EG) was preheated at 70°C for 15 minutes to form the Ethaline solution (**Figure 3.2e**). The preheating phase was considered complete at 70°C (**Figure 3.2f**).

- **Mixing and Heating Stage**,

  The choline chloride (ChCl) and ethylene glycol (EG) were mixed and heated for an extended period using a heater until a homogeneous solution was achieved (**Figure 3.2g**). After approximately 60 minutes, It was confirmed, through measurements taken with a thermometer, that a homogeneous Ethaline mixture was obtained at the selected temperature (**Figure 3.2h**). At this final stage, the ionic liquid preparation process was complited by cooling the mixture to room temperature.

In summary, the Ethaline solution was initially heated to 70°C until a homogeneous structure was attained. The homogeneous Ethaline solution, achieved after approximately 60 minutes, was allowed to cool to room temperature, finalizing the ionic liquid preparation process.

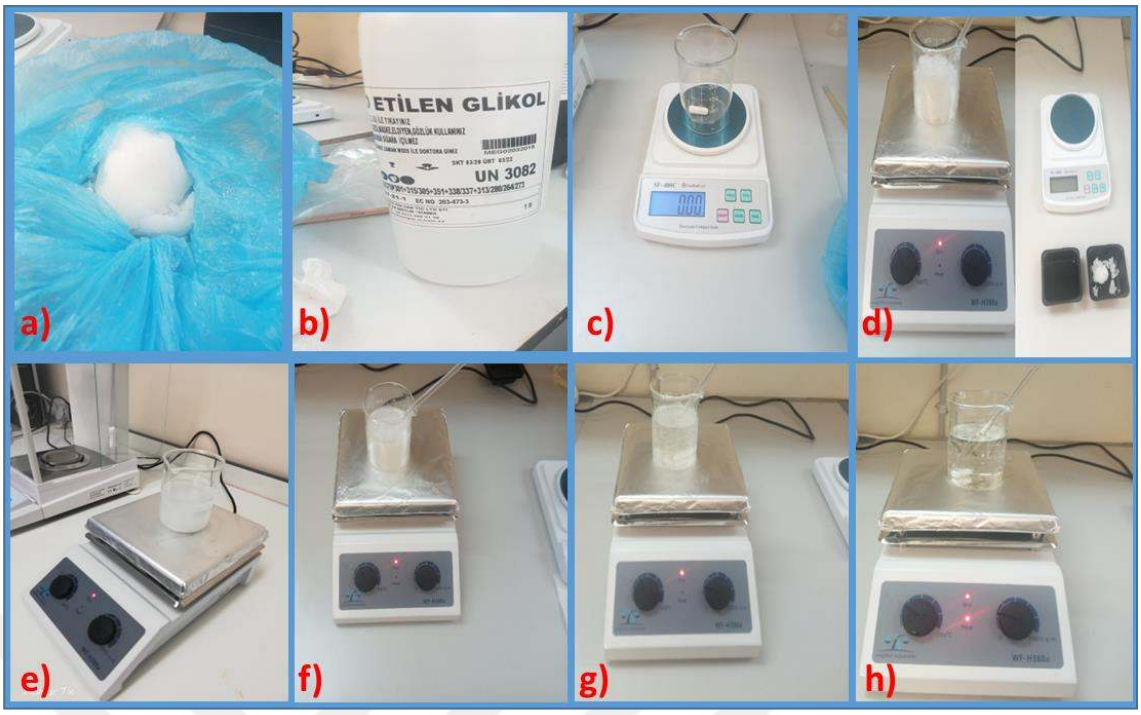

Figure 3.2 Photographs during the Ethaline preparation process a) choline chloride (ChCl); b) ethylene glycol (EG); c) Measuring all chemical materials with laboratory scale; d) Adding of 100 grams ChCl and 88 grams EG into a beaker; e) heating ethaline solution at 70 °C for 15 minutes; f) Heating the Ethaline solution with mixing until the temperature reaches approximately 70 °C; g) After 30 minutes, continuing to heating with stirring; h) After approximately 60 minutes, homogeneous Ethaline mixture was obtained.

The next step in the experimental procedure is the choice and preparation of the graphite substrate coating alloys indicated below, which comes after the preparation of the Deep Eutectic Solvent Ethaline mixture.

- **Element Selection for Electrode Modification**,

  In the electrode modification process, it was decided to employ manganese (Mn) and copper (Cu) elements for modifying the graphite substrate. These elements were found to be effective in enhancing the properties and performance of the selected coating process.

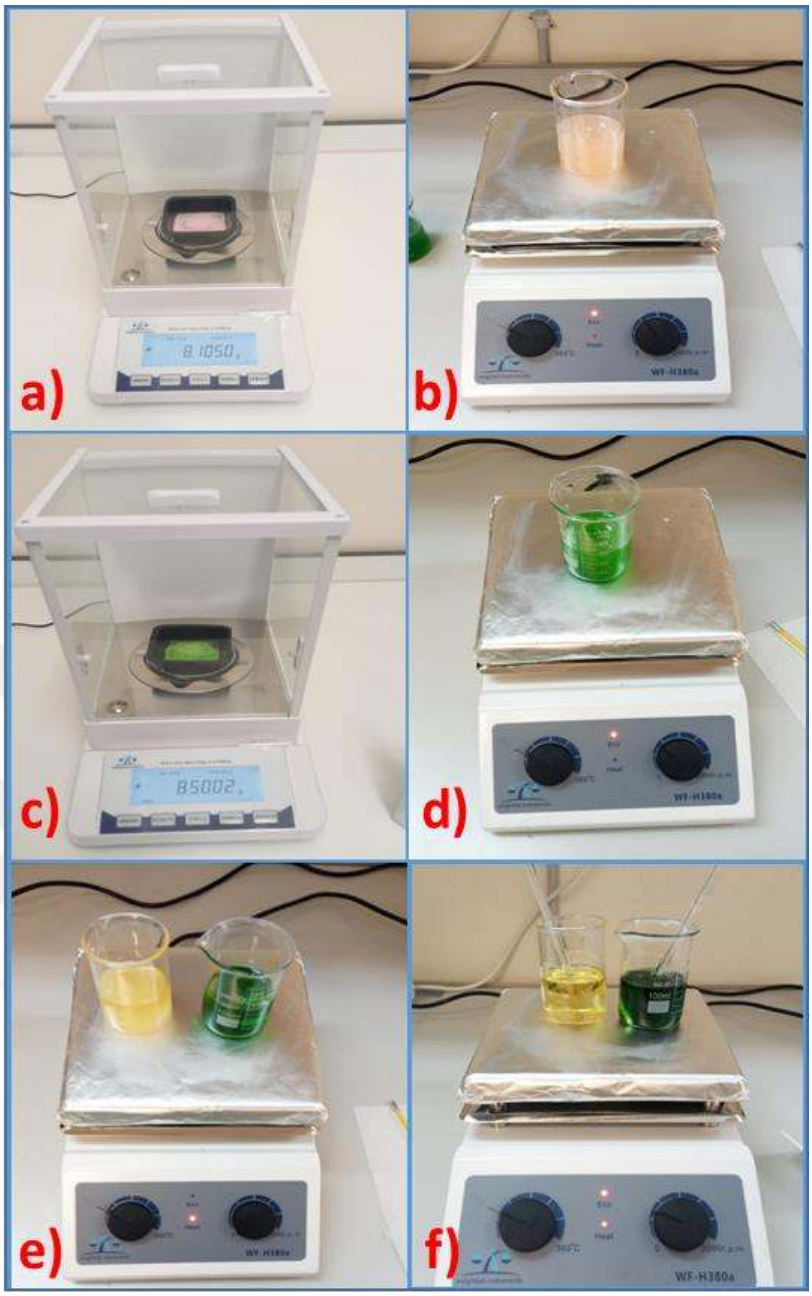

Figure 3.3 Photographs of the preparation of the growth electrolyte for coating alloys a) weighing powder of MnCl2; b) in transferred into Ethaline in; c) weighing CuCl2; d) transferred int Ethaline; e) Preheating the mixtures of MnCl2 and CuCl2; f) After approximately 60 minutes, MnCl2 and CuCl2 solutions were obtained at 60°C

- **Weighing of Chemical Components and Solution Preparation**,

  $MnCl_2$ and $CuCl_2$ powders were separately weighed on precision balances. In total, 8.1 grams of $MnCl_2$ (**Figure 3.3a**) were added to 50

mL of Ethaline solution (**Figure 3.3b**), and 8.5 grams of $CuCl_2$ (**Figure 3.3c**) were added to another 50 mL of Ethaline solution (**Figure 3.3d**). Both solutions were prepared to have a concentration of 1 M $MnCl_2$ and 1 M $CuCl_2$.

- **Preheat Stage**,

  The mixtures of $MnCl_2$ and $CuCl_2$ were preheated at 70°C for 15 minutes in separate beakers(**Figure 3.3e**).

- **Mixing and Heating Stage**,

  The $MnCl_2$ and $CuCl_2$ solutions in Ethalinewere mixed at 70°C after the heater was set, and heating continued until a homogeneous structure was achieved over an extended period. After approximately 600 minutes, the mixture temperatures were monitored with a thermometer, and the desired homogeneous structure was attained and the process was then concluded (**Figure 3.3f**).

Ethaline solutions with 1 M $MnCl_2$ and 1 M $CuCl_2$ were consequently produced separately. A new beaker was filled with an equal mixture of the two liquids. 0.5 M $MnCl_2$ + 0.5 M $CuCl_2$ mixture in Ethaline solution was obtained. Ethaline solutions containing 1 M $MnCl_2$ and 1 M $CuCl_2$ seperately and containin and the mixture of 0.5 M $MnCl_2$ + 0.5 M $CuCl_2$ in Ethaline were prepared for cyclic voltammetry process. Modified electrodes based on Mn-Cu alloys were transferred different electrolyte for scanning between two selected potentials. The final stage of the preparation of chemical solutions involves the preparation of scanning electrolyte solutions.

- **Preparation of Solution Electrolytes,**

  To prepare 1 M Na_2SO_4 electrolyte solution, 71.02 grams (0.5 moles) of Na_2SO_4 (sodium sulfate) were initially measured. Then, distilled water was used to form a total volume of 500 mL solution. The Na_2SO_4 chemical was slowly added to distilled water and water was added to complete a 500 mL solution. During this process, continuous stirring was applied to ensure the formation of a homogeneous mixture. When the sodium sulfate (Na_2SO_4) was completely dissolved in the water, a 1 M Na_2SO_4 solution was successfully obtained.

  To prepare the electrolyte solutions, we initially measured out the necessary chemicals. For the 1 M Na_2SO_4 solution, 71.02 grams (0.5 moles) of

Na_2SO_4 (Sodium sulfate) were used. Similarly, for the 1 M KOH solution, 28.05 grams (0.5 moles) of KOH (potassium hydroxide) were measured. The next step involved creating a total volume of 500 mL for each solution by using distilled water. While adding the respective chemicals to 500 mL of solution, ensuring that thorough mixing and dissolution occurred. Continuous stirring was applied throughout this process to guarantee the formation of homogeneous mixtures. Once all the sodium sulfate (Na_2SO_4) or potassium hydroxide (KOH) were completely dissolved in the water, we successfully obtained 1 M Na_2SO_4 and 1 M KOH solutions. As a final step, the equal volumes of these two solutions were mixed in a new beaker, resulting in an electrolyte solution consisting of 0.5 M KOH + 0.5 M Na_2SO_4. This meticulously prepared electrolyte solution was then ready for use in the experimental procedures.

3.4 Electrochemical Characterization of Mn-Cu Alloy Coating on Graphite Sample

In this study, flexible supercapacitor electrodes were fabricated by electrochemically depositing manganese-copper alloys onto graphite-based samples. By using various potentials, the manganese-copper alloy electrodes were put through a potentiostatic technique procedure on graphite electrodes. Both uncoated and alloy-coated electrodes' chemical, structural, and morphological characteristics were carefully examined.

The modified electrodes were then submerged in solutions containing potassium hydroxide (KOH) and sodium sulfate (Na_2SO_4), as well as solutions containing combinations of these two electrolytes in equal amounts, to reveal their electrochemical behaviors. Utilizing chronocoulometric, chronoamperometric, cyclic voltammetric, and cyclic polarisation techniques, the electrochemical properties of both pure graphite and coated graphite electrodes were examined. These attributes included capacitance calculations, stability, energy storage capabilities, and rate-limiting reactions.

3.4.1 Chronocoulometric

The chronocoulometric analysis method was used to apply -1.6 V, -1.9 V, and -2.2 V potentials to graphite-based samples in Ethaline solution containing 0.5 M $MnCl_2$

+ $CuCl_2$ at 60 °C for 150 seconds. This allowed us to determine the growth of manganese and copper alloys by electrochemical deposition on the graphite electrode. The potentiostat was controlled using a VersaSTAT 3, Princeton Applied Research model potentiostat manufactured by AMATEK Company (USA).

This research demonstrates the growth of a manganese and copper alloy on a graphite electrode over 150 seconds at potentials of -1.6 V, -1.9 V, and -2.2 V as well as the alloy's capacity and charging period. The electrochemical plating procedure can be optimized using this data to produce the optimum manganese copper alloy for graphite electrodes. Chronocoulometric results was obtained by the integration of chronoamperometry data.

3.4.2 Chronoamperometry

In the coating process of the electrodes, a mixture solution prepared in Ethaline at a concentration of 0.5 M $MnCl_2$ + 0.5 M $CuCl_2$ was used as the growth solution. This solution was heated to 60°C for electrochemical deposition. Graphite-based film, wire, and fabric samples were set as the working electrode, platinum wire as the reference electrode, and platinum part as the counter electrode.

The samples were subjected to electrodeposition with the potentiostatic method for 150 seconds at different potentials (-1.6 V,-1.9 V, and -2.2 V). The electrodeposition process was carried out by the potentiostatic method. The potentiostat was controlled using a VersaSTAT 3, Princeton Applied Research model potentiostat manufactured by AMATEK Company (USA). As a result of this process, a series of graphite-based film, wire, and fabric electrodes with Mn-Cu coating were obtained by electrodeposition at different potentials.

3.4.3 Cyclic Voltammetry

These tests were run to check how Mn-Cu-coated and bare (uncoated) graphite electrodes performed electrochemically. The VersaSTAT 3, Princeton Applied Research model produced by AMATEK Company (USA) was used to conduct cyclic voltammetry investigations in a three-electrode system.

In these tests, an Ag/AgCl reference electrode and a titanium working electrode with a platinum coating were employed in a saturated KCl solution. Because manganese is electroactive in Na_2SO_4 and copper electrode is active in KOH , it

was decided to employ, these two electrolytes with the mixture of 0.5 M KOH + 0.5 M Na_2SO_4 were used as electrolytes.

Initially, 20 scanning cycles of graphite electrodes between potential values ranging from -1.0 V to 0.5 V were performed on them at a scanning rate of 50 mV s^{-1}. While the first nine scan rates (100 mV s^{-1}, 50 mV s^{-1}, 25 mV s^{-1}) are cycled three times. Respectively, the next scan rate is two scan cycles for 10 mV s^{-1}, and finally, for a scan rate of 100 mV s^{-1}, 9 cycles were performed. The electrode surface area was kept constant as 1 cm^2.

Cyclic voltammetry plots were used to determine the most recent values for the oxidation and reduction peaks. Graphs were created also utilizing the logarithm of these values and the logarithm of the applied potential scanning rates to find rate limiting reaction. The results and comments were thoroughly explored in the study. An efficient evaluation technique would be to use these graphs to examine the electrochemical behavior of coating manganese and copper based alloys on graphite electrodes.

3.5 Non-Electrochemical Characterization of Mn-Cu Alloy Coating on Graphite Sample

The performance of flexible electrodes, a crucial field of study for the fabrication of energy storage technologies, has been the main emphasis of this experiment study. Samples of graphite with coatings of manganese and copper based film are crucial materials that would be examined in the construction of these electrodes. In this context, characterization methods such as X-ray diffraction (XRD), Fourier Transform Infrared Spectroscopy (FTIR), and scanning electron microscopy (SEM) have been employed. XRD was utilized to analyze the crystallinity of the electrodes, FTIR provided insights into their compositional structure, and SEM allowed for the observation of surface morphology.

These methods have made it possible to examine the composition, structural characteristics, and surface morphology of the manufactured flexible electrodes in great detail. The characterization results have given important insights into these electrodes' design and performance optimization. This discovery provides a basic step that will provide insight into subsequent research projects aimed at advancing the development of flexible electrodes.

3.5.1 X-Ray Diffractometer (XRD) Analysis

Compared to UV radiation, X-rays are higher intensity, more frequent, and have shorter wavelengths. These characteristics, which resemble the guiding parameters of crystals, demonstrate how X-rays may be used to examine the crystal structure of matter.

The XRD characterisation was obtained using the Automate II XRD instrument, which was made in Japan by the Rigaku Company. By aiming X-rays at the samples, the XRD apparatus gauges the strength of the rays that are reflected. These data lead to the analysis of intensity peaks, which helps identify variations in crystal structure. The samples were subjected to 1.54 Å X-rays from the CuKα source, and the samples were examined within a 2°–80° angle range.

Mn-Cu modification coatings obtained to the graphite surface of the samples at different voltage values were analyzed. The purpose of obtaining these results was to ascertain the modifications in the electrodes' crystal structure. It has offered vital information for comprehending the characteristics, performance, and crystal formations of electrodes.

3.5.2 Fourier Transform Infrared Spectroscopy (FTIR) Analysis

Fourier Transform Infrared Spectroscopy (FTIR) uses the infrared region of the electromagnetic spectrum. By the absorption and emission process of infrared light directed towards the sample, it acquires a wide range of data at high resolution. It is capable of analyzing solids, liquids, and gases in this way. In this study, Vertex 70v model Fourier transform infrared spectroscopy (FTIR) of the United States-based Bruker Company was used in the characterization of bare graphite and Mn-Cu alloy-coated graphite electrodes.

In the experiment, a coating process of 150 seconds was applied at voltage values of -1.6, -1.9, and -2.2 V at 60 °C, respectively, and at the end of this process, the obtained samples and uncoated graphite were subjected to FTIR analysis, infrared rays were sent to them and the transmission of these rays from the surface was recorded. The obtained data were then presented and analyzed in graphs.

It is a crucial instrument for researching the existence and crystal structure of Mn-Cu alloy on the electrode surface, in particular. In this experiment, the chemical compositions of the electrodes and the efficiency of the coating process were

assessed using the findings of FTIR spectroscopy analysis. The stability and caliber of the coating process are largely determined by this analysis procedure.

CHAPTER IV
RESULTS AND DISCUSSION

To fully comprehend the electrochemical characteristics of electrodes and electrolytes, this extensive study includes the application of a variety of electrochemical techniques, such as the potentiostatic method, cyclic voltammetry, and cyclic polarization. These methods offer insightful information regarding the electrochemical processes occurring inside the system as well as the chemical reactions taking place on electrode surfaces during cycling (charging-discharging).
Likewise, this study goes beyond electrochemical analyses by incorporating non-electrochemical methods. In this study X-ray Diffraction (XRD), Fourier Transform Infrared Spectroscopy (FTIR), and Scanning Electron Microscopy (SEM) techniques were used for investigating the compositional, structural, and morphological features of manganese-copper-based electrodes.

4.1 Growth of Manganese-Copper (Mn-Cu) Coating on Graphite

A series of comprehensive studies are set to focus on the utilization of manganese-copper (Mn-Cu) coated flexible graphite sheets for energy storage devices, alongside the fabrication of flexible electrodes through manganese and copper coated graphite filaments. The alloy coating was electrodeposited on flexible graphite films, graphite wires, and graphite fabrics.
These graphite samples are coated and examined by the potentiostatic method in an in-Ethaline solution containing 0.5 M $MnCl_2$ + 0.5 M $CuCl_2$ by applying -1.9 V at 60 ^oC for 150 seconds. Next, the graphite substrates (working electrode) are subjected to the cyclic voltammetry method to reveal if Mn-Cu could be coated on the selected surface. The core objective of this study is to understand the usability Mn-Cu film on graphite electrodes, thereby enhancing the surface properties of the electrodes.
Mn-Cu modified electrodes, based on graphite coated tapes, neat graphite wires, and graphite fabric, have been prepared as substrates. However, the optimization of plating conditions, particularly electroplating potentials, emerges as a requisite for

the effective growth of Mn-Cu alloys. Consequently, meticulous scrutiny was directed toward the growth conditions of the electrodes, and then resulting in obtaining the suitable electrocoating potentials.

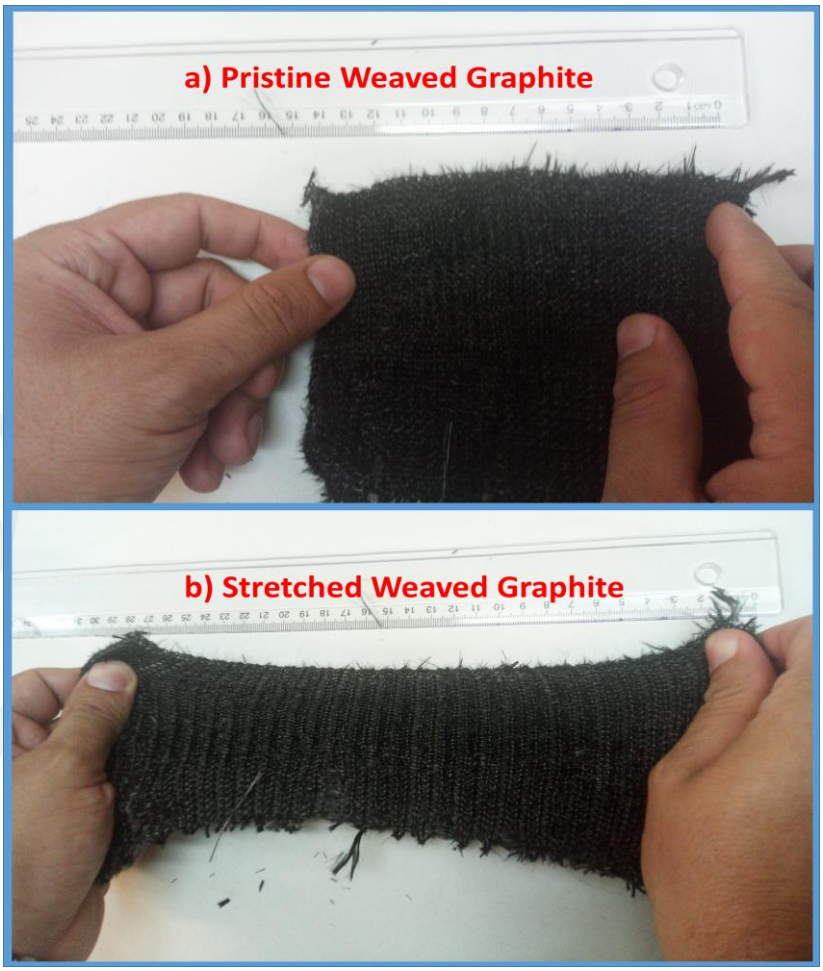

Figure 4.1 Photograph of a) pristine knitted graphite fabric and b) stretched form of the same fabric.

This comprehensive study involves the application of various electrochemical techniques such as the potentiostatic method, cyclic voltammetry, and cyclic polarization to unravel the electrochemical properties of the electrodes and electrolytes. Moreover, it encompasses non-electrochemical investigations (including XRD, FTIR, and SEM) that provide insights into the structural and electrochemical behaviors of the electrodes.

The fact that the graphite-based fabric structure has a three-dimensional (3D) (**shown in Figure 4.1**) structure is advantageous in terms of increasing the surface area of the flexible electrodes and optimizing the capacitance values. However, since a more controlled environment is required for electrochemical

characterization, it seems appropriate to also use the two-dimensional (2D) structure of graphite in cyclic voltammogram experiments. This approach was considered an important step to better understand the electrochemical behavior of the electrode surface.

Consequently, in this section, the growth conditions required for the application of Mn-Cu coatings to graphite electrodes are analysed.The electrochemical and nonelectrochemical properties of the electrodes has been examined. These results have the potential to develop more efficient electrode materials for flexible energy storage devices in the future.

The findings from the literature review and the experimental results shown in **Figure 4.2** make it clear that the factor of electrolyte composition offers an advantage for electrochemical operations. With the help of the graphs in **Figure 4.2,** we can better understand how composition affects the electrochemical processes by showing how it may help to reveal the probable potential for alloy coating.

The cyclic voltammetry method has been used to explore and characterize the behavior of metal ions, including manganese, copper, and their mixed ions, in electrochemical reactions. In electrochemical reactions, it has been found that the composition could influence the redox reaction of the Ethaline.

To better understand the electrochemical behavior of the electrodes, a thorough analysis of the growth conditions necessary for the deposition of Mn-Cu coatings onto graphite electrodes has been carried out. These findings demonstrate how the composition influences the formation of electrode materials.

Red line in Figure 4.2.a is cyclic voltammogram responses of graphite in Ethaline including Cu^{2+} ions. Oxidation and reduction of copper is observed at around -0.5 V. Redox reactions of Mn^{2+} have been observed (see green line of Figure 4.2.a). Reduction of Mn starts at around -1.5 V which could be associated to the growth of Mn.

These peaks do not belong to graphite electrode as black line in Figure 4.2.b which is cyclic voltammogram of graphite in pure Ethaline do not illustrate redox peaks.

Oxidation and reduction peaks of Ethaline having both ions (Cu^{2+} and Mn^{2+}) appears (see blue line of in Figure 4.2.b). The application of potential less than 1.5 V could cause the growth of Mn-Cu alloy.

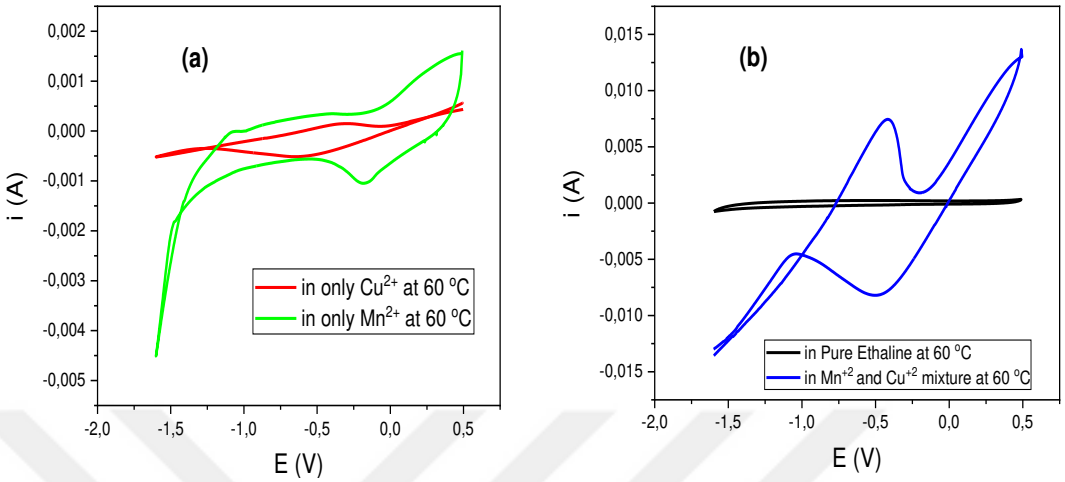

Figure 4.2 Cyclic voltammogram results of bare graphite in a) Ethaline having $CuCl_2$ (red line) and Ethaline having $MnCl_2$ (red line) and; b) pure Ethaline (black line) and Ethaline having both $CuCl_2$ and $MnCl_2$ (blue line). The scan rate and temperature of the experiments are 50 mV s^{-1} and 60 °C.

The chronoamperometry method was employed for electrodeposition of manganese and copper metals onto graphite tapes, graphite wires, and graphite fabrics. This electrochemical process was achieved using AMATEK Company's (USA) VersaSTAT 3 potentiostat (Princeton Applied Research model potentiostat presented in **Figure 4.3**).

During the growth electrochemical processes, counter and reference electrodes of platinum and silver wire were respectively utilized **(Figure 4.3b, c,d)**. When the modified electrodes were cycled in aqueous solutions, the reference electrode was changed as silver/silver chloride electrode.

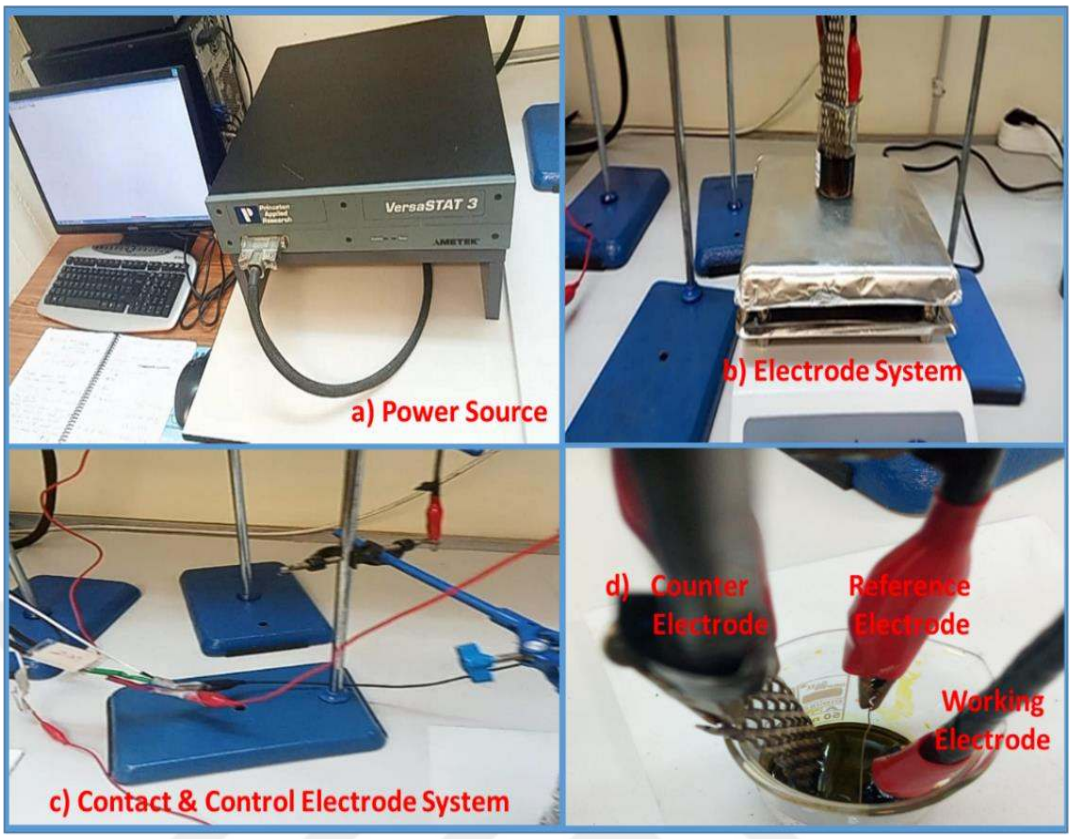

Figure 4.3 Photograph of a) AMATEK Company's (USA) VersaSTAT 3 potentiostat; b) electrochemical electrode process system; c) contact and control electrode system; d) counter, reference, and working electrodes of platinum, silver wire, and graphite substrate.

First of all, the mixture solution was allowed to be heated at 60 °C for 180 minutes, in an Ethaline deep eutectic solvent solution containing 0.5 M Mn^{+2} and 0.5 M Cu^{+2}. Afterward, graphites having 1 cm^2 area were immersed in Ethaline deep eutectic solvent solution containing 0.5 M Mn^{+2} and 0.5 M Cu^{+2}. Graphite surface coating of manganese and copper alloy was achieved by these electrochemical processes carried out for 150 seconds at -1.6 V, -1.9 V and -2.2 V potentials, respectively. Graphite based substrates which were used as working electrode are demonstrated in **Figure 4.4**.

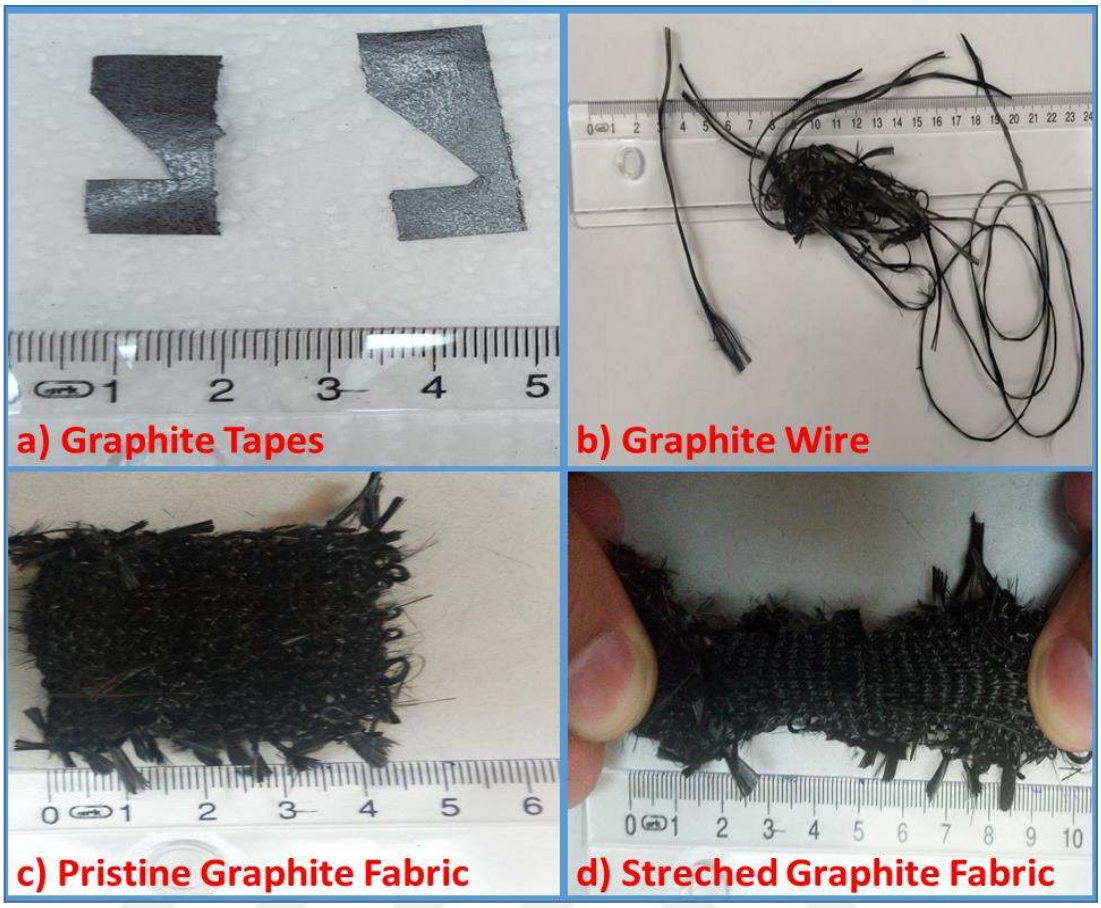

Figure 4.4 Photograph of a) graphite tape; b) graphite wire; c) pristine graphite fabric and; d) stretched graphite fabric

The data in **Figure 4.5** show how manganese and copper metals are coated on a sample of graphite tapes, graphite wires, and graphite fabrics (**Figure 4.4**) by the electrodeposition process and how the current density changes over time. In particular, the results in **Figure 4.5a, b, and c** display that the current density of the electrodeposition process increased for 60 seconds, but almost stabilized after a certain time. This indicates that the graphite surface area of the manganese and copper alloy decreases over time and therefore the coating speed decreases. The results illustrate that the electrochemical coating process takes place gradually and the coating speed stabilizes when a certain thickness is reached.

In line with this information, it helped us to understand how manganese and copper metals could be coated on different graphite forms by electrodeposition process and to understand the electrochemical properties of the obtained coatings. It also

allowed us to observe our accuracy in the time stability of the current density of the electrodeposition at certain potentials.

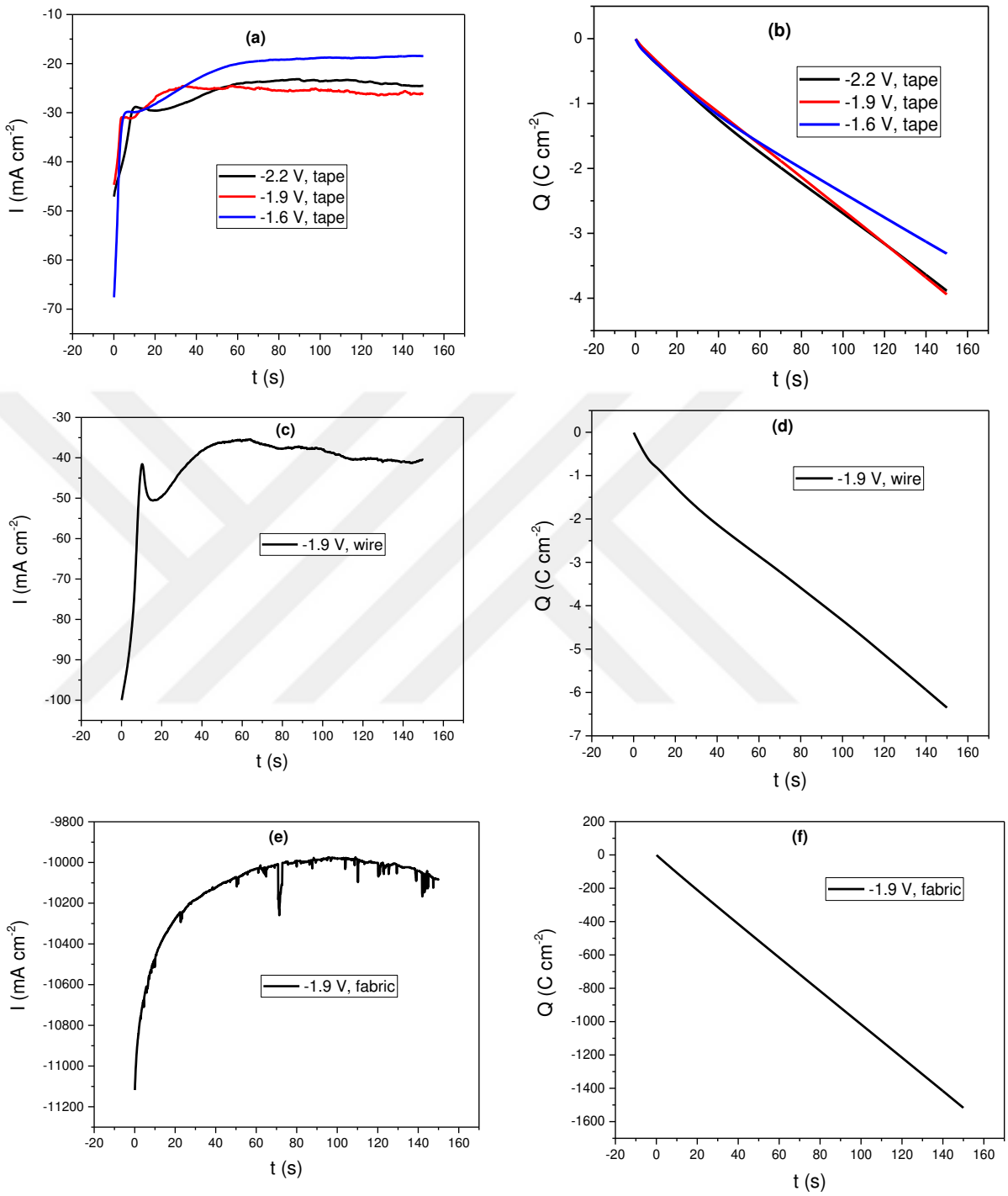

Figure 4.5 The chronoamperometry and chronocoulometry responses of Mn-Cu growth at 60 ^{o}C for 150 seconds a) chronoamperometry data of Mn-Cu alloy growth on graphite coated tape by application of -2.2 V (black line), -1.9 V (red line) and -1.6 V

(blue line). b) chronocoulometry data of the growth given in panel a. c) Chronoamperometry results of the alloy on graphite wire by application of -1.9 V. d) chronocoulometry data of the growth given in panel c. e) Chronoamperometry responses of the alloy on graphite fabric by application of -1.9 V. f) chronocoulometry data of the growth given in panel d. The electrodeposition bath is Ethaline having 0.5 M Mn^{2+} and 0.5 M Cu^{2+}

On the other hand, it displays chronocoulometric data of the electrochemical deposition of a manganese-copper-based layer on the graphite electrode in **Figure 4.5b, d, and f.** According to this graph data, the charge change will be accordingly a stabilized line over time if the current flux approaches a constant value with time. This shows that the electrochemical reaction has reached equilibrium and the current is stable.

It is known that the current graph expresses the change in the amount of charge (coulomb) carried in a certain time, for this reason, over time, a constant current results in a steady build-up of charge. When the current is high, the charge accumulation starts quickly and then increases more quickly over time. This indicates that the electrochemical process is proceeding steadily and that the current does not change with time.

4.1.1 XRD Results of Mn-Cu Alloy Deposited Graphite Substrate

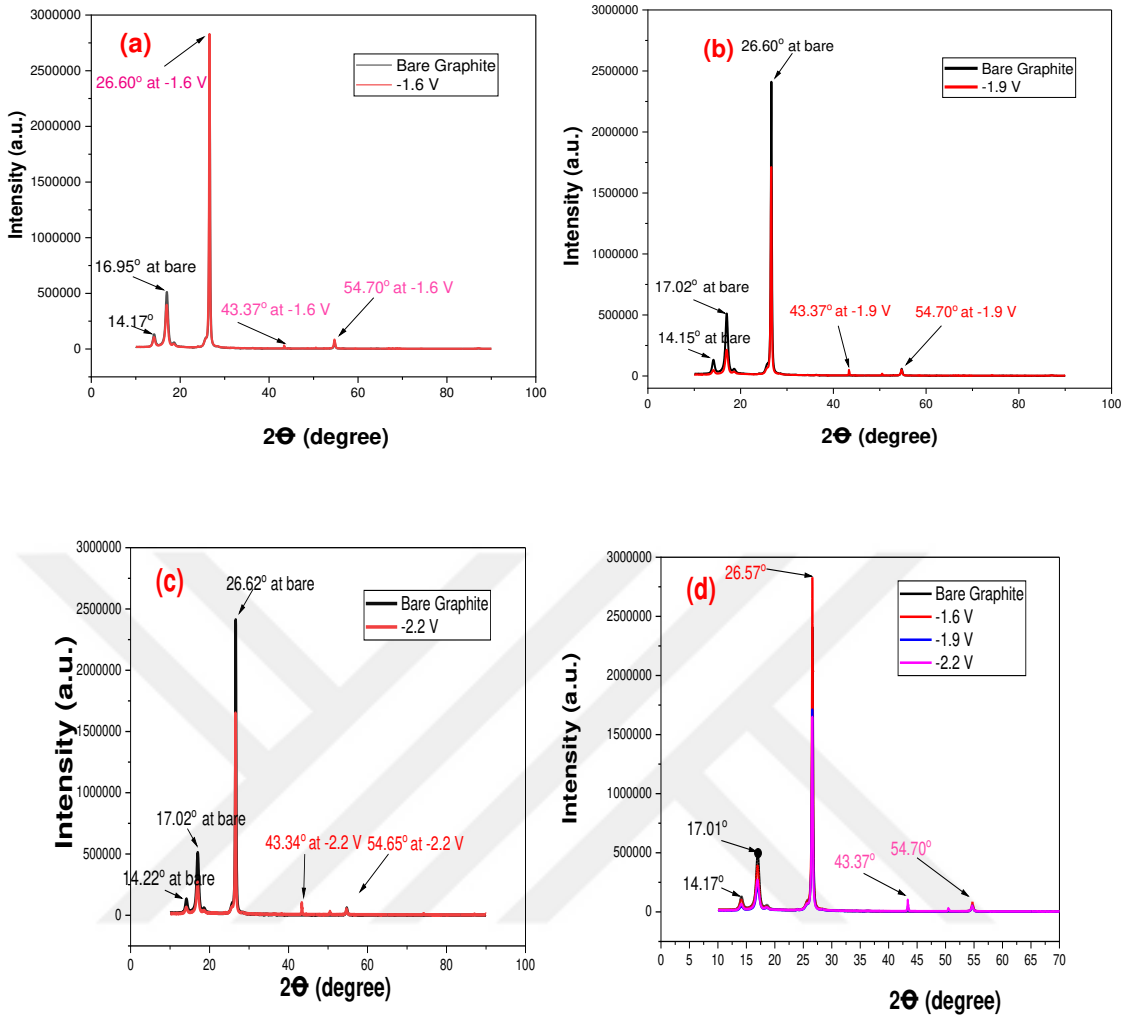

Figure 4.6 The plot of XRD results of **(a)** at -1.6 V for manganese and copper film-coated graphite electrodeposited in Ethaline deep eutectic solvent for 150 seconds at 60°C (red line) and uncoated graphite (black line); **(b)** at -1.9 V for manganese and copper film-coated graphite electrodeposited in Ethaline deep eutectic solvent for 150 seconds at 60°C (red line) and uncoated graphite (black line); **(c)** at -2.2 V for manganese and copper film-coated graphite electrodeposited in Ethaline deep eutectic solvent for 150 seconds at 60°C (red line) and uncoated graphite (black line);**(d)**) at -1.6 V (red line), at -1.9V (blue line), at -2.2 V (pink line) and uncoated graphite (black line)

The different XRD peaks between Mn-Cu alloy-coated and uncoated graphite samples are shown **in Figure 4.6.** In the case of pure graphite, a distinct peak at around 2θ = 26.5° and a smaller peak at 2θ = 54.5° are observed. Therefore, the XRD yield of bare graphite is observed at 26.57° with a distinct peak (**Figure 4.6a**). This (black line in **Figure 4.6a**) is known to be the basic peak of bare graphite [17], [79]. These peaks correspond to the (002) and (004) planes, with d-spacing values of approximately 3.5 Å and 1.9 Å, respectively. These results emphasize the integrity of the graphite structure by reflecting the distinctive XRD pattern of bare graphite [17], [79]. Furthermore, literature surveys have shown that the XRD patterns of copper and graphite have different peak reactions due to their distinct crystal structures. Peak positions for pure graphite are approximately 26.5°, 43–45°, 56°, and 77°, whereas peak positions for copper are roughly 44°, 53°, and 74°. Additionally, fundamental peak positions for manganese can be observed at approximately 37° [80]–[83].

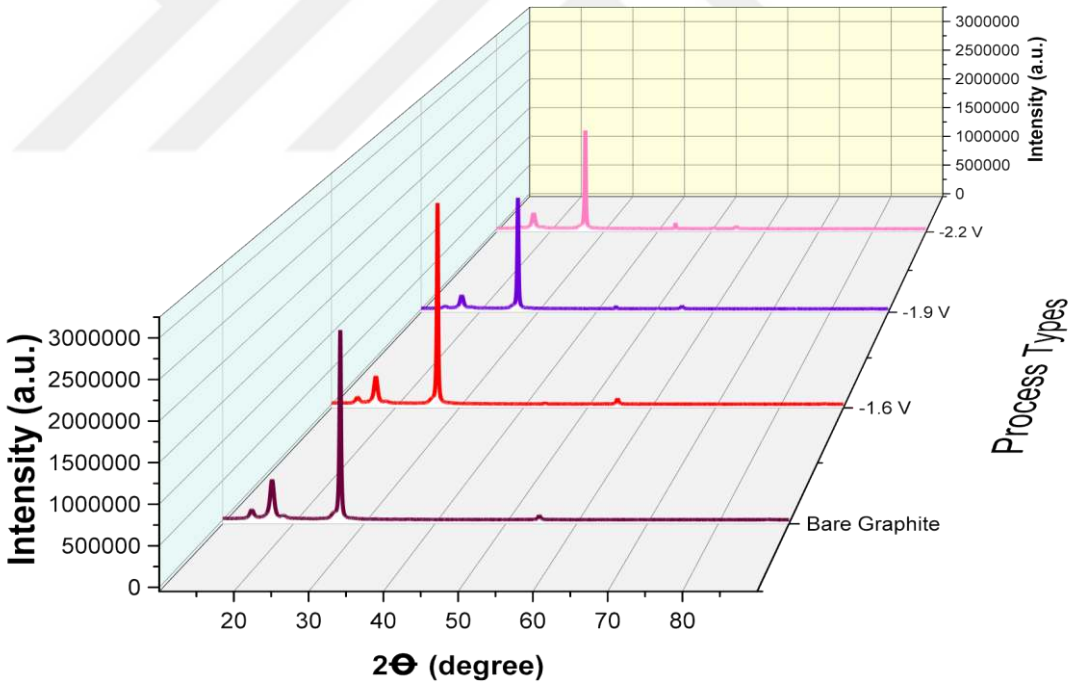

Figure 4.7 The 3D plot of XRD results for manganese and copper film-coated graphite electrodeposited in Ethaline deep eutectic solvent for 150 seconds at 60°C at -1.6 V (red line); at -1.9V (blue line); at -2.2 V (pink line); and uncoated graphite (black line)

When graphite samples coated with Mn-Cu alloy are subjected to XRD analysis at various voltages, smaller sharp peaks than bare graphite have been observed at approximately 2θ = 14.2°, 17.0°, 43.3°, and 54.6°. The presence of Mn-Cu alloys and different occurred such as Mn, Cu metal or alloy structure may be suggested by these peaks. Whereas, these smaller peaks, closely resemble the XRD pattern of pure graphite (this can be seen by examining the 3D graph in **Figure 4.7**), demonstrating that the coating procedure substantially conserved the basic crystal structure of graphite [17].

Moreover, the XRD results of Mn-Cu alloy-coated graphite have shown a decrease in peak intensity when graphite is coated. Particularly, the peak intensity at 14° and 17° for Mn-Cu alloy coatings obtained at -1.6, -1.9, and -2.2 V is lower than that of bare graphite (this can be seen by examining the 3D graph in **Figure 4.7**). This shows that the coating procedure changed the graphite surface, producing XRD results that were different from what would have happened with bare graphite. These findings highlight the possible influence Mn-Cu alloy coatings may occur on the surface of graphite [82],[83].

4.1.2 FTIR Results of Mn-Cu Alloy Deposited Graphite Substrate

The results of the Fourier Transform Infrared Spectroscopy (FTIR) analysis that was performed to improve the characterization of Mn-Cu alloy coated and uncoated graphite electrodes are shown in **Figure 4.8**. These findings could be used for understanding the chemical composition and structure of the electrodes. No significant peak rise-drop formation is observed in bare graphite.

However, a drop peak development is observed at approximately 1700 cm^{-1} (**Figure 4.8a**). **Figure 4.8b** shows that prominent peaks are formed on the electrode due to the deposition of Mn-Cu alloy on the surface of the graphite electrode at -1.6 V potential. At the same time, fluctuating peaks between 1750 and 1100 cm^{-1} are observed (**in Figure 4.8b**). As the electrodes grow with more negative deposition potentials, this peak becomes more dominant and sharper.

In addition, with a potential of -1.9 V (**Figure 4.8c**), a peak formation between 3300-3500 cm^{-1} is sharply observed in the support electrode where the Mn-Cu alloy

is electrochemically deposited. At a potential of -2.2 V (**Figure 4.8d**), the same peak is observed in the range of 3000-1800 cm^{-1}. **Figure 4.8c** and **Figure 4.8d** of the FTIR spectra graph display a significant resemblance to the results at potentials of -1.9 V and -2.2 V. **Figure 4.8e** would make this more clear. This similarity indicates that the coating process is relatively stable, and similar coating results can be obtained even under different experimental conditions.

In other words, even if different potentials have been applied, the coating process is quite consistent in terms of chemical composition and produces similar results. This shows that the Mn-Cu coating method is dependable and repeatable, making it appropriate for obtaining consistent outcomes under different application circumstances. Mn-Cu based cotings on graphite were transferred to aqueous solutions.

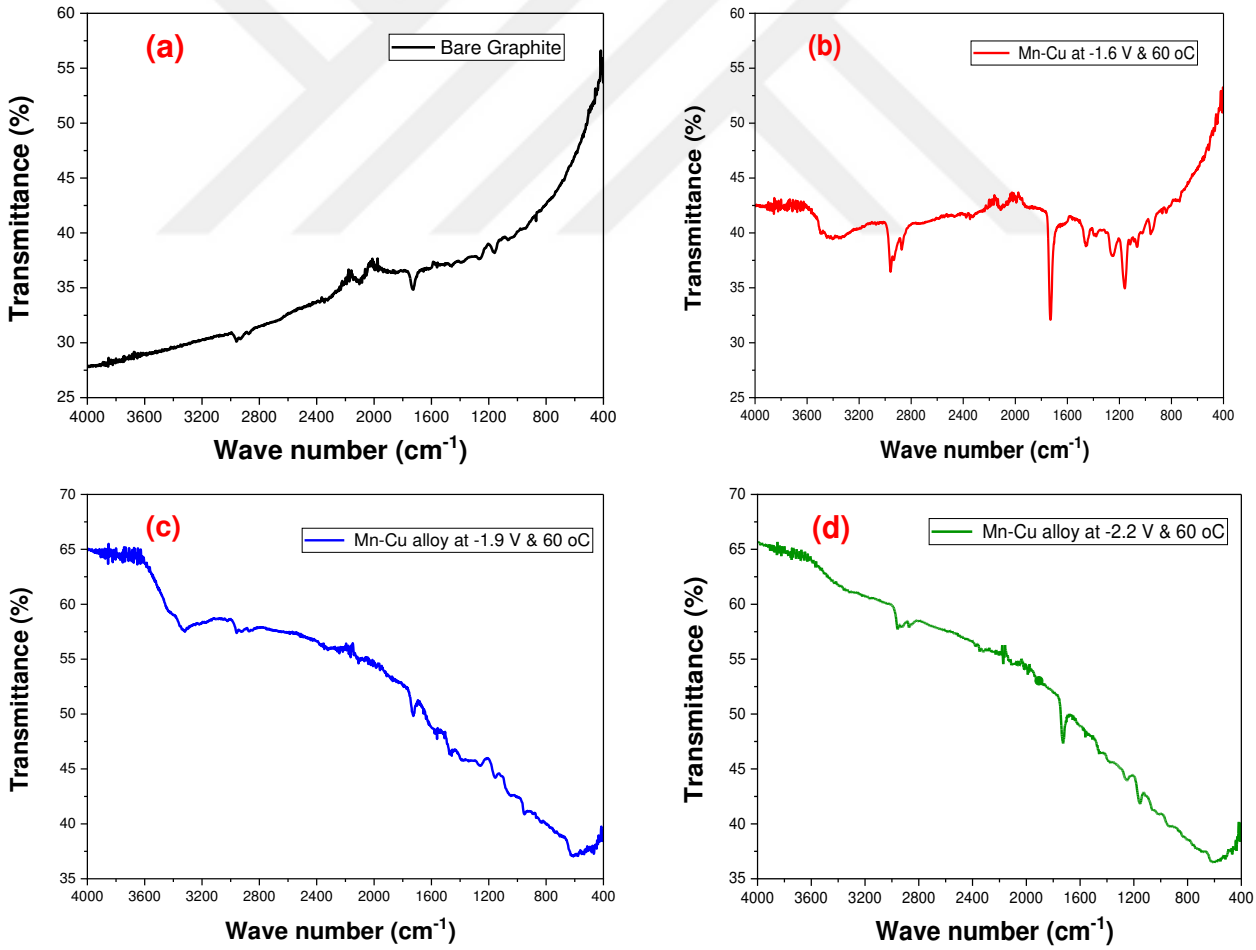

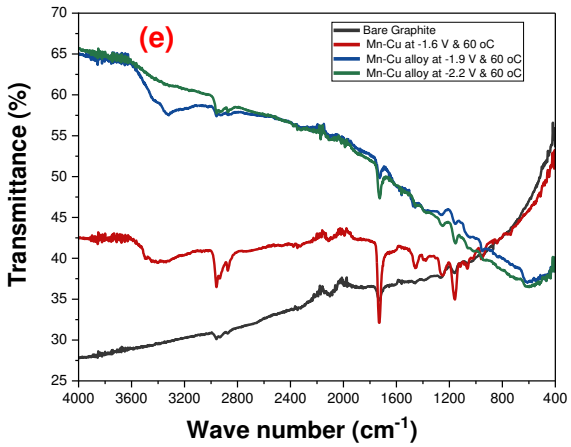

Figure 4.8 FTIR spectroscopy results of a) bare graphite; b) Mn-Cu alloy coated on graphite at -1.6 V & 60 ^{o}C; c) Mn-Cu alloy coated on graphite at -1.9 V & 60 ^{o}C; d) Mn-Cu alloy coated on graphite at -2.2 V & 60 ^{o}C; e) The comparison of all electrodes

4.2 Characterisation of the Alloys on Flexible Graphite

4.2.1 Mn-Cu Electrodeposited by Application of -1.6 V

In the initial stage, graphite surfaces were coated with Mn-Cu films by under a constant potential of -1.6 V using a solution containing 0.5 M Mn^{+2} and 0.5 M Cu^{+2} ions in Ethaline deep eutectic solvent. This process enabled the deposition of metal alloys onto the graphite surfaces. Then, the electrodes were immersed in different electrolyte liquids determined as 1 M Na_2SO_4 and 1 M HCl in the range of -1 to 0.5 V with the same scanning rate.

Cyclic voltammetry tests were performed at the same scanning rate to examine their electrochemical behavior. Upon evaluating the results of the cyclic voltammetry tests, as depicted in **Figure 4.9a, c** the current density in the HCl based electrolyte decreases upon cycling and reduction-oxidation peaks become stable after tens of cycling and current ranged from -0.5 mA cm^{-2} to +0.5 mA cm^{-2}. Additionally, in the Na_2SO_4 electrolyte, this value corresponds to peaks within the range of -4 mA cm^{-2} to +1 mA cm^{-2}.

The current graph is stable meaning that this electrolyte could be used for cycling in the area of energy storage devices. Moreover, upon reviewing **Figure 4.9b, d**, it became evident that the cyclic stability of HCl acid was lower compared to that of

Na_2SO_4 electrolyte, and cyclic stability did not establish quickly. Therefore, we concluded that HCl acid is not suitable for electrochemical tests.

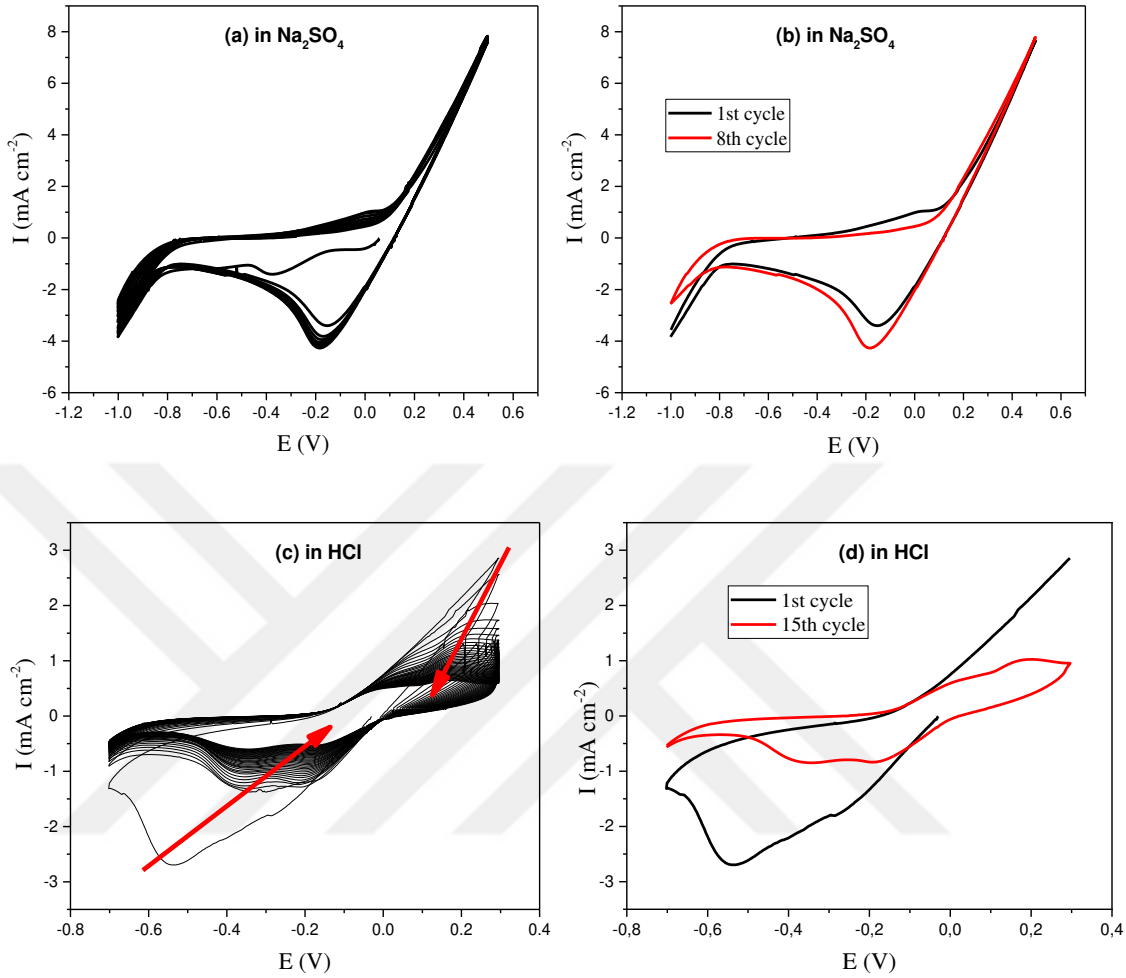

Figure 4.9 a) The cyclic voltammetry responses of Mn-Cu alloys cycling in 1 M Na_2SO_4. b) 1st and 8th cycle of Mn-Cu alloy in 1 M Na_2SO_4. c) Cyclic voltammetry responses of Mn-Cu alloys cycling in 1 M HCl. b) first and 15th cycle of Mn-Cu alloy in 1 M HCl. The electrodes were electrodeposited by application of -1.6 V in Ethaline containing Mn^2 and Cu^{2+} ions.

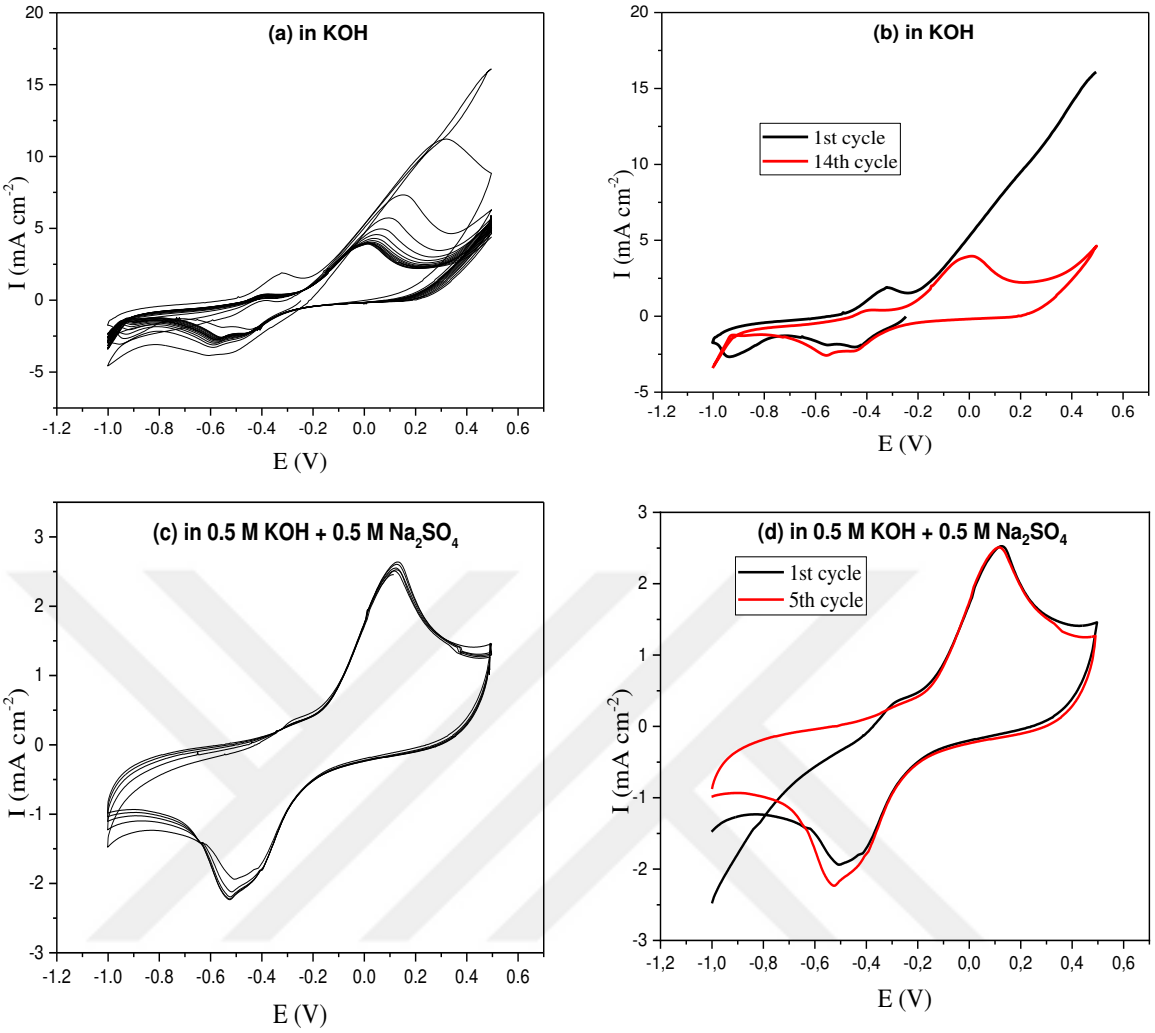

Figure 4.10 a) The cyclic voltammetry responses of Mn-Cu alloys cycling in 1 M KOH. b) 1st and 14th cycle of Mn-Cu alloy in 1 M KOH. c) cyclic voltammetry responses of Mn-Cu alloys cycling in 0.5 M Na_2SO_4 + 0.5 M KOH. d) 1st and 5th cycle of Mn-Cu alloy in 0.5 M Na_2SO_4 + 0.5 M KOH. The electrodes were electrodeposited by application of -2.2 V in Ethaline containing Mn^2 and Cu^{2+} ions

Furthermore, with insights gained from the results of cyclic voltammetry tests conducted in various electrolytes, an important role of electrolyte selection in influencing electrochemical properties and energy storage capacity have been discovered. The coating process, which was carried out by applying a potential of -2.2 V to the graphite surfaces by using Ethaline deep eutectic solvent solution containing 0.5 M Mn^{+2} and 0.5 M Cu^{+2}, was completed. Then, cyclic voltammetry tests were performed in the potential window range of -1 to 0.5 V, at the same

scanning speed. **Figure 4.10** illustrated the decrease of current upon cycling. However, the current responses evolves and become stable. **Figure 4.10c** illustrates the area under the current-voltage curve of the mixing electrolyte is higher than that of the other electrolyte. **Figure 4.10c** confirms that the mixed electrolyte is a more efficient option in terms of charge storage capacity.

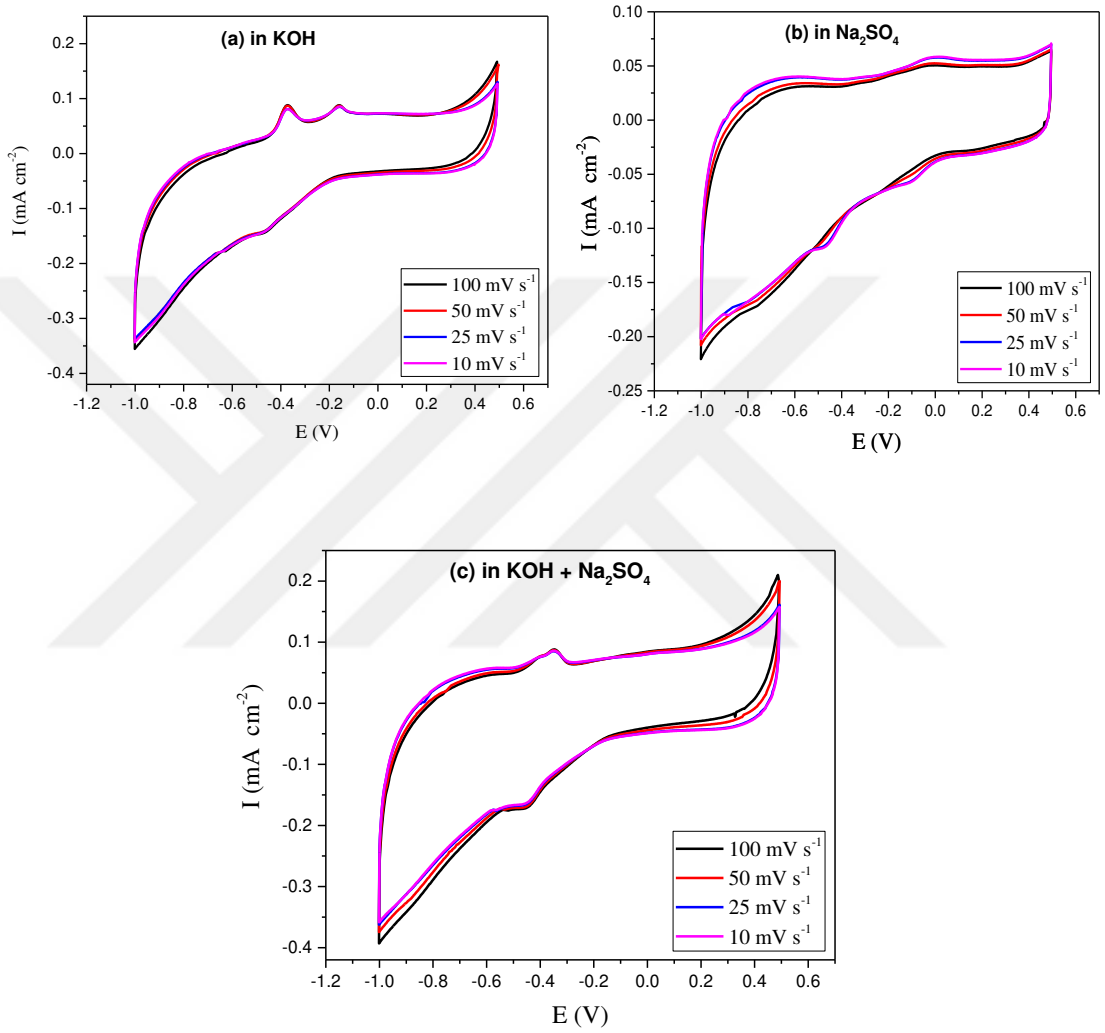

Figure 4.11 The cyclic voltammograms of bared graphite tape in a) 1 M KOH; b) 1 M Na_2SO_4 and; c) 0.5 M KOH and 0.5 M Na_2SO_4

Figure 4.11 shows cyclic voltammogram of bare graphite in three different electrolytes. Bare graphite tapes have been used in a variety of investigations to better understand their electrochemical characteristics. This series of studies' main goal was to learn how to the role of scan rates on the surface of bare graphite and analyze its electrochemical behavior under diverse circumstances.

Different electrolyte solutions were used to better understand the electrodes' electrochemical characteristics. These solutions included 1 M KOH and 1 M Na_2SO_4 as well as the combination of 0.5 M KOH and 0.5 M Na_2SO_4. Additionally, different scan rates (100 mV/s, 50 mV/s, 25 mV/s, and 10 mV/s) were used while adjusting the electrode potential within the range of -1 V to 0.5 V.

According to the results of the experiments, it was observed that the current density in the electrolyte corresponded to reduction-oxidation peak points varying between -0.3 mA cm^{-2} and +0.1 mA cm^{-2}. These findings indicate that electrochemical reactions take place on the electrode surface and can vary under different electrolyte conditions. It can be observed from the graphs in **Figure 4.11a, b, and c** that the results are not significantly impacted by the different scan rates. It demonstrates that regardless of the scanning rate, electrochemical reactions take place on the electrode surface in a consistent manner. These results provide important insights into comprehending the electrochemical properties of uncoated graphite tapes.

To determine the effects of different solution compositions and voltage levels on the electrochemical performance of Mn-Cu coatings and approach optimal values, a preliminary study was conducted. In this preliminary study, processes were carried out using different solutions with varying compositions and concentrations, such as KOH, Na_2SO_4, and 0.5 M KOH + 0.5 M Na_2SO_4, employing three uniform voltage levels (-1.6, -1.9, and -2.2 V) for each solution. In this case, consistent voltage levels were applied for each solution. As a result of these processes, it was observed that the coating had a significant impact on the electrochemical performance of the electrodes (**in Figure 4.12**). Particularly, in processes conducted within 1 M KOH, 1 M Na_2SO_4, and 0.5 M KOH + 0.5 M Na_2SO_4 mixed solutions, it was noted that the different voltage levels (-1.6, -1.9, and -2.2 V) did not yield the same. As can be seen in **Figure 4.12**, the cyclic voltammogram responses of the alloy-based coatings were examined by comparing the current values of bare graphite and Mn-Cu coated graphite in the solutions of 1 M KOH, 1 M Na_2SO_4, and the mixture of 0.5 M KOH + 0.5 M Na_2SO_4. The current value given by bare graphite in three solutions is approximately 0.4 mA **(in Figure 4.11a, b, c)**. Mn-Cu coated graphite has been observed to provide around 4 mA in 1 M KOH solution **(in Figure 4.12a)** and about 6 mA in 1 M Na_2SO_4 solution **(in Figure 4.12b)**. However, the current value generated by Mn-Cu coated graphite tapes at a potential of -1.9 V in a

mixture of solution of 0.5 M KOH and 0.5 M Na_2SO_4 was calculated to be around 6.5 mA (**in Figure 4.12c).**

As a result of the cyclic voltammogram data, it was observed that the electrochemical performance of Mn-Cu-coated graphite was significantly higher compared to that of bare graphite. In this context, it was determined that the optimal operating voltage was -1.9 V, and it was planned to continue the experiments using three different solvents. These experiments is important steps toward further optimizing the electrochemical performance.

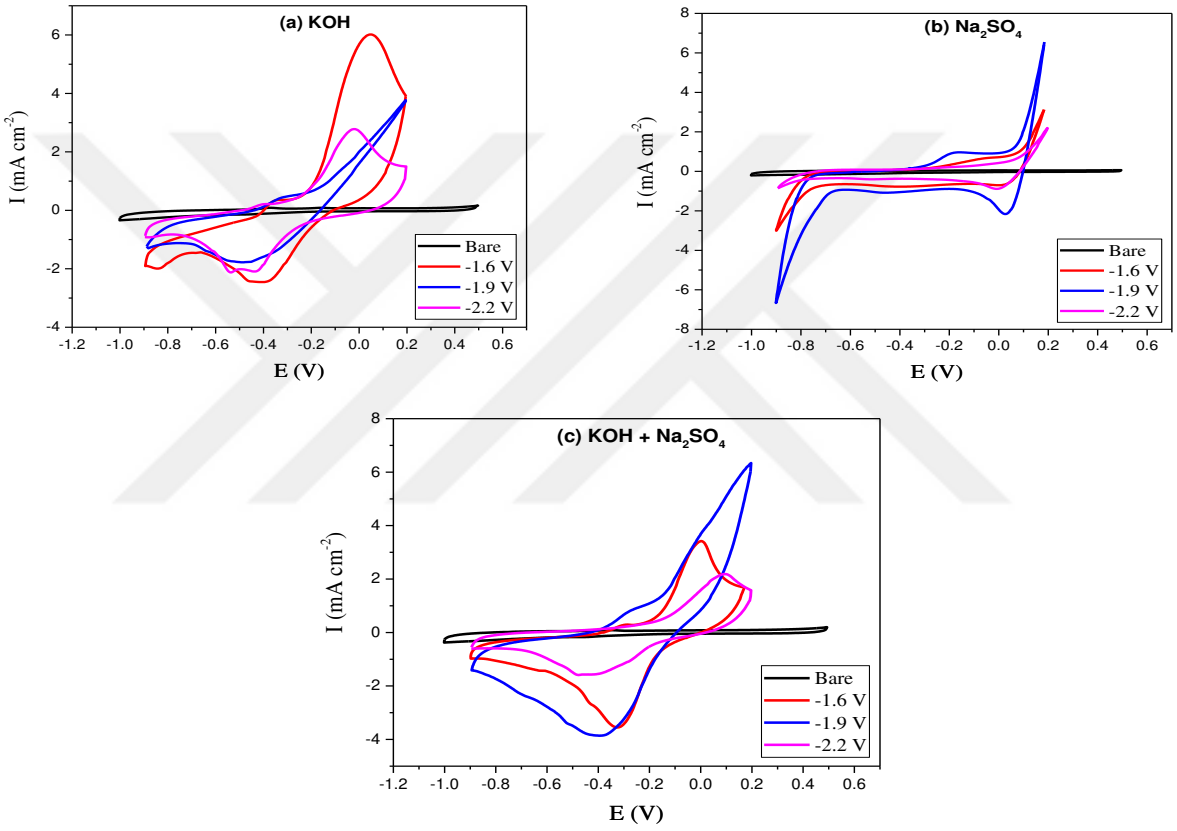

Figure 4.12 The cyclic voltammogram results of all types of graphite films cycled a) in 1 M KOH (v = 50 mV s^{-1}). b) 1 M Na_2SO_4 (v = 50 mV s^{-1}). c) 0.5 M Na_2SO_4 + 0.5 M KOH (v = 50 mV s^{-1})

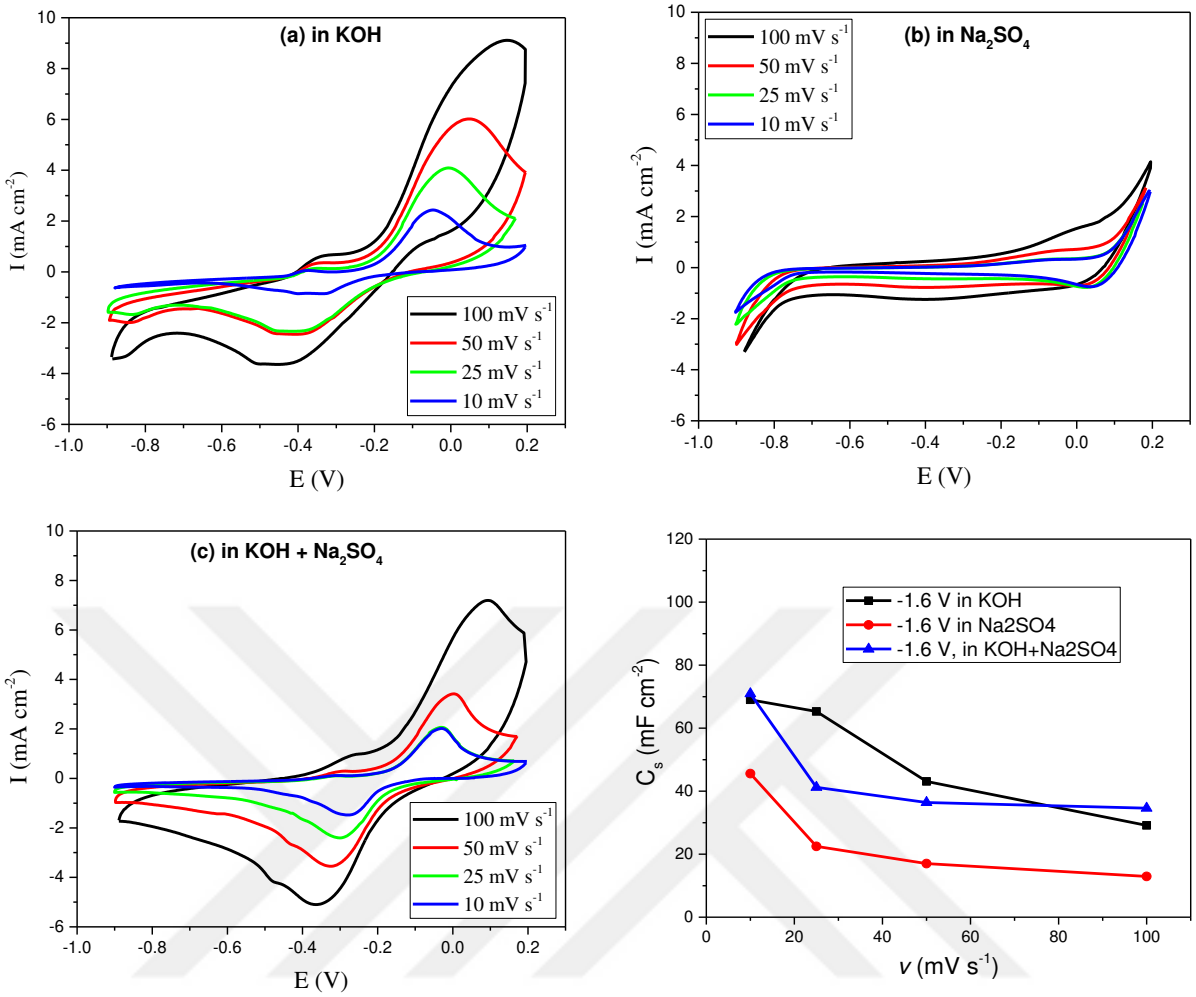

Figure 4.13 The cyclic voltammetry data Mn-Cu coated from Ethaline Deep Eutectic Solvent on graphite by application of -1.6 V and now cycling in a) 1 M KOH; b) 1 M Na_2SO_4 and; c) an electrolyte consisting of 0.5 M KOH and 0.5 M Na_2SO_4. The scan rates are given in the panels. d) Plot of the area capacitance of the electrodes given in panel a, panel b, and panel c depending on scanning speed.

Figure 4.13 is obtained when the experiment was carried out by taking Mn-Cu coated graphite samples obtained by applying -1.6 V potential using Ethaline Deep Eutectic Solvent. Then, the samples were subjected to cyclic voltammetry experiments in three different electrolyte solutions (1 M KOH, 1 M Na_2SO_4, and 0.5 M KOH + 0.5 M Na_2SO_4) with electrode potentials ranging from -0.9 V to 0.2 V. Different scan rates (100 mV/s, 50 mV/s, 25 mV/s, and 10 mV/s) were used for these studies. To improve the interpretation of the experimental results, the experiment's goal is to analyze the data through comparison analysis. This study includes a comparative analysis process to better understand the electrochemical

performance of the Mn-Cu-coated flexible graphite and to examine its interaction properties with the electrolyte. Upon analyzing the cyclic voltammetry graph in **Figure 4.13,** the electrochemical behavior of Mn-Cu-coated samples in different electrolytes was observed. Particularly, at a scan rate of 100 mV/s, the current density values in **Figure 4.13a** and **4.13c** are found to be between -3 and 8.5 mA cm^{-2} and between -5 and 7 mA cm^{-2}, respectively. Furthermore, the cyclic voltammetry curve of **Figure 4.13c** exhibits a more effective result in terms of the area under the curve compared to **Figure 4.13a**. This indicates that the electrolyte of **Figure 4.13c** enhances electrochemical performance by utilizing a greater surface area for enhanced storage capacity.

All graphs in **Figure 4.13** show the increase in the current density of Mn-Cu alloys obtained at different electrode potentials with the increase in scanning speed. These observations explain that the current density in electrochemical reactions is a reflection of the rate of charge transfer. As the scanning speed increases, the amount of charge transfer per unit time increases, increasing current density. The data shown in **Figure 4.13b**, however, also show a distinct scenario. Current density maxima are observed in this figures at -3 and 3 mA cm^{-2}. Comparatively to **Figure 4.13a** and; **4.13c**, this figure's area under the curve is noticeably smaller. This implies that the electrolyte in **Figure 4.13b** has less storage capacity and electrochemical capacity than the covered surfaces of the other samples.

As a result, it can be observed from the comparisons between **Figure 4.13a, 13b,** and **13c** that the electrochemical behavior varies according to the scan rate and electrolyte conditions. These findings offer important information about how Mn-Cu-coated graphite tapes operate electrochemically in various electrolytes. Furthermore, these experiments represent significant steps toward optimizing the electrochemical properties and performance of the coated layers. These findings pave the way for further advancements in tailoring the electrochemical behavior of coated graphite surfaces.

The specific capacitance (C) is generally expressed using the following formula:

$$C = \frac{2}{A \cdot \Delta V} \int \frac{I \, dV}{v} \qquad (4.1)$$

Where:

- C is the specific capacitance (F cm^{-2}),
- I represents the current density (A cm^{-2}),
- ΔV stands for the potential difference (V),
- v signifies the scan rate (mV s^{-1}),
- A is the area of active materials of the working electrode (cm^2)

Specific capacitance refers to the amount of charge stored on an electrode surface during an electrochemical process. The scanning rate, on the other hand, indicates the speed of the electrode potential in voltammetry experiments. Referring to **Figure 4.13d**, the relationship between specific capacitance and scan rate is inversely proportional. That is, as the scanning speed increases, the specific capacitance decreases.

Table 4.1 Specific capacitance values of Mn-Cu coated graphite tapes electrodeposited at -1.6 V potential depending on the varying scanning rates in different electrolyte solutions

Scan Rate (mV s^{-1})	**Specific Capacitance in KOH (mF cm^{-2})**	**Specific Capacitance in Na_2SO_4 (mF cm^{-2})**	**Specific Capacitance in KOH + Na_2SO_4 (mF cm^{-2})**
100	29	13	35
50	43	17	36
25	65	23	41
10	69	46	71

The same conclusion may be drawn about this by looking at the experimental data in **Table 4.1**. At higher scan rates (e.g., 100 mV/s), the measured specific capacitance value in the KOH electrolyte is 29 mF cm^{-2}. As the scan rate decreases (e.g., 10 mV/s), the specific capacitance value increases, and reaching 69 mF cm^{-2}. This indicates that slower scan rates (higher time scale) allow for greater charge storage capacity on the electrode surface.

Similarly, under Na_2SO_4 electrolyte, increasing the scan rate leads to lower specific capacitance values. The capacitance value starts at 13 mF cm^{-2} at 100 mV/s scan rate and increases to 46 mF cm^{-2} at 10 mV/s scan rate. This trend suggests that lower scan rates result in higher capacitance values under Na_2SO_4 electrolyte. The trend is consistent when a combination of both electrolytes (KOH + Na_2SO_4) is used. The capacitance value starts at 35 mF cm^{-2} at higher scan rates (e.g., 100 mV/s) and increases to 71 mF cm^{-2} at lower scan rates (e.g., 10 mV/s). In conclusion, decreasing the scan rate allows for more charge storage on the electrode surface, leading to higher capacitance values. Moreover, different electrolyte solutions (KOH, Na_2SO_4, and KOH + Na_2SO_4) exhibit similar trends, with capacitance values increasing as the scan rate decreases.

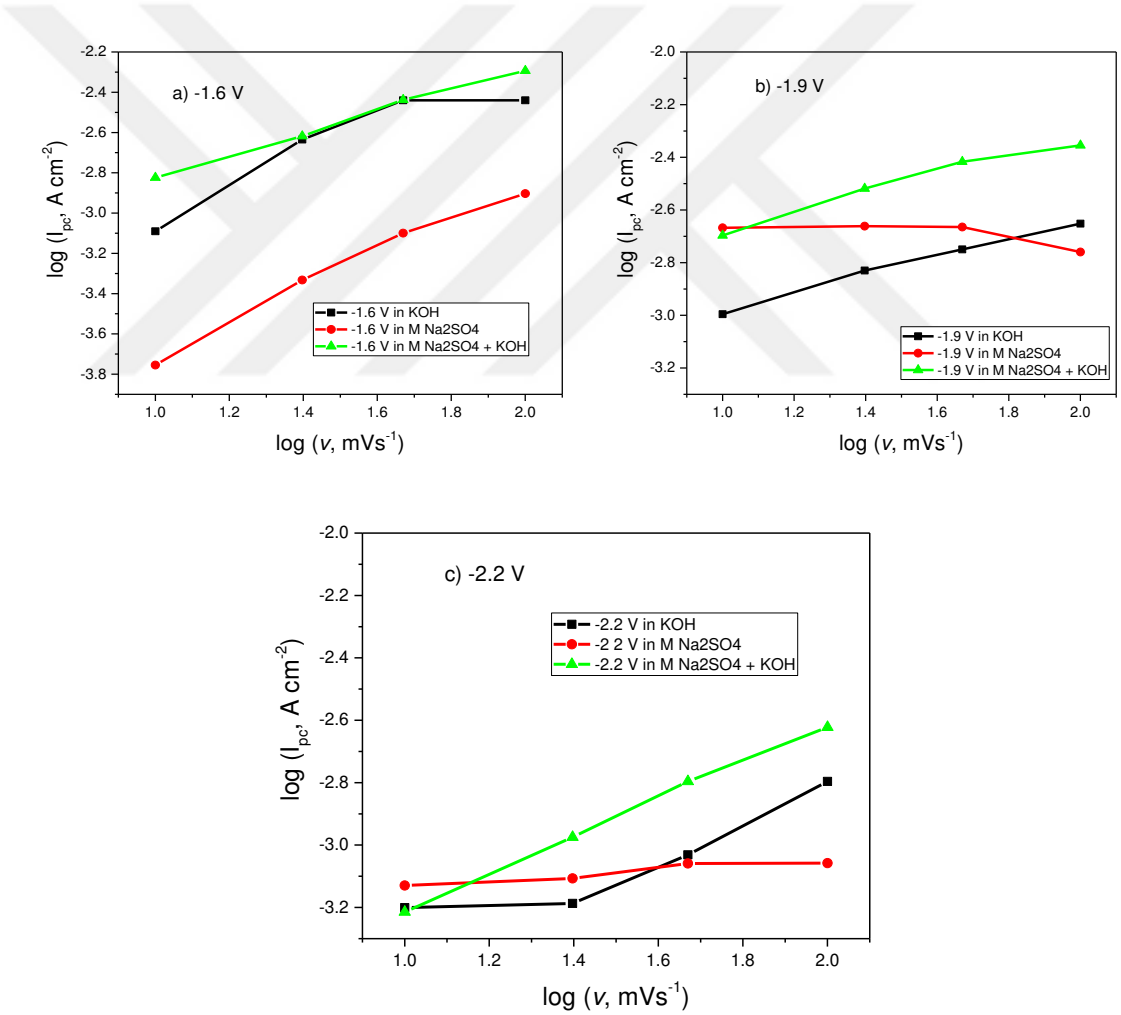

Figure 4.14 Plot of logarithm of current againes logarithm of scan rate (logi vs logv) for reduction of Mn-Cu electrodes obtained in Ethaline deep eutectic solvent by applying a) -1.6 V; b) -1.9 V and; c) -2.2 V. The

cycling electrolyte of electrodes is aqueous KOH (black line), Na_2SO_4 (red line), and a mixture of Na_2SO_4 and KOH

The reaction mechanism between electrodes and electrolytes could be controlled by electron transfer and/or mass transport. The limiting reaction (kinetic-controlled or diffusion-controlled) could give information related to the usefulness of the electrochemical system (electrodes and electrolytes) in specific applications. The limiting reaction can be obtained by using Cottrell Equation (4.2). The Cottrell equation is expressed as follows:

$$i=n*F*A*C_{\infty}*\left(\sqrt[2]{\frac{D}{\pi*t}}\right) \qquad (4.2)$$

Where:

- i, current (Amperes)
- n, the number of electrons transferred in the electrochemical reaction
- F, Faraday's constant (Coulombs per electron)
- A, electrode surface area (cm^2)
- C_{∞}, initial concentration of the electrochemical species in the solution (mol/cm^3)
- D, diffusion coefficient (cm^2/s)
- t, time (seconds)

Table 4.2 The equation between the logarithm of reduction peak current and the logarithm of scan rate deduced from Figure 4.14

Growth Potential	KOH	Na_2SO_4	Na_2SO_4 + KOH
-1.6 V	y = -0.21x – 2.1	y = -0.28x – 2.6	y = -0.18x – 2.1
-1.9 V	y = -0.11x – 2.5	y = 0.028x – 2.8	y = -0.11x – 2.2
-2.2 V	y = -0.14x – 2.7	y = -0.026x – 3.0	y = -0.20x – 2.4

The values of current peaks and the scan rate for the modified electrodes were obtained from reduction peaks of electrodes cycled in KOH, Na_2SO_4, and the mixture of these two electrolyte given in **Figure 4.13a, b, and c,** respectively. As the oxidation peaks of the Mn-Cu electrode in Na_2SO_4 electrolyte (**Figure 4.13c**)

are not clear, only their reduction peaks were considered to identify and compare the rate-limiting reactions between electrodes and the electrolytes. The equation between the logarithm of reduction peak current and the logarithm of scan rate deduced from

Figure 4.13a, b, and c is presented in Error! Reference source not found.. The Cottrell equation could be summarised that the logarithm of the current peak and the logarithm of the square root of the scan rate are linear for diffusional controlled reactions. However, the logarithm of the current peak and the logarithm of the square root of the scan rate for all Mn-Cu electrodes electrodeposited from Ethaline is less than 0.5. This indicates that the rate-limiting reaction of Mn-Cu-modified electrodes is not a diffusional controlled mechanism. [84]–[86]

4.2.2 Mn-Cu Electrodeposited by Application of -1.9 V

When comparing **Figure 4.15** to **Figure 4.13,** a distinct difference in the data obtained from the common electrolytes is observed. For instance, in **Figure *4.15***, the current density values at a scan rate of 100 mV/s generally range between -2 and 4 mA cm^{-2} on average. These values decrease as the scan rate decreases. Notably, the current density values in **Figure *4.15*.b**, are comparatively lower. In the Na_2SO_4 electrolyte, the current density values vary between -1 and 7 mA cm^{-2}. Furthermore, in the 1 M KOH + 1 M Na_2SO_4 electrolyte, the values span from -4 to 8 mA cm^{-2}.

If making the graphs attention to **Figure 4.13,** , the current density values range between -3 and 8 mA cm^{-2} for KOH electrolyte. In the Na_2SO_4 electrolyte, these values span between -1 and 4 mA cm^{-2}. In the 1M KOH + 1M Na_2SO_4 electrolyte, the values fluctuate between -5 and 7 mA cm^{-2}. At a scan rate of 100 mV/s, a specific capacitance of 12 mF cm^{-2} is attained while utilizing the KOH electrolyte. This outcome is consistent with the finding that the specific capacitance rises when the scan rate drops (**as shown in Table 4.3**). Inferred from this is that slower scan rates enable more favorable surface reactions and efficient charge transfer processes.

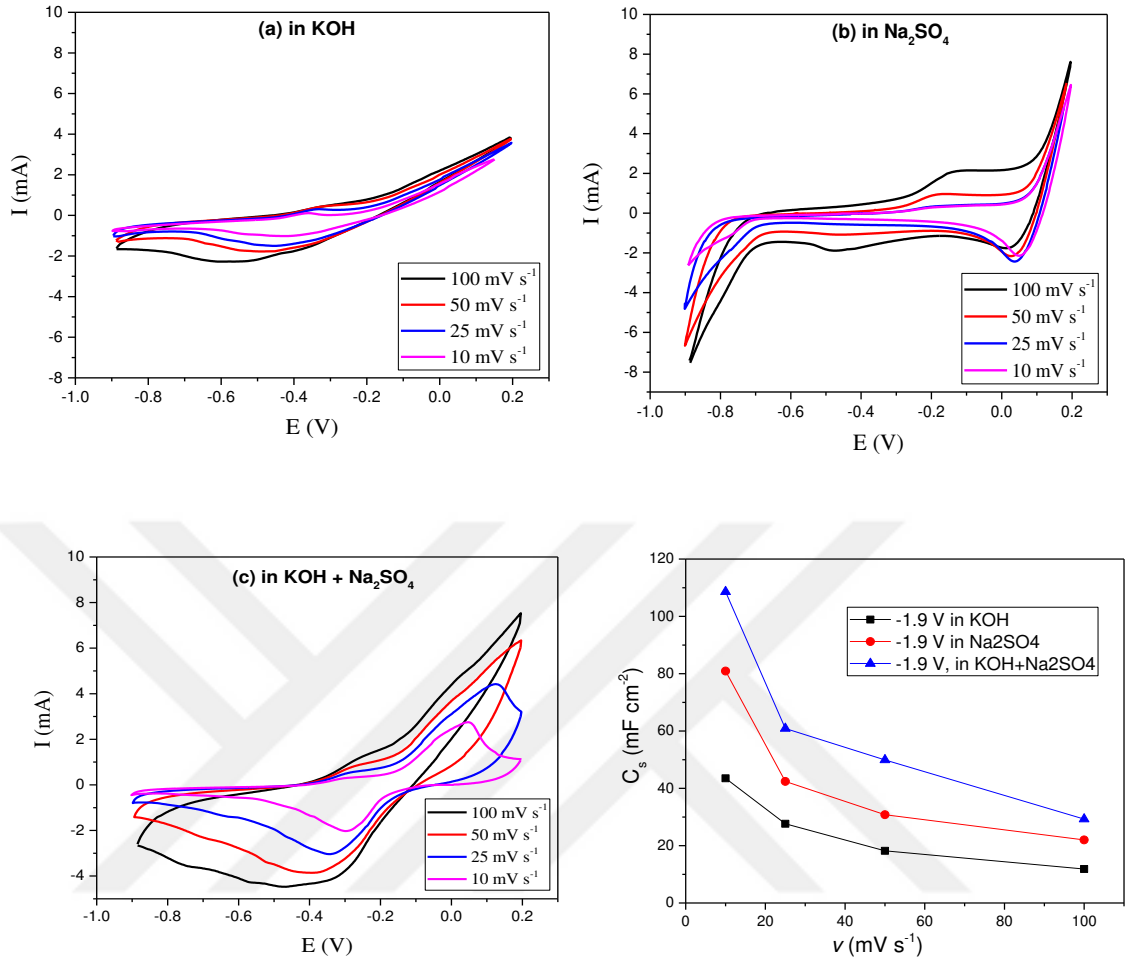

Figure 4.15 The cyclic voltammograms of Mn-Cu alloy in a) 1 M KOH; b) 1 M Na_2SO_4 and; c) an electrolyte consisting of 0.5 M KOH and 0.5 M Na_2SO_4. Mn-Cu alloy coating on graphite tapes were obtained in Ethaline deep eutectic solvent by applying a constant voltage of -1.9 V. d) Plot of the area capacitance of the electrodes given in panel a, panel b, and panel c depending on scanning speed.

On the other hand, when the Na_2SO_4 electrolyte is employed, the specific capacitance value at a scan rate of 100 mV/s is 22 mF cm^{-2} (**as indicated in Table 4.3**). When utilizing the mixed KOH + Na_2SO_4 electrolyte, the specific capacitance value at a scan rate of 100 mV/s is measured at 29 mF cm^{-2}.

Table 4.3 Specific capacitance values of Mn-Cu coated graphite tapes at -1.9 V potential depending on the varying scanning rates in different electrolyte solutions

Scan Rate ($mV\ s^{-1}$)	**Specific Capacitance ($mF\ cm^{-2}$) in KOH**	**Specific Capacitance ($mF\ cm^{-2}$) in Na_2SO_4**	**Specific Capacitance ($mF\ cm^{-2}$) in KOH + Na_2SO_4**
100	12	22	29
50	18	31	50
25	28	42	61
10	43	81	109

The observations based on the slopes of the equations in Error! Reference source not found. and **Figure 4.14** provide important insights into rate-limiting reaction. Here are the observations and predictions regarding diffusion based on the slopes of these equations:

- KOH electrolyte, at -1.6 V, the slope value is approximately -0.2146. This slope value represents the response of the reaction's rate to the scan rate in the KOH electrolyte. Since the slope value is negative, it indicates that the reaction rate decreases with increasing scan rate. This signifies a reaction does not occur under just diffusion control.

- Na_2SO_4 electrolyte, at -1.9 V, the slope value is -0.1112. This negative slope value also suggests that the reaction decreases in response to the scan rate. Once again, it indicates not only diffusional control mechanism.

- Na_2SO_4 + KOH mixture, at -1.6 V and -1.9 V, the slope values are -0.1772 and -0.1128, respectively. In both cases, the negative slope values indicate that the reaction is not purely diffusion-controlled. This is consistent even when a mixture of electrolytes is used.

In summary, the results obtained based on the slopes of these equations indicate that the studied electrochemical reactions are not under diffusion control. This implies that the reaction rate varies with the scan rate, and diffusion does not play a

crucial role in the reaction mechanism. It could be concluded that the reaction mechanism of Mn-Cu electrodes is likely to have a different rate-determining reaction mechanism and is not exclusively related to diffusion. As a result, we may conclude that all of these findings are related to electrode material, surface area, electrolyte composition coating process conditions, etc. Many factors provide important predictive information for the design and optimization of electrochemical systems.

4.2.3 Mn-Cu Electrodeposited by Application of -2.2 V

The photographs of Mn-Cu coating of graphite are presented in **Figure 4.16**. Analyzing the data in **Figure 4.17**, we ascertain that in the KOH electrolyte, the current density values range from -3 to 4 mA cm^{-2}. In the Na_2SO_4 electrolyte, these values vary between -1 and 2 mA cm^{-2}. For the 1 M KOH + 1 M Na_2SO_4 electrolyte, the values fall within the range of -2.5 to 3 mA cm^{-2}. Exploring the factors underlying these discrepancies, we find that at higher scan rates, the time allocated to the redox reaction diminishes, resulting in higher peak current values, especially at higher voltages.

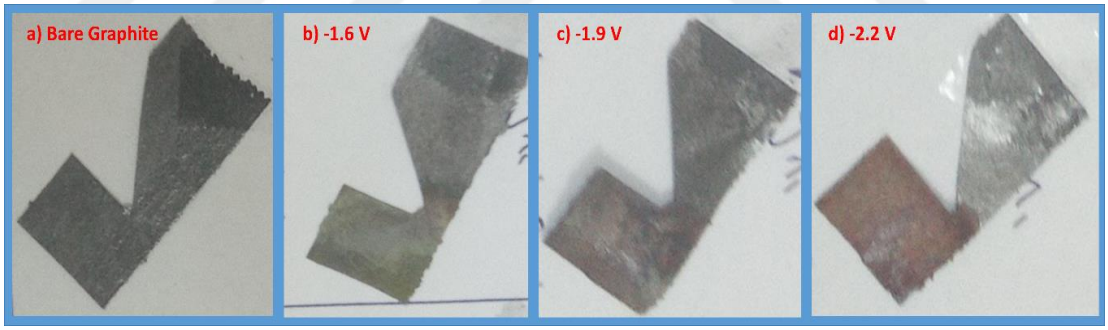

Figure 4.16 Photograph of a) bare graphite; b) Mn-Cu alloy coating on graphite tapes obtained in Ethaline deep eutectic solvent by applying a constant voltage of -1.6V; c) Mn-Cu alloy coating on graphite tapes obtained in Ethaline deep eutectic solvent by applying a constant voltage of -1.9 V; d) Mn-Cu alloy coating on graphite tapes obtained in Ethaline deep eutectic solvent by applying a constant voltage of -2.2 V

Additionally, considering the alloy deposition process, we note that lower negative voltage values generally lead to sparser and thinner coating layers **(Figure 4.16).** As ions are gradually transported to the surface, the coating layer becomes more

irregular and filled with voids. However, at higher negative voltages, denser and more compact coating layers were observed (**Figure 4.16c, d**). Faster ion transport at higher voltages seems to yield a more homogeneous layer. All these processes, supported by our graphical data, collectively highlight the effects of different voltage levels and scan rates on the electrochemical coating process.

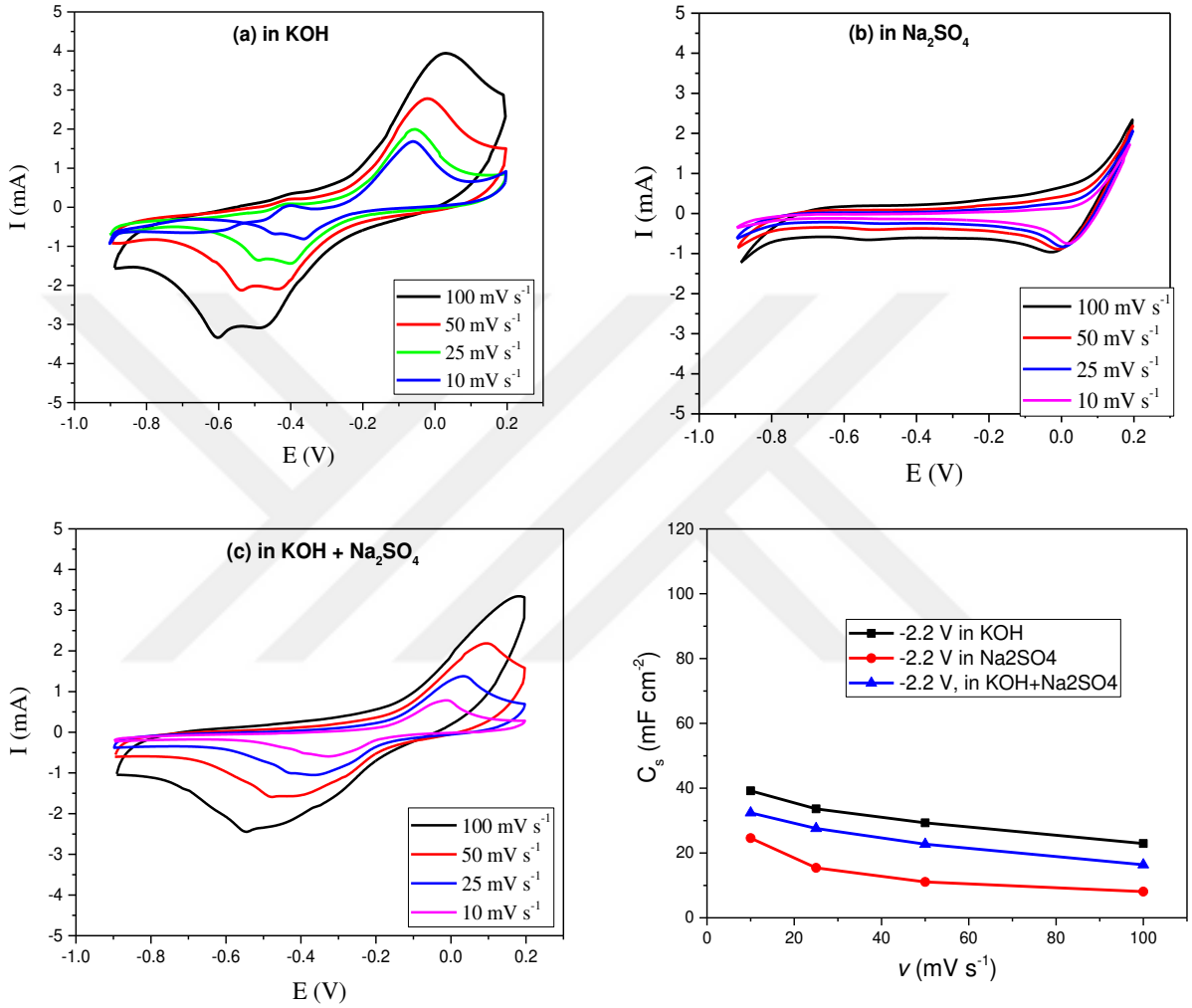

Figure 4.17 The cyclic voltammograms of Mn-Cu alloy in a) 1 M KOH; b) 1 M Na_2SO_4 and; c) an electrolyte consisting of 0.5 M KOH and 0.5 M Na_2SO_4. Mn-Cu alloy coating on graphite tapes were obtained in Ethaline deep eutectic solvent by applying a constant voltage of -2.2 V. d) Plot of the areal capacitance of the electrodes given in panel a, panel b, and panel c depending on scanning speed.

Comparing previous experimental figures by analyzing the graphs of **Figure 4.17**, in contrast to what was anticipated under the same scanning speed and electrolyte conditions, the flexible graphite samples coated at higher voltage exhibit lower

current peaks. Numerous predictable and unforeseen causes can be responsible for this behavior and it might be related to how electro-coating works. Because they carry more energy at higher voltages, the ions in the electrolyte could move to the surface layer more quickly. A more compact and dense coating layer may have occurred as a result. On the other hand, a coating layer may have become thinner and thinner because the ions carry less energy at lower voltages.

The coating process also may be influenced by greater diffusion. In this case, the rate at which ions are transported to the electrode surface becomes more effective in determining the current density. This case may result in a gradual rise in current density and hence, smaller current peaks. Besides, it is important to consider the role of the electrolyte. The tendency to produce intermediates or ions with poor diffusion coefficients may rise at higher voltages, which may limit ion mobility and result in lower current peaks. It should be noted, however, that although this explanation provides a reasonable perspective of the observed behavior, the electro-coating process is complex and influenced by numerous factors.

Table 4.4 Specific capacitance values of Mn-Cu coated graphite tapes at -2.2 V potential depending on the varying scanning rates in different electrolyte solutions

Scan Rate ($mV\ s^{-1}$)	**Specific Capacitance ($mF\ cm^{-2}$) in KOH**	**Specific Capacitance ($mF\ cm^{-2}$) in Na_2SO_4**	**Specific Capacitance ($mF\ cm^{-2}$) in KOH + Na_2SO_4**
100	23	8	16
50	29	11	23
25	34	15	28
10	39	25	32

Figure 4.17 and **Table 4.4** present specific capacitance values obtained at various scanning rates in different electrolyte solutions: KOH, Na_2SO_4, and a mixture of KOH + Na_2SO_4. These data provide valuable insights into the relationship between electrolyte compositions, scanning rates, and specific capacitance values. Upon examination, a clear trend emerges in the specific capacitance values across the

different electrolyte solutions. In the case of the KOH electrolyte, a scanning rate of 100 mV/s yields a specific capacitance of 23 mF cm^{-2}. However, as the scan rate is lowered (e.g., 10 mV/s), a noticeable increase in the specific capacitance value, reaching as high as 39 mF cm^{-2} was observed. This result probably highlights the favorable ion conductivity of the KOH electrolyte, leading to a higher capacitance. As the scanning rate is reduced, the specific capacitance increases, indicating that slower scan rates allow for more surface reactions and efficient charge transfer processes.

Conversely, when the Na_2SO_4 electrolyte is employed, a scanning rate of 100 mV/s results in a specific capacitance of 8 mF cm^{-2}, which then rises to 25 mF cm^{-2} when the scan rate is decreased to 10 mV/s. This outcome suggests that the presence of larger sulfate ions could restrict surface reactions and consequently lower the capacitance. When utilizing the KOH + Na_2SO_4 mixed electrolyte solution, specific capacitance values fall within an intermediate range.

This finding underscores a balance between the high-capacitance characteristics of the KOH electrolyte and the limitations posed by the Na_2SO_4 electrolyte. These experimental results reveal the critical role of electrolyte composition and scanning rate in shaping specific capacitance values. The interplay between ion conductivity and surface reaction dynamics becomes evident, demonstrating the complex nature of energy storage mechanisms in these systems. Such insights are pivotal for the optimization and design of energy storage devices for various applications.

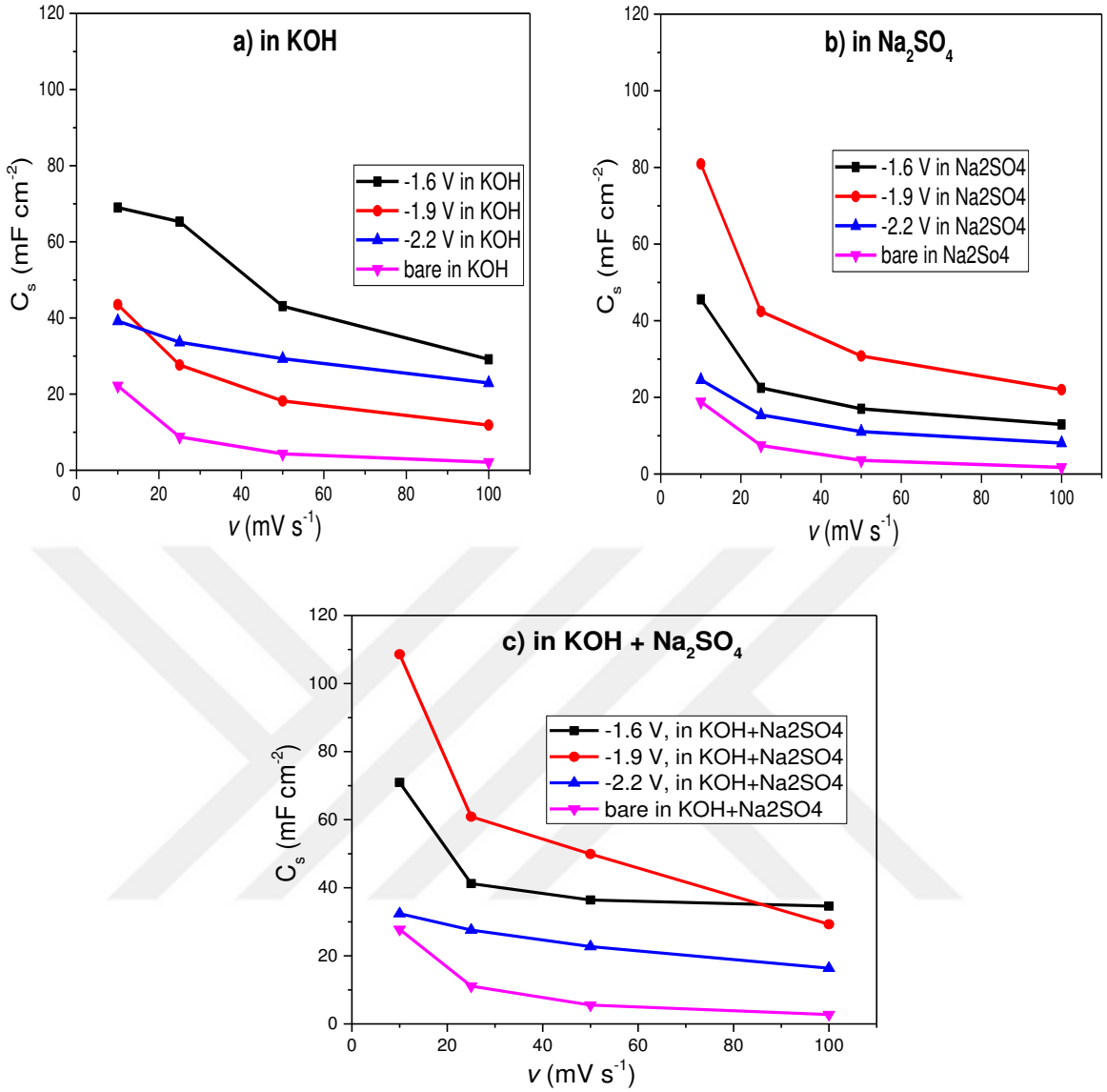

Figure 4.18 Specific capacitance of Mn-Cu based alloy on graphite depending on the applied coating voltage at different values a) cycled in 1 M KOH; b) cycled 1 M Na_2SO_4 and; c) cycled in the mixture of 0.5 M KOH and 0.5 M Na_2SO_4 at various scanning speed.

When examining the graphs in **Figure 4.18** individually, the results obtained under different coating voltages offer valuable insights. Firstly, the KOH electrolyte data, acquired at a -1.6 V coating voltage greatly outperforms the data obtained at other coating voltages (**Figure 4.18a**). These results demonstrate how the electrolyte and the coating voltage of -1.6 V improve and increase the electrode's capacitance

properties. Notably, even better results were obtained in comparison to the uncoated graphite-specific capacitance values and the -1.9 V and -2.2 V coatings. This demonstrates the potential of slower scan speeds to accommodate a higher capacity for charge storage on the electrode surface and highlights the critical importance of selecting the right electrolyte.

Analyzing the data acquired under a coating voltage of -1.9 V similarly reveals a tendency similar to the data shown **in Figure 4.18a**. The reported specific capacitance value in the KOH electrolyte is 12 mF cm^{-2} at higher scan rates (for example, 100 mV/s). The specific capacitance value rises to a maximum of 43 mF cm^{-2} when the scan rate falls (for example, to 10 mV/s). When evaluating the results acquired in the Na_2SO_4 electrolyte under a -1.9 V coating voltage, the same pattern is observe. Higher specific capacitance values are produced when the scan rate is reduced. For instance, the specific capacitance is 22 mF cm^{-2} at a scan rate of 100 mV/s but increases to 81 mF cm^{-2} with a scan rate of 10 mV/s (**in Figure 4.18b**).

The study of data obtained using the mixed KOH + Na_2SO_4 electrolyte also yielded similar results. It is obvious that for scan rate measurements, the best results are obtained with a constant -1.9 V coating voltage. For instance, the specific capacitance value is 29 mF cm^{-2} at a scan rate of 100 mV/s, but it increases to 109 mF cm^{-2} with a scan rate of 10 mV/s (**in Figure 4.18c**).

Additionally, the high capacitance characteristics of the 0.5 M KOH + 0.5 M Na_2SO_4 concentrated electrolyte are supported by the capacitance values under the -1.6 V coating voltage. These experimental graphs demonstrate, in conclusion, how important electrolyte composition and scan rate are in determining certain capacitance values. The complicated nature of these systems' energy storage mechanisms is underlined by the relationship between ion conductivity and surface response kinetics.

4.3 Characterisation of the Alloys Coated on Graphite Wire

In the study of **Figure 4.19** experiment, a mixing solution was first made that deep eutectic solvent was based on Ethaline and contained copper ions (Cu^{+2}) and manganese ions (Mn^{+2}). For 180 minutes, this blending solution was heated to 60

°C. After that, 1 cm worth of graphite wires were obtained. These graphite wires were submerged in a substantial Ethaline-based eutectic solution that also contained copper and manganese ions.

The surface coating of manganese and copper alloyed graphite wires was obtained using the electrochemical coating method at -1.9 V potential for 150 sec. It was subjected to cyclic voltammetry at different scanning rates (100 mV/s, 50 mV/s, 25 mV/s, and 10 mV/s) by applying electrode potential in the range of -1 V to 0.5 V. Different electrolyte solutions were used to better understand and compare the electrochemical properties of the electrodes.

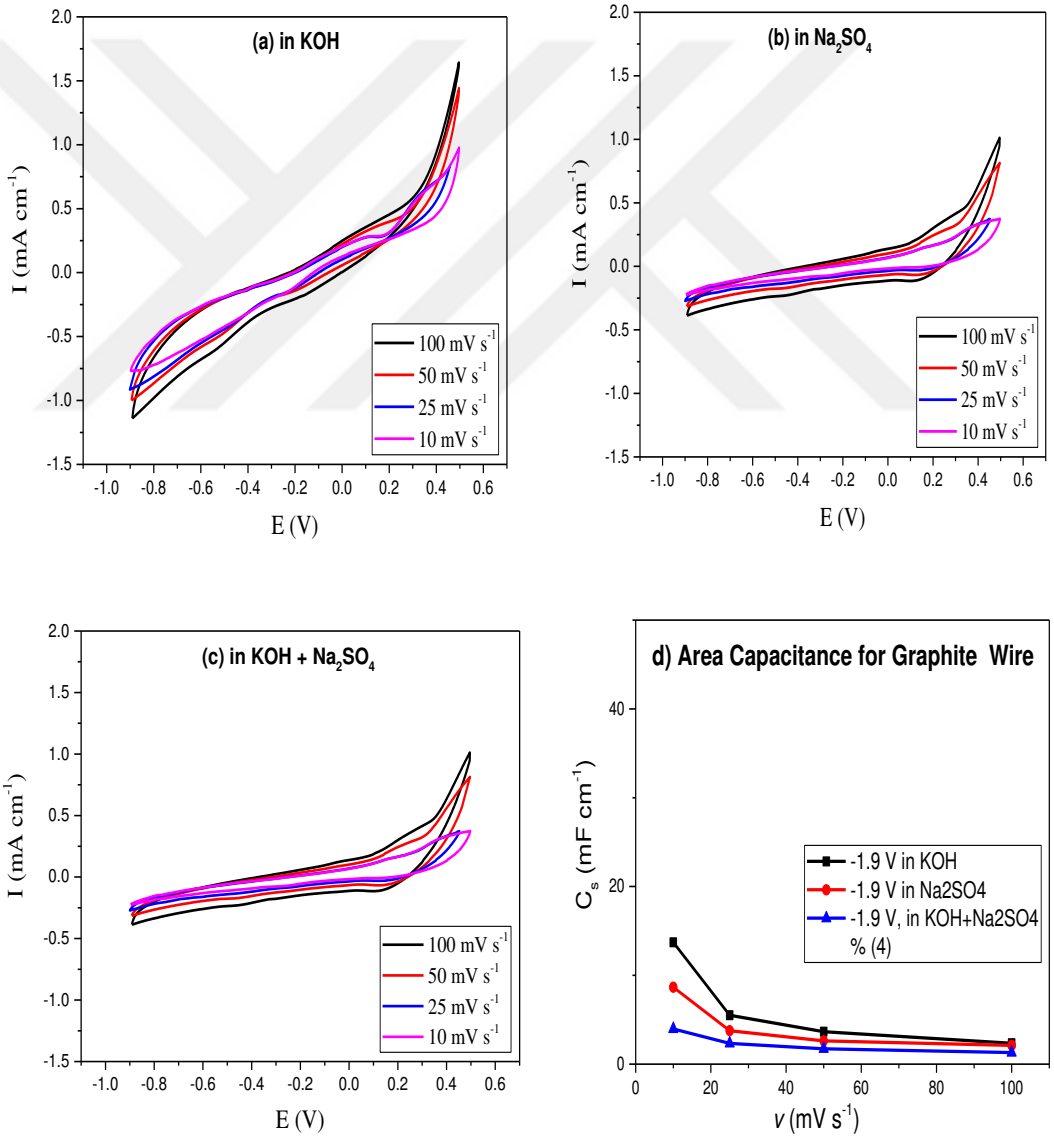

Figure 4.19 The cyclic voltammograms of Mn-Cu alloy in a) 1 M KOH; b) 1 M Na_2SO_4 and; c) an electrolyte consisting of 0.5 M KOH and 0.5 M Na_2SO_4. Mn-Cu alloy coating on graphite wires were obtained in Ethaline deep eutectic solvent by applying a constant voltage of -1.9 V. d) Plot of the areal capacitance of the electrodes given in panel a, panel b, and panel c depending on scanning speed.

These solutions contain 1 M KOH and 1 M Na_2SO_4 and a combination of 0.5 M KOH with 0.5 M Na_2SO_4. When we examine the graphs in **Figure 4.19a, b, and c**, we can see that the current density in the KOH electrolyte changes between -1 and 1.5 mA cm^{-2} for the CV curve with a scanning rate of 100 mV/s. However, in the Na_2SO_4 electrolyte, these values range from -0.3 to 1 mA cm^{-2}. When 0.5 M KOH 0.5 M Na_2SO_4 electrolytes are utilised, the readings vary between -0.3 and 1 mA cm^{-2} and this value decreases as the scan rate decreases.

These findings demonstrate the impact of various electrolytes and scanning rates on the development of manganese and copper coatings on graphite wire. Lower current density values are obtained when KOH and Na_2SO_4 electrolytes are combined, and these values go even lower as the scanning speed is slower. These tests demonstrate the electrochemical characteristics of graphite wire surface coatings and how they alter in various environments.

This goal study of **Figure 4.20** is to thoroughly examine the electrochemical behavior of bare graphite wire surfaces using cyclic voltammogram testing in an experimental setting. For this purpose, various electrolyte solutions have been utilized; used examples include solutions such as 1 M KOH, 1 M Na_2SO_4 and the mixture of 0.5 M KOH with 0.5 M Na_2SO_4, which are encompassed within this scope. Furthermore, an electrode potential range varying from -1 V to 0.5 V has been examined and it is made experimental of different scan rates (100 mV/s, 50 mV/s, 25 mV/s, and 10 mV/s).

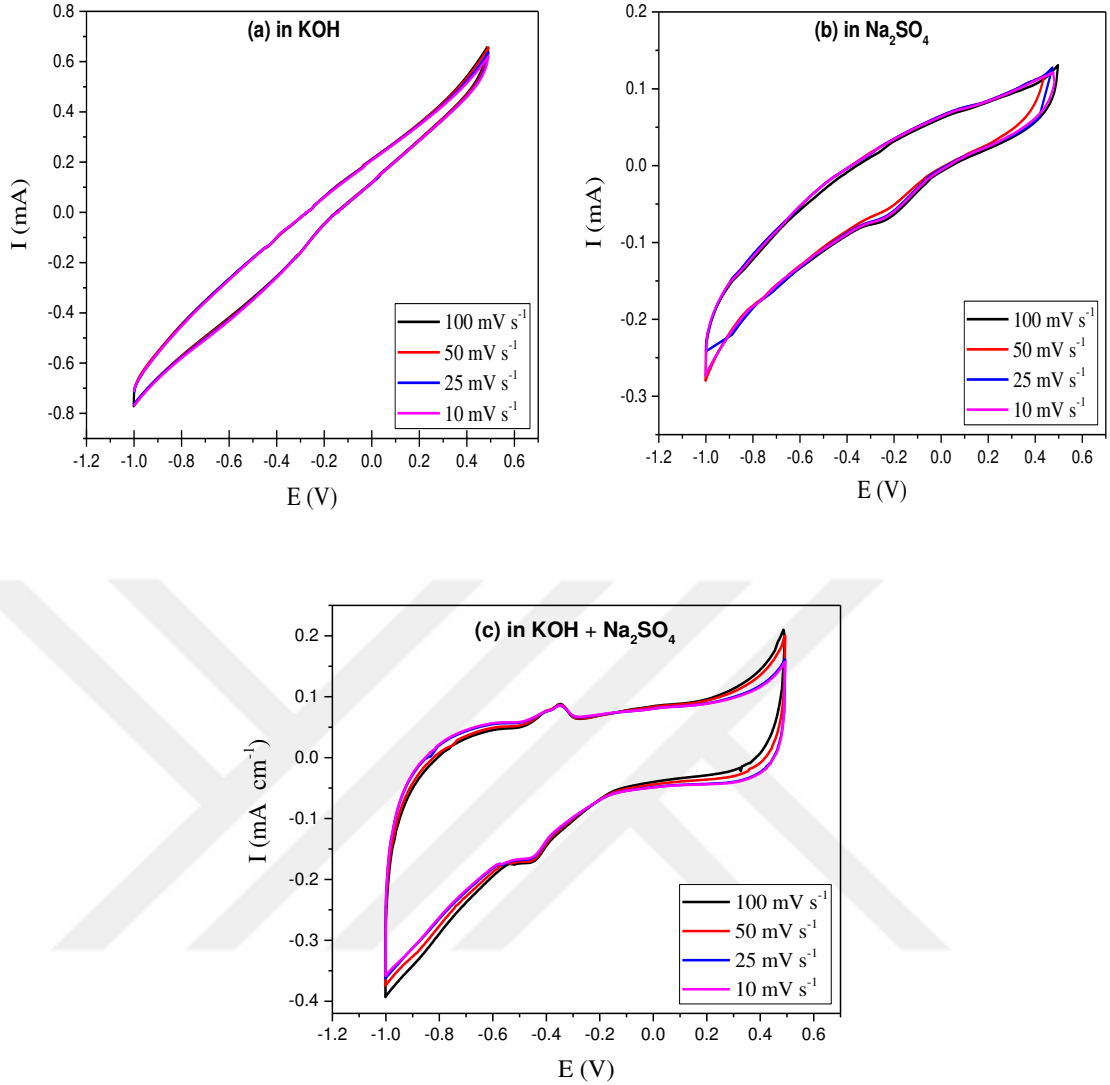

Figure 4.20 The cyclic voltammograms of bare graphite wires in a) 1 M KOH; b) 1 M Na_2SO_4 and; c) an electrolyte consisting of 0.5 M KOH and 0.5 M Na_2SO_4

When the result of examining the graphs in **Figure 4.20a, b, c**, it is observed that for CV curves at a scan rate of 100 mV/s, the obtained current density within the KOH electrolyte varies between -0.7 and 0.7 mA cm^{-1}. However, when Na_2SO_4 electrolyte is employed, these values fluctuate between -0.3 and 0.25 mA cm^{-1}.

When a mixture of 0.5 M KOH and 0.5 M Na_2SO_4 is used, the recorded readings exhibit variations within the range of -0.35 to 0.2 mA cm^{-1}. In general, it is observed that as the scan rate decreases, the obtained current density remains relatively constant.

These results indicate that the scan rate does not significantly impact the electrochemical reactions on the surface of the bare electrode. In this context, a novel perspective is offered for understanding the electrochemical properties of bare graphite wires. Furthermore, an important series of experiments have been conducted to compare the effects of different electrolyte solutions and voltage levels on the electrochemical performance of Mn-Cu-coated graphite wires, aiming to achieve optimal results. Cyclic voltammetry data reveals that Mn-Cu-coated graphite wires demonstrate higher electrochemical performance compared to bare graphite wires.

The specific capacitance (C) is generally expressed using the following equation:

$$C = \frac{2}{l \cdot \Delta V} \int \frac{I \, dV}{v} \qquad (4.3)$$

Where:

- C is the specific capacitance (F cm^{-1}),
- I represents the current density (A cm^{-1}),
- ΔV stands for the potential difference (V),
- v signifies the scan rate (mV s^{-1}),
- l is the area of active materials loaded in the working electrode (cm)

.

Table 4.5 Specific capacitance values of Mn-Cu coated graphite wires at -1.9 V potential depending on the varying scanning rates in different electrolyte solutions

Scan Rate (mV s^{-1})	**Specific Capacitance (mF cm^{-1}) in KOH**	**Specific Capacitance (mF cm^{-1}) in Na_2SO_4**	**Specific Capacitance (mF cm^{-1}) in KOH + Na_2SO_4**
100	2	2	1
50	4	3	2
25	6	4	2
10	14	9	4

The graphite wire samples were obtained at a plating voltage of -1.9 V and then, these samples used for the specific capacitance processes in various electrolytes exhibit a reducing tendency, as can be seen by looking at the data from **Figure**

4.19d and **Table 4.5** within the context of this study. When treating a graphite wire, the length measurement is taken into account rather than the surface area (**4.3**). In this procedure, "specific capacitance" refers to the quantity of charge held along the electrode's length during an electrochemical reaction, and "scan rate" designates the pace at which the electrode potential changes during voltammetry studies. Upon scrutiny of **Figure 4.19d**, the obtained outcome highlights an inversely proportional relationship between specific capacitance and scan rate. In this context, to investigate the variation of specific capacitance concerning length, the experimental data from **Table 4.5** are also utilized.

For example, at higher scanning rates (for example, 100 mV/s) with KOH electrolyte, the specific capacitance measured against the length of the electrode is 2 mF cm^{-1}. On the other hand, as the scanning rate decreases (for example, 10 mV/s), the specific capacitance value increases to 14 mF cm^{-1}. Similarly, a lower scanning rate with Na_2SO_4 electrolyte leads to higher specific capacitance values.

For instance, the capacitance value, which is initially at the level of 2 mF cm^{-1} according to the electrode length at a scanning speed of 100 mV/s, increases to 9 mF cm^{-1} at a scanning speed of 10 mV/s. This indicates that lower scanning rates produce higher capacitance values relative to the electrode length. The same trend is observed when the combination of both electrolytes (KOH + Na_2SO_4) is used. At higher scan rates (eg, 100 mV/s) the capacitance value is initially 1 mF cm^{-1}, increasing to 4 mF cm^{-1} at lower scan rates (eg 10 mV/s).

4.4 Characterisation of the Alloys Coated on Graphite Fabric

Various electrolyte solutions were employed to better comprehend and compare the electrochemical characteristics of the electrodes. These solutions included a combination of 1 M KOH and 1 M Na_2SO_4, along with 0.5 M KOH and 0.5 M Na_2SO_4. The electode is knitted graphite fabric consisting of only graphite filaments.

These findings underscore the impact of different electrolytes and scanning rates on the development of manganese and copper coatings on the graphite fabric samples. The combination of KOH and Na_2SO_4 electrolytes yields lower current density values, and this trend is further pronounced as the scanning rate decreases. These

experimental trials serve to elucidate the electrochemical properties of graphite fabric surface coatings and their responsiveness to varying environmental conditions.

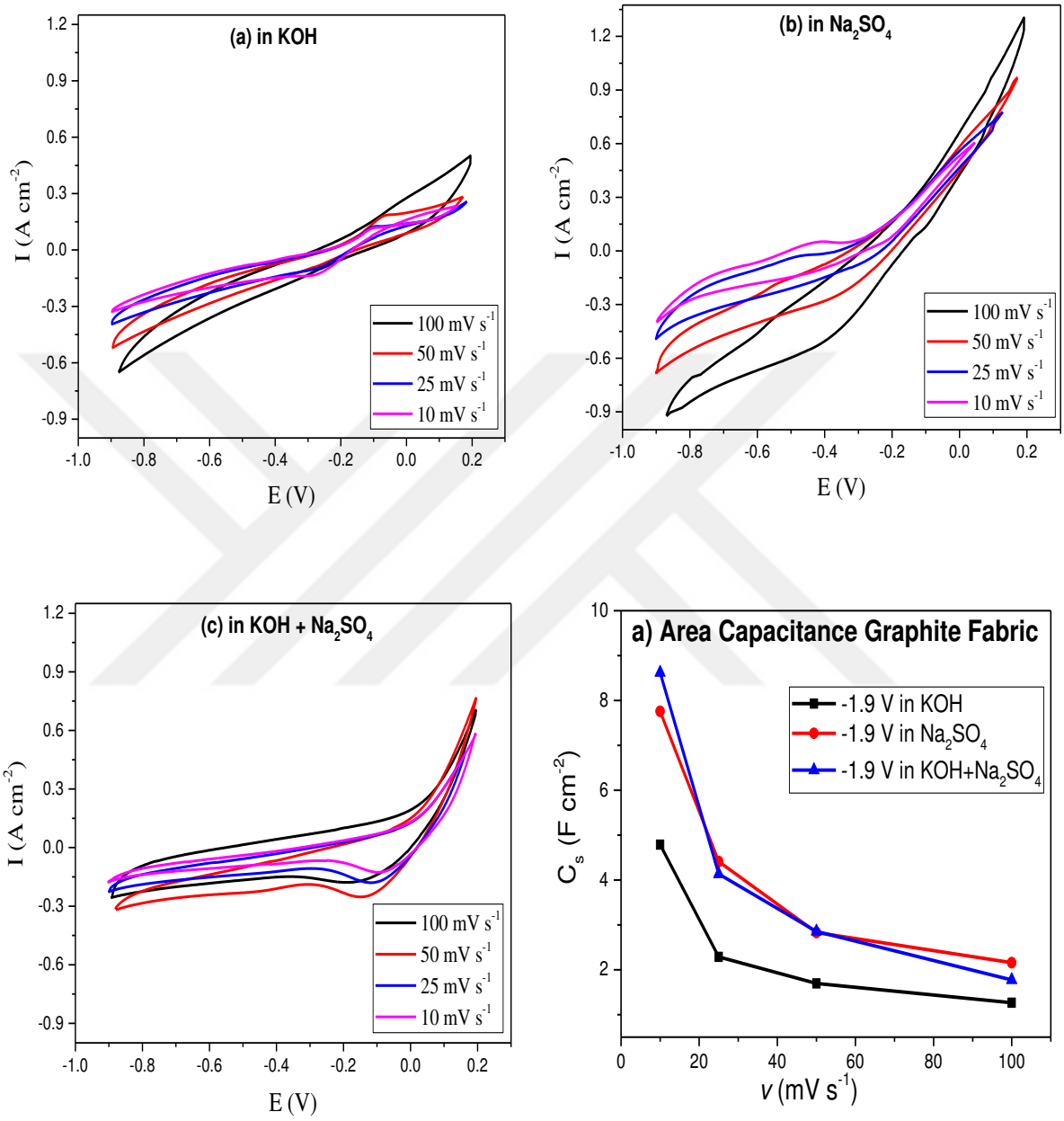

Figure 4.21 The cyclic voltammograms of Mn-Cu alloy in a) 1 M KOH; b) 1 M Na_2SO_4 and; c) an electrolyte consisting of 0.5 M KOH and 0.5 M Na_2SO_4. Mn-Cu alloy coating on graphite fabrics were obtained in Ethaline deep eutectic solvent by applying a constant voltage of -1.9 V. d) Plot of the area capacitance of the electrodes given in panel a, panel b, and panel c depending on scanning speed.

Upon analyzing the graphs depicted in **Figure 4.21a, b**, and **c**, it becomes evident that, for the CV curve conducted with a scanning rate of 100 mV/s, the current density in the KOH electrolyte varies between -0.65 and 0.5 A cm^{-2}. In contrast, within the Na_2SO_4 electrolyte, these values range from -0.9 to 1.2 A cm^{-2}. When utilizing the 0.5 M KOH and 0.5 M Na_2SO_4 electrolytes, the readings fluctuate between -0.3 and 0.75 A cm^{-2}, with this value diminishing as the scanning rate decreases.

Moreover, when we compare these experimental data with **Figure 4.19** and **Figure 4.11,** a clear difference emerges mean current density values according to electrolyte types and scanning speeds. The results of the experiment data **in Figure 4.21** show higher current density values than the other experiments. In addition, high values are provided as the area under the CV curves. These comparisons show the positive effects of manganese and copper coatings on graphite fabric of different electrolyte types and scanning rates.

Table 4.6 Specific capacitance values of Mn-Cu coated graphite fabrics at -1.9 V potential depending on the varying scanning rates in different electrolyte solutions

Scan Rate ($mV\ s^{-1}$)	**Specific Capacitance (F cm^{-2}) in KOH**	**Specific Capacitance (F cm^{-2}) in Na_2SO_4**	**Specific Capacitance (F cm^{-2}) in KOH + Na_2SO_4**
100	1	2	2
50	2	3	3
25	2	4	4
10	5	8	9

Based on the experiment data presented in **Table 4.6** and **Figure 4.21d**, the analysis conducted revolves around specific capacitance measurements performed at different scan rates (mV/s). Similar trends may be seen in the relationships between scan rate and specific capacitance in the electrolytes 1 M Na_2SO_4 and 0.5 M KOH + Na_2SO_4 **(Figure 4.21d)**. For instance, in the Na_2SO_4 electrolyte, the specific capacitance is 2 F cm^{-2} at a scan rate of 100 mV/s, whereas a scan rate reduction to

10 mV/s increases the specific capacitance value to 8 F cm^{-2} (**Table 4.6**). The electrolyte combination of KOH and Na_2SO_4 shows a similar tendency. For instance, the specific capacitance in the 0.5 M KOH + Na_2SO_4 electrolyte is 2 F cm^{-2} at a scan rate of 100 mV/s, but the specific capacitance increases to 9 F cm^{-2} at a scan rate of 10 mV/s (**Table 4.6**). Specific capacitance has similar values that are larger at Na_2SO_4 electrolyte and electrolyte combination of KOH and Na_2SO_4. However, when using the 1 M KOH electrolyte, different behavior is observed. When the scan rate is lowered from 100 to 10 mV/s, the specific capacitance in this electrolyte rises from 1 F cm^{-2} to 5 F cm^{-2} (**Table 4.6**).

In conclusion, comparable measurements conducted under different electrolytes and similar scan rates demonstrate that lower scan rates correspond to higher specific capacitance values on the electrode surface. While this trend is consistent and higher values are observed in 1 M Na_2SO_4 and 0.5 M KOH + Na_2SO_4 electrolytes, a different behavior; at lower values is evident in the context of the 1 M KOH electrolyte **(Figure 4.21d)**.

In the scope of our study, comprehensive examinations were conducted on samples of different forms, namely Graphite Tapes (**Figure 4.11**), Graphite Wires (**Figure 4.19**), and Graphite Fabric (**Figure 4.21**), and the obtained results were carefully evaluated. Upon reviewing these analyses and observations, it becomes evident that Mn-Cu alloy-coated Graphite Fabric presents a substantial advantage in terms of specific capacitance compared to the other two forms.

Particularly, compared to the other types, the alloy-based coating used on the graphite fabric results in a nearly 1000-fold increase in specific capacitance. These results highlight the flexible Mn-Cu-coated graphite fabric's enormous potential for supercapacitor applications. By expanding the surface area of the graphite fabric, the alloy coating dramatically improves capacitance and allows for more charge storage. The voltage value employed during the coating process, the time of the voltage, the coating temperature, and the alloy components used all play significant roles in affecting capacitance improvement.

In this respect, it could be said that the Mn-Cu alloy-based coating of graphite fabric bears major importance for supercapacitor technology based on previous literature studies and the results of the experimental procedures given here,

primarily because of the significant rise in capacitance values. This growth may result in better energy storage. This increase could potentially lead to enhanced energy storage capacity. However, further research endeavors should be directed toward optimizing the coating process, investigating the effects of different alloy components, and assessing the performance in practical applications.

CHAPTER V
CONCLUSION

Evaluation of the data, findings and analysis obtained as a result of this thesis study are as follows;

- **Usage of Ethaline Deep Eutectic Solvent**; ethaline deep eutectic solvent was the main solvent used in this experiment. This solvent is a unique kind of ionic liquid that has a broad temperature range. This characteristic makes it possible to conduct electrochemical reactions at low temperatures. Morever, the low viscosity and excellent conductivity of ethylene lead to a uniform dispersion of the electrochemical solution.
- **Reasons for Choosing Mn-Cu Alloy**; the aim of choosing the components Cu (copper) and Mn (manganese) is to improve the electrodes' electrical performance. Because of their excellent conductivity and efficiency in energy storage devices, these two metals are chosen. Using Mn-Cu alloy increased the durability and capacitance of the electrodes.
- **Use of KOH and Na_2SO_4 as Electrolytes**; Potassium Hydroxide (KOH) and Sodium Sulfate (Na_2SO_4) are electrolytes that enable ion movement in the electrochemical cell. Because of its high conductivity, KOH is well suited to help ions travel across electrodes. This experiment assessed the effects of different, including Na_2SO_4, which is a general electrolyte used in a electrochemical applications. As the result, electrode performance and the rate of electrochemical reactions was impacted by the choice of electrolyte.
- **Role of Alloy Based Graphite Hybrid Fabric**; alloy based hybrid fabric included of graphite not only makes the electrodes more physically durable, but because of its large surface area, it can also enhance the possibility of electrochemical reactions. This fabric can help coat the electrode uniformly, which can optimize the energy storage capacity.Moreover, its flexible construction can strengthen the electrode's resistance to mechanical loads and improve cycle stability.

In conclusion, significant advances in the field of energy storage technologies have been made possible by a combination of factors such as the compatible use of Ethaline deep eutectic solvent, Mn-Cu alloy, specific electrolyte combinations and alloy-based graphite hybrid fabric. The effective combination of these elements has resulted in critical properties such as flexibility, durability and high performance of the electrodes.The findings of this study can be considered an important resource in the design of future energy storage solutions for wearable technologies, biomedical devices and portable electronic applications. Carefully integrating these elements into industrial studies can make a significant contribution to the development of more durable, flexible and high-performance energy storage systems.

REFERENCES

[1] M. S. Guney and Y. Tepe, “Classification and assessment of energy storage systems,” Renewable and Sustainable Energy Reviews, vol. 75, pp. 1187–1197, Aug. 2017, doi: 10.1016/j.rser.2016.11.102.

[2] J. Mitali, S. Dhinakaran, and A. A. Mohamad, “Energy storage systems: a review,” Energy Storage and Saving, vol. 1, no. 3, Sep. 2022, doi: 10.1016/j.enss.2022.07.002.

[3] M. A. Hannan et al., “Battery energy-storage system: A review of technologies, optimization objectives, constraints, approaches, and outstanding issues,” J Energy Storage, vol. 42, p. 103023, Oct. 2021, doi: 10.1016/j.est.2021.103023.

[4] Y. Yang, S. Bremner, C. Menictas, and M. Kay, “Battery energy storage system size determination in renewable energy systems: A review,” Renewable and Sustainable Energy Reviews, vol. 91, pp. 109–125, Aug. 2018, doi: 10.1016/j.rser.2018.03.047.

[5] J. Ho, T. R. Jow, and S. Boggs, “Historical introduction to capacitor technology,” IEEE Electrical Insulation Magazine, vol. 26, no. 1, Jan. 2010, doi: 10.1109/MEI.2010.5383924.

[6] Poonam, K. Sharma, A. Arora, and S. K. Tripathi, “Review of supercapacitors: Materials and devices,” J Energy Storage, vol. 21, Feb. 2019, doi: 10.1016/j.est.2019.01.010.

[7] F. R. Kalhammer and T. R. Schneider, “Energy Storage,” Annual Review of Energy, vol. 1, no. 1, Nov. 1976, doi: 10.1146/annurev.eg.01.110176.001523.

[8] Ş. & G. Z. A. Efe, “Battery Technology from Past to Present. European Journal of Science and Technology,” vol. 32, pp. 947–955, 2021.

[9] X. Luo, J. Wang, M. Dooner, and J. Clarke, “Overview of current development in electrical energy storage technologies and the application potential in power system operation,” Appl Energy, vol. 137, pp. 511–536, Jan. 2015, doi: 10.1016/j.apenergy.2014.09.081.

[10] H. L. Ferreira, R. Garde, G. Fulli, W. Kling, and J. P. Lopes, “Characterisation of electrical energy storage technologies,” Energy, vol. 53, pp. 288–298, May 2013, doi: 10.1016/j.energy.2013.02.037.

[11] J. C. Beardsall, C. A. Gould, and M. Al-Tai, “Energy storage systems: A review of the technology and its application in power systems,” in 2015 50th International Universities Power Engineering Conference (UPEC), IEEE, Sep. 2015, pp. 1–6. doi: 10.1109/UPEC.2015.7339794.

[12] A. González, E. Goikolea, J. A. Barrena, and R. Mysyk, “Review on supercapacitors: Technologies and materials,” Renewable and Sustainable Energy Reviews, vol. 58, pp. 1189–1206, May 2016, doi: 10.1016/j.rser.2015.12.249.

[13] M. Vangari, T. Pryor, and L. Jiang, “Supercapacitors: Review of Materials and Fabrication Methods,” Journal of Energy Engineering, vol. 139, no. 2, pp. 72–79, Jun. 2013, doi: 10.1061/(ASCE)EY.1943-7897.0000102.

[14] H.-Q. Li, Y.-G. Wang, C.-X. Wang, and Y.-Y. Xia, “A competitive candidate material for aqueous supercapacitors: High surface-area graphite,” J Power Sources, vol. 185, no. 2, pp. 1557–1562, Dec. 2008, doi: 10.1016/j.jpowsour.2008.08.079.

[15] M. E. Sahin, F. ; Blaabjerg, and A. Sangwongwanich, “A Review on Supercapacitor Materials and Developments,” Turkish Journal of Materials, vol. 5, no. 2, pp. 10–24, 2020, [Online]. Available: https://www.scienceliterature.com/index.php/tjom/article/view/10-24

[16] A. González, E. Goikolea, J. A. Barrena, and R. Mysyk, “Review on supercapacitors: Technologies and materials,” Renewable and Sustainable Energy Reviews, vol. 58, pp. 1189–1206, May 2016, doi: 10.1016/j.rser.2015.12.249.

[17] A. Yavuz, M. Bedir, and A. Tunç, “Manganese – iron coated flexible graphite sheet having a wide potential window for energy storage devices,” J Energy Storage, vol. 50, p. 104253, Jun. 2022, doi: 10.1016/j.est.2022.104253.

[18] Z. S. Iro, C. Subramani, and S. S. Dash, “A Brief Review on Electrode Materials for Supercapacitor,” Int J Electrochem Sci, vol. 11, no. 12, pp. 10628–10643, Dec. 2016, doi: 10.20964/2016.12.50.

[19] A. Yavuz, M. Artan, and N. F. Yilmaz, “The effect of growth potential on the self-discharge behavior of Cu–Ni-based alloy electrodes,” Journal of Physics and Chemistry of Solids, vol. 169, p. 110872, Oct. 2022, doi: 10.1016/j.jpcs.2022.110872.

[20] E. Niknam, H. Naffakh-Moosavy, and M. Ghahraman Afshar, “Electrochemical Performance of Nickel Foam Electrode in Potassium Hydroxide and Sodium Sulfate Electrolytes for Supercapacitor Applications,” Journal of Composites and Compounds, vol. 4, no. 12, pp. 149–152, Sep. 2022, doi: 10.52547/jcc.4.3.3.

[21] A.-L. Brisse, P. Stevens, G. Toussaint, O. Crosnier, and T. Brousse, “Ni(OH)2 and NiO Based Composites: Battery Type Electrode Materials for Hybrid Supercapacitor Devices,” Materials, vol. 11, no. 7, p. 1178, Jul. 2018, doi: 10.3390/ma11071178.

[22] K. K. Purushothaman, M. Cuba, and G. Muralidharan, “Supercapacitor behavior of α-MnMoO4 nanorods on different electrolytes,” Mater Res Bull, vol. 47, no. 11, pp. 3348–3351, Nov. 2012, doi: 10.1016/j.materresbull.2012.07.027.

[23] “IRENA (2023), World Energy Transitions Outlook 2023, Volume 1, International Renewable Energy Agency”.

[24] L. Wagner, “Overview of energy storage methods Research,” 2007.

[25] D. Behçet KOCAMAN, ENERJİ DEPOLAMA TEKNOLOJİLERİ. 2021. [Online]. Available: www.iksadyayinevi.com

[26] M. A. Hannan, M. M. Hoque, A. Mohamed, and A. Ayob, “Review of energy storage systems for electric vehicle applications: Issues and challenges,” Renewable and Sustainable Energy Reviews, vol. 69. Elsevier Ltd, pp. 771–789, Mar. 01, 2017. doi: 10.1016/j.rser.2016.11.171.

[27] M. Winter and R. J. Brodd, “What Are Batteries, Fuel Cells, and Supercapacitors?,” Chem Rev, vol. 104, no. 10, Oct. 2004, doi: 10.1021/cr020730k.

[28] F. Putois, “Market for nickel-cadmium batteries,” J Power Sources, vol. 57, no. 1–2, Sep. 1995, doi: 10.1016/0378-7753(95)02243-0.

[29] A. M. Abdalla et al., “Innovative lithium-ion battery recycling: Sustainable process for recovery of critical materials from lithium-ion batteries,” J Energy Storage, vol. 67, Sep. 2023, doi: 10.1016/j.est.2023.107551.

[30] C. M. Hayner, X. Zhao, and H. H. Kung, “Materials for Rechargeable Lithium-Ion Batteries,” Annu Rev Chem Biomol Eng, vol. 3, no. 1, Jul. 2012, doi: 10.1146/annurev-chembioeng-062011-081024.

[31] B. Scrosati and J. Garche, “Lithium batteries: Status, prospects and future,” J Power Sources, vol. 195, no. 9, pp. 2419–2430, May 2010, doi: 10.1016/j.jpowsour.2009.11.048.

[32] N. Chawla, N. Bharti, and S. Singh, “Recent Advances in Non-Flammable Electrolytes for Safer Lithium-Ion Batteries,” Batteries, vol. 5, no. 1, Feb. 2019, doi: 10.3390/batteries5010019.

[33] D. Pletcher, H. Zhou, G. Kear, C. T. J. Low, F. C. Walsh, and R. G. A. Wills, “A novel flow battery—A lead-acid battery based on an electrolyte with soluble lead(II),” J Power Sources, vol. 180, no. 1, May 2008, doi: 10.1016/j.jpowsour.2008.02.024.

[34] Ş. EFE and Z. A. GÜNGÖR, “Geçmişten Günümüze Batarya Teknolojisi,” European Journal of Science and Technology, Jan. 2022, doi: 10.31590/ejosat.1048673.

[35] D. Pletcher, H. Zhou, G. Kear, C. T. J. Low, F. C. Walsh, and R. G. A. Wills, “A novel flow battery—A lead-acid battery based on an electrolyte with soluble lead (II): Part VI. Studies of the lead dioxide positive electrode,” J Power Sources, vol. 180, no. 1, pp. 630–634, 2008.

[36] M. F. Cowlishaw, “The characteristics and use of lead-acid cap lamps,” Trans. British Cave Research Association, vol. 1, no. 4, pp. 199–214, 1974.

[37] A. A. Kebede, T. Kalogiannis, J. Van Mierlo, and M. Berecibar, “A comprehensive review of stationary energy storage devices for large scale renewable energy sources grid integration,” Renewable and Sustainable Energy Reviews, vol. 159, May 2022, doi: 10.1016/j.rser.2022.112213.

[38] P. Kumari, M. Shandilya, M. Lal, and R. Rai, “High dielectric materials for supercapacitors,” Smart materials for smart living, p. 95, 2017.

[39] I. Melkiyur et al., “A comprehensive review on novel quaternary metal oxide and sulfide electrode materials for supercapacitor: Origin, fundamentals, present perspectives, and future aspects,” Renewable and Sustainable Energy Reviews, vol. 173, p. 113106, Mar. 2023, doi: 10.1016/j.rser.2022.113106.

[40] J. Ho, T. R. Jow, and S. Boggs, “Historical introduction to capacitor technology,” IEEE Electrical Insulation Magazine, vol. 26, no. 1, Jan. 2010, doi: 10.1109/MEI.2010.5383924.

[41] Y. Shao et al., “Design and Mechanisms of Asymmetric Supercapacitors,” Chem Rev, vol. 118, no. 18, pp. 9233–9280, Sep. 2018, doi: 10.1021/acs.chemrev.8b00252.

[42] V. Molahalli, C. K, M. K. Singh, M. Agrawal, S. G. Krishnan, and G. Hegde, “Past decade of supercapacitor research – Lessons learned for future innovations,” J Energy Storage, vol. 70, Oct. 2023, doi: 10.1016/j.est.2023.108062.

[43] J. Sung and C. Shin, “Recent Studies on Supercapacitors with Next-Generation Structures,” Micromachines (Basel), vol. 11, no. 12, p. 1125, Dec. 2020, doi: 10.3390/mi11121125.

[44] M. Şahin, F. Blaabjerg, and A. Sangwongwanich, “A Comprehensive Review on Supercapacitor Applications and Developments,” Energies (Basel), vol. 15, no. 3, p. 674, Jan. 2022, doi: 10.3390/en15030674.

[45] X.-L. Wu and A.-W. Xu, “Carbonaceous hydrogels and aerogels for supercapacitors,” J. Mater. Chem. A, vol. 2, no. 14, pp. 4852–4864, 2014, doi: 10.1039/C3TA13929H.

[46] A. G. Pandolfo and A. F. Hollenkamp, “Carbon properties and their role in supercapacitors,” J Power Sources, vol. 157, no. 1, pp. 11–27, Jun. 2006, doi: 10.1016/j.jpowsour.2006.02.065.

[47] D. Zhang, C. Tan, W. Zhang, W. Pan, Q. Wang, and L. Li, “Expanded Graphite-Based Materials for Supercapacitors: A Review,” Molecules, vol. 27, no. 3, p. 716, Jan. 2022, doi: 10.3390/molecules27030716.

[48] S. Ghosh, G. R. Rao, and T. Thomas, “Analysis of Charge Storage Behavior in Redox-electrolyte Based Battery-like-systems: A Case Study on Zr-doped Ceria,” ChemistrySelect, vol. 5, no. 5, pp. 1628–1639, Feb. 2020, doi: 10.1002/slct.201904761.

[49] P. Kurzweil, “Supercapacitors: Electrochemical double-layer capacitors,” in Reference Module in Chemistry, Molecular Sciences and Chemical Engineering, Elsevier, 2023. doi: 10.1016/B978-0-323-96022-9.00045-1.

[50] B. Deka and K.-H. Cho, “BiFeO3-Based Relaxor Ferroelectrics for Energy Storage: Progress and Prospects,” Materials, vol. 14, no. 23, p. 7188, Nov. 2021, doi: 10.3390/ma14237188.

[51] A. Bothe, S. E. M. Pourhosseini, P. Ratajczak, F. Béguin, and A. Balducci, “Analysis of thermal and electrochemical properties of electrical double-layer capacitors by using an in-situ simultaneous thermal analysis cell,” Electrochim Acta, vol. 444, p. 141974, Mar. 2023, doi: 10.1016/j.electacta.2023.141974.

[52] L. Köps, F. A. Kreth, M. Klein, and A. Balducci, “An in-depth investigation into the influence of temperature on the electrochemical behavior of electric double-

layer capacitors containing ethyl isopropyl sulfone-based electrolytes," J Power Sources, vol. 581, p. 233480, Oct. 2023, doi: 10.1016/j.jpowsour.2023.233480.

[53] B. Zhao et al., "A high-energy, long cycle-life hybrid supercapacitor based on graphene composite electrodes," Energy Storage Mater, vol. 7, pp. 32–39, Apr. 2017, doi: 10.1016/j.ensm.2016.11.010.

[54] J. Libich, J. Máca, J. Vondrák, O. Čech, and M. Sedlaříková, "Supercapacitors: Properties and applications," J Energy Storage, vol. 17, pp. 224–227, Jun. 2018, doi: 10.1016/j.est.2018.03.012.

[55] S. Zallouz, S. N. Pronkin, J.-M. Le Meins, C. Pham-Huu, and C. Matei Ghimbeu, "New development in carbon-based electrodes and electrolytes for enhancement of supercapacitor performance and safety," in Renewable Energy Production and Distribution Volume 2, Elsevier, 2023, pp. 353–408. doi: 10.1016/B978-0-443-18439-0.00011-2.

[56] C. An, Y. Zhang, H. Guo, and Y. Wang, "Metal oxide-based supercapacitors: progress and prospectives," Nanoscale Adv, vol. 1, no. 12, pp. 4644–4658, 2019, doi: 10.1039/C9NA00543A.

[57] N. Kurra and Q. Jiang, "Supercapacitors," in Storing Energy, Elsevier, 2022, pp. 383–417. doi: 10.1016/B978-0-12-824510-1.00017-9.

[58] J. Libich, J. Máca, J. Vondrák, O. Čech, and M. Sedlaříková, "Supercapacitors: Properties and applications," J Energy Storage, vol. 17, pp. 224–227, Jun. 2018, doi: 10.1016/j.est.2018.03.012.

[59] A. Afif, S. M. Rahman, A. Tasfiah Azad, J. Zaini, M. A. Islan, and A. K. Azad, "Advanced materials and technologies for hybrid supercapacitors for energy storage – A review," J Energy Storage, vol. 25, p. 100852, Oct. 2019, doi: 10.1016/j.est.2019.100852.

[60] M. Z. Iqbal and U. Aziz, "Supercapattery: Merging of battery-supercapacitor electrodes for hybrid energy storage devices," J Energy Storage, vol. 46, p. 103823, Feb. 2022, doi: 10.1016/j.est.2021.103823.

[61] N. Wu et al., "Recent Advances of Asymmetric Supercapacitors," Adv Mater Interfaces, vol. 8, no. 1, Jan. 2021, doi: 10.1002/admi.202001710.

[62] S.-M. Chen, R. Ramachandran, V. Mani, and R. Saraswathi, "Recent Advancements in Electrode Materials for the High-performance Electrochemical Supercapacitors: A Review," Int J Electrochem Sci, vol. 9, no. 8, pp. 4072–4085, Aug. 2014, doi: 10.1016/S1452-3981(23)08076-8.

[63] P. Sharma and V. Kumar, “Current Technology of Supercapacitors: A Review,” Journal of Electronic Materials, vol. 49, no. 6. Springer, pp. 3520–3532, Jun. 01, 2020. doi: 10.1007/s11664-020-07992-4.

[64] S. W. Bokhari et al., “Advances in graphene-based supercapacitor electrodes,” Energy Reports, vol. 6, pp. 2768–2784, Nov. 2020, doi: 10.1016/j.egyr.2020.10.001.

[65] S. Najib and E. Erdem, “Current progress achieved in novel materials for supercapacitor electrodes: mini-review,” Nanoscale Adv, vol. 1, no. 8, pp. 2817–2827, 2019, doi: 10.1039/C9NA00345B.

[66] S. S. Siwal, Q. Zhang, N. Devi, and V. K. Thakur, “Carbon-Based Polymer Nanocomposite for High-Performance Energy Storage Applications,” Polymers (Basel), vol. 12, no. 3, p. 505, Feb. 2020, doi: 10.3390/polym12030505.

[67] Z. S. Iro, C. Subramani, and S. S. Dash, “A Brief Review on Electrode Materials for Supercapacitor,” Int J Electrochem Sci, vol. 11, no. 12, pp. 10628–10643, Dec. 2016, doi: 10.20964/2016.12.50.

[68] N. I. Jalal, R. I. Ibrahim, and M. K. Oudah, “A review on Supercapacitors: types and components,” J Phys Conf Ser, vol. 1973, no. 1, p. 012015, Aug. 2021, doi: 10.1088/1742-6596/1973/1/012015.

[69] P. Forouzandeh, V. Kumaravel, and S. C. Pillai, “Electrode Materials for Supercapacitors: A Review of Recent Advances,” Catalysts, vol. 10, no. 9, p. 969, Aug. 2020, doi: 10.3390/catal10090969.

[70] H. Gupta, M. Kumar, D. Sarkar, and P. W. Menezes, “Recent technological advances in designing electrodes and electrolytes for efficient zinc ion hybrid supercapacitors,” Energy Advances, vol. 2, no. 9, pp. 1263–1293, 2023, doi: 10.1039/D3YA00259D.

[71] J. Jiang, Y. Li, J. Liu, X. Huang, C. Yuan, and X. W. D. Lou, “Recent Advances in Metal Oxide-based Electrode Architecture Design for Electrochemical Energy Storage,” Advanced Materials, vol. 24, no. 38, pp. 5166–5180, Oct. 2012, doi: 10.1002/adma.201202146.

[72] Z. S. Iro, C. Subramani, and S. S. Dash, “A brief review on electrode materials for supercapacitor,” International Journal of Electrochemical Science, vol. 11, no. 12. Electrochemical Science Group, pp. 10628–10643, 2016. doi: 10.20964/2016.12.50.

[73] M. J. Carmezim and C. F. Santos, “Electrolytes in Metal Oxide Supercapacitors,” in Metal Oxides in Supercapacitors, Elsevier, 2017, pp. 49–78. doi: 10.1016/B978-0-12-810464-4.00003-6.

[74] M. Pershaanaa, S. Bashir, S. Ramesh, and K. Ramesh, “Every bite of Supercap: A brief review on construction and enhancement of supercapacitor,” J Energy Storage, vol. 50, p. 104599, Jun. 2022, doi: 10.1016/j.est.2022.104599.

[75] K. Karuppasamy et al., “Ionic Liquid-Based Electrolytes for Energy Storage Devices: A Brief Review on Their Limits and Applications,” Polymers (Basel), vol. 12, no. 4, p. 918, Apr. 2020, doi: 10.3390/polym12040918.

[76] S. Islam et al., “Recent Advancements in Electrochemical Deposition of Metal-Based Electrode Materials for Electrochemical Supercapacitors,” The Chemical Record, vol. 22, no. 7, Jul. 2022, doi: 10.1002/tcr.202200013.

[77] M. Z. Iqbal, S. Zakar, and S. S. Haider, “Role of aqueous electrolytes on the performance of electrochemical energy storage device,” Journal of Electroanalytical Chemistry, vol. 858, p. 113793, Feb. 2020, doi: 10.1016/j.jelechem.2019.113793.

[78] E. Bekaert, L. Buannic, U. Lassi, A. Llordés, and J. Salminen, “Electrolytes for Li- and Na-Ion Batteries: Concepts, Candidates, and the Role of Nanotechnology,” in Emerging Nanotechnologies in Rechargeable Energy Storage Systems, Elsevier, 2017, pp. 1–43. doi: 10.1016/B978-0-323-42977-1.00001-7.

[79] Q. T. Ain, S. H. Haq, A. Alshammari, M. A. Al-Mutlaq, and M. N. Anjum, “The systemic effect of PEG-nGO-induced oxidative stress in vivo in a rodent model,” Beilstein Journal of Nanotechnology, vol. 10, pp. 901–911, Apr. 2019, doi: 10.3762/bjnano.10.91.

[80] N. V. Gandhare et al., “An efficient and one-pot synthesis of 2,4,5-trisubstituted imidazole compounds catalyzed by copper nanoparticles,” Journal of the Chinese Advanced Materials Society, vol. 3, no. 4, pp. 270–279, Oct. 2015, doi: 10.1080/22243682.2015.1068134.

[81] W. Huang, J. Li, and Y. Xu, “Nucleation/Growth Mechanisms and Morphological Evolution of Porous MnO2 Coating Deposited on Graphite for Supercapacitor,” Materials, vol. 10, no. 10, p. 1205, Oct. 2017, doi: 10.3390/ma10101205.

[82] P. Porta, G. Moretti, M. Musicanti, and A. Nardella, “Characterization of copper-manganese mixed oxides,” Catal Today, vol. 9, no. 1–2, pp. 211–218, Mar. 1991, doi: 10.1016/0920-5861(91)85026-5.

[83] S.-E. Fateen, A. Khedr, O. Elkady, S. Azer, and Omar. Abdel-Salam, “Copper-Graphite Nanocomposite Electrodes for the Electrochemical Reduction of Carbon Dioxide to Methanol. ,” BOOK, Apr. 2016.

[84] B. Talluri, M. L. Aparna, N. Sreenivasulu, S. S. Bhattacharya, and T. Thomas, “High entropy spinel metal oxide (CoCrFeMnNi)3O4 nanoparticles as a high-performance supercapacitor electrode material,” J Energy Storage, vol. 42, p. 103004, Oct. 2021, doi: 10.1016/j.est.2021.103004.

[85] M. Opitz, J. Yue, J. Wallauer, B. Smarsly, and B. Roling, “Mechanisms of Charge Storage in Nanoparticulate TiO2 and Li4Ti5O12 Anodes: New Insights from Scan rate-dependent Cyclic Voltammetry,” Electrochim Acta, vol. 168, pp. 125–132, Jun. 2015, doi: 10.1016/j.electacta.2015.03.186.

[86] P. M. Shafi et al., “Sr- and Fe-substituted LaMnO3 Perovskite: Fundamental insight and possible use in asymmetric hybrid supercapacitor,” Energy Storage Mater, vol. 45, pp. 119–129, Mar. 2022, doi: 10.1016/j.ensm.2021.11.028.

[87] M. Sharma, S. Gao, E. Mäder, H. Sharma, L. Y. Wei, and J. Bijwe, “Carbon fiber surfaces and composite interphases,” Compos Sci Technol, vol. 102, pp. 35–50, Oct. 2014, doi: 10.1016/j.compscitech.2014.07.005.

[88] S. Chou, H.-C. Chen, and H.-E. Chen, “ carbon fiber fabric reinforced epoxy resin composites,” Compos Sci Technol, vol. 45, no. 1, pp. 23–35, Jan. 1992, doi: 10.1016/0266-3538(92)90119-N.

[89] S. Wang, Z. Li, X. Gong, F. Hou, and J. Liang, “Self-Assembly and Properties of Elastic Nanocellulose-Carbon Airgel with Ordered Porosity by Template-Free Directional Freezing,” Coatings, vol. 13, no. 7, p. 1297, Jul. 2023, doi: 10.3390/coatings13071297.

[90] “The structure of graphite,” Proceedings of the Royal Society of London. Series A, Containing Papers of a Mathematical and Physical Character, vol. 106, no. 740, pp. 749–773, Dec. 1924, doi: 10.1098/rspa.1924.0101.

[91] M. D. Stoller, S. Park, Y. Zhu, J. An, and R. S. Ruoff, “Graphene-Based Ultracapacitors,” Nano Lett, vol. 8, no. 10, pp. 3498–3502, Oct. 2008, doi: 10.1021/nl802558y.

[92] P. M. Shafi et al., “Sr- and Fe-substituted LaMnO3 Perovskite: Fundamental insight and possible use in asymmetric hybrid supercapacitor,” Energy Storage Mater, vol. 45, pp. 119–129, Mar. 2022, doi: 10.1016/j.ensm.2021.11.028.

[93] S. L. Medway, C. A. Lucas, A. Kowal, R. J. Nichols, and D. Johnson, “In situ studies of the oxidation of nickel electrodes in alkaline solution,” Journal of Electroanalytical Chemistry, vol. 587, no. 1, pp. 172–181, Feb. 2006, doi: 10.1016/j.jelechem.2005.11.013.

[94] D. Michell, D. A. J. Rand, and R. Woods, “A study of ruthenium electrodes by cyclic voltammetry and X-ray emission spectroscopy,” J Electroanal Chem Interfacial Electrochem, vol. 89, no. 1, pp. 11–27, May 1978, doi: 10.1016/S0022-0728(78)80027-8.

[95] X. Nie, M. R. Esopi, M. J. Janik, and A. Asthagiri, “Copper Electrodes: The Role of the Kinetics of Elementary Steps,” Angewandte Chemie, vol. 125, no. 9, pp. 2519–2522, Feb. 2013, doi: 10.1002/ange.201208320.

[96] K. Vijayamohanan, T. S. Balasubramanian, and A. K. Shukla, “Rechargeable alkaline iron electrodes,” J Power Sources, vol. 34, no. 3, pp. 269–285, Apr. 1991, doi: 10.1016/0378-7753(91)80093-D.

[97] M. Morita, C. Iwakura, and H. Tamura, “The anodic characteristics of manganese dioxide electrodes prepared by thermal decomposition of manganese nitrate,” Electrochim Acta, vol. 22, no. 4, pp. 325–328, Apr. 1977, doi: 10.1016/0013-4686(77)85081-0.

[98] S. Palmas, F. Ferrara, A. Vacca, M. Mascia, and A. M. Polcaro, “Behavior of cobalt oxide electrodes during oxidative processes in alkaline medium,” Electrochim Acta, vol. 53, no. 2, pp. 400–406, Dec. 2007, doi: 10.1016/j.electacta.2007.01.085.

[99] Zh. A. Boeva and V. G. Sergeyev, “Polyaniline: Synthesis, properties, and application,” Polymer Science Series C, vol. 56, no. 1, pp. 144–153, Sep. 2014, doi: 10.1134/S1811238214010032.

[100] G. B. Street, S. E. Lindsey, A. I. Nazzal, and K. J. Wynne, “The Structure and Mechanical Properties of Polypyrrole,” Molecular Crystals and Liquid Crystals, vol. 118, no. 1, pp. 137–148, Feb. 1985, doi: 10.1080/00268948508076201.

CURRICULUM VITAE

Name Surname	**HÜSEYİN FAAL**

EDUCATION

2021- Continues	**M.Sc. in Materials Science and Engineering** Material Science and Engineering, Gaziantep University
2017 to 2021	**Metallurgy and Materials Engineering** Metallurgy and Materials Engineering, Gaziantep University
2015 to 2020	**Mechanical Engineering** Mechanical Engineering, Gaziantep University

PROFESSIONAL EXPERIENCE

2022 to 2023	**Weaving Product Engineer - RAVANDA CARPET, Gaziantep** Controlled daily production efficiency of looms, created workloads, tracked orders, and oversaw general production tracking and control.
2020 to 2021	**Assistant of Business Manager - SIRMA CARPET, Gaziantep** Responsible for weaving, apparel, and production follow-up, yield tracking, and quality control.

ORIENTATION EXPERIENCE

Jan.2020 to April 2020	**Internship - SIRMA CARPET, Gaziantep** Conducted compulsory internship including workflow in weaving, time study tracking, production tracking in apparel, glue consumption analysis, and cost calculation in the finishing machine.
Jun. 2014 to Sep. 2014	**Summer Internship - TPAO Inc., Batman** Actively participated in exploration, drilling, well completion, perforation, and other production stages at TPAO Inc. in Batman.